

**International  
Journal of  
Engineering  
Technologies  
(IJET)**

**ISSN: 2149-0104**

**Volume: 1  
No: 1  
March 2015**

**© Istanbul Gelisim University Press, 2015**  
Certificate Number: 23696  
All rights reserved.

*International Journal of Engineering Technologies is an international peer-reviewed journal and published quarterly. The opinions, thoughts, postulations or proposals within the articles are but reflections of the authors and do not, in any way, represent those of the Istanbul Gelisim University.*

**CORRESPONDENCE and COMMUNICATION:**

Istanbul Gelisim University Faculty of Engineering and Architecture  
Cihangir Mah. Şehit P. Onb. Murat Şengöz Sk. No: 8  
34315 Avcılar / Istanbul / TURKEY  
**Phone:** +90 212 4227020 **Ext.** 221  
**Fax:** +90 212 4227401  
**e-Mail:** [ijet@gelisim.edu.tr](mailto:ijet@gelisim.edu.tr)  
**Web site:** <http://ijet.gelisim.edu.tr>  
<http://dergipark.ulakbim.gov.tr/ijet>

**Printing and binding:**

Anka Matbaa  
Sertifika No: 12328  
Tel: +90 212 5659033 - 4800571  
e-Posta: [ankamatbaa@gmail.com](mailto:ankamatbaa@gmail.com)

*International Journal of Engineering Technologies (IJET) is included in:*



**Turkish**  
**JournalPark**  
ACADEMIC



**INTERNATIONAL JOURNAL OF ENGINEERING TECHNOLOGIES (IJET)**  
**International Peer-Reviewed Journal**  
**Volume 1, No 1, March 2015, ISSN: 2149-0104**

**Owner on Behalf of Istanbul Gelisim University**  
Rector Prof. Dr. Burhan AYKAÇ

**Editor-in-Chief**  
Prof. Dr. İlhami ÇOLAK

**Associate Editor**  
Dr. Selin ÖZÇİRA  
Dr. Mehmet YEŞİLBUDAK

**Layout Editor**  
Seda ERBAYRAK

**Proofreader**  
Özlemnur ATAOL

**Copyeditor**  
Evrin GÜLEY

**Contributor**  
Ahmet Şenol ARMAĞAN

**Cover Design**  
Tarık Kaan YAĞAN

## **Editorial Board**

Professor İlhami COLAK, Istanbul Gelisim University, Turkey

Professor Dan IONEL, Regal Beloit Corp. and University of Wisconsin Milwaukee, United States

Professor Fujio KUROKAWA, Nagasaki University, Japan

Professor Marija MIROSEVIC, University of Dubrovnik, Croatia

Prof. Dr. Şeref SAĞIROĞLU, Gazi University, Graduate School of Natural and Applied Sciences, Turkey

Professor Adel NASIRI, University of Wisconsin-Milwaukee, United States

Professor Mamadou Lamina DOUMBIA, University of Québec at Trois-Rivières, Canada

Professor João MARTINS, University/Institution: FCT/UNL, Portugal

Professor Yoshito TANAKA, Nagasaki Institute of Applied Science, Japan

Dr. Youcef SOUFI, University of Tébessa, Algeria

Prof.Dr. Ramazan BAYINDIR, Gazi Üniversitesi, Turkey

Professor Goce ARSOV, SS Cyril and Methodius University, Macedonia

Professor Tamara NESTOROVIĆ, Ruhr-Universität Bochum, Germany

Professor Ahmed MASMOUDI, University of Sfax, Tunisia

Professor Tsuyoshi HIGUCHI, Nagasaki University, Japan

Professor Abdelghani AISSAOUI, University of Bechar, Algeria

Professor Miguel A. SANZ-BOBI, Comillas Pontifical University /Engineering School, Spain

Professor Mato MISKOVIĆ, HEP Group, Croatia

Professor Nilesh PATEL, Oakland University, United States

Assoc. Professor Juan Ignacio ARRIBAS, Universidad Valladolid, Spain

Professor Vladimir KATIC, University of Novi Sad, Serbia

Professor Takaharu TAKESHITA, Nagoya Institute of Technology, Japan

Professor Filote CONSTANTIN, Stefan cel Mare University, Romania

Assistant Professor Hulya OBDAN, Istanbul Yildiz Technical University, Turkey

Professor Luis M. San JOSE-REVUELTA, Universidad de Valladolid, Spain

Professor Tadashi SUETSUGU, Fukuoka University, Japan

Associate Professor Zehra YUMURTACI, Istanbul Yildiz Technical University, Turkey

Dr. Rafael CASTELLANOS-BUSTAMANTE, Instituto de Investigaciones Eléctricas, Mexico

Assoc. Prof. Dr. K. Nur BEKIROGLU, Yildiz Technical University, Turkey

Professor Gheorghe-Daniel ANDREESCU, Politehnica University of Timisoara, Romania

Dr. Jorge Guillermo CALDERÓN-GUIZAR, Instituto de Investigaciones Eléctricas, Mexico

Professor VICTOR FERNÃO PIRES, ESTSetúbal/Polytechnic Institute of Setúbal, Portugal

Dr. Hiroyuki OSUGA, Mitsubishi Electric Corporation, Japan

Associate Professor Serkan TAPKIN, Istanbul Gelisim University, Turkey

Professor Luis COELHO, ESTSetúbal/Polytechnic Institute of Setúbal, Portugal

Professor Furkan DINCER, Mustafa Kemal University, Turkey

Professor Maria CARMEZIM, ESTSetúbal/Polytechnic Institute of Setúbal, Portugal

Associate Professor Lale T. ERGENE, Istanbul Technical University, Turkey

Dr. Hector ZELAYA, ABB Corporate Research, Sweden

Professor Isamu MORIGUCHI, Nagasaki University, Japan

Associate Professor Kiruba SIVASUBRAMANIAM HARAN, University of Illinois, United States

Associate Professor Leila PARSA, Rensselaer Polytechnic Institute, United States

Professor Salman KURTULAN, Istanbul Technical University, Turkey

Professor Dragan ŠEŠLIJA, University of Novi Sad, Serbia

Professor Birsen YAZICI, Rensselaer Polytechnic Institute, United States

Assistant Professor Hidenori MARUTA, Nagasaki University, Japan

Associate Professor Yilmaz SOZER, University of Akron, United States

Associate Professor Yuichiro SHIBATA, Nagasaki University, Japan

Professor Stanimir VALTCHEV, Universidade NOVA de Lisboa, (Portugal) + Burgas Free University, (Bulgaria)

Professor Branko SKORIC, University of Novi Sad, Serbia

Dr. Cristea MIRON, Politehnica University in Bucharest, Romania

Dr. Nobumasa MATSUI, MHPS Control Systems Co., Ltd, Japan

Professor Mohammad ZAMI, King Fahd University of Petroleum and Minerals, Saudi Arabia

Associate Professor Mohammad TAHA, Rafik Hariri University (RHU), Lebanon

Assistant Professor Kyungnam KO, Jeju National University, Republic of Korea

Dr. Guray GUVEN, Conductive Technologies Inc., United States

Dr. Tuncay KAMAŞ, Eskişehir Osmangazi University, Turkey

## **From the Editor**

Dear Colleagues,

On behalf of the editorial board of International Journal of Engineering Technologies (IJET), I would like to share our happiness to publish the first issue of IJET. My special thanks are for members of editorial board, editorial team, referees, authors and other technical staff.

Please find the first issue of International Journal of Engineering Technologies at <http://dergipark.ulakbim.gov.tr/ijet>. We invite you to review the Table of Contents by visiting our web site and review articles and items of interest. IJET will continue to publish high level scientific research papers in the field of Engineering Technologies as an International peer-reviewed scientific and academic journal of Istanbul Gelisim University.

Thanks for your continuing interest in our work,

**Professor ILHAMI COLAK**  
**Istanbul Gelisim University**  
[icolak@gelisim.edu.tr](mailto:icolak@gelisim.edu.tr)

---

<http://dergipark.ulakbim.gov.tr/ijet>  
**Print ISSN: 2149-0104**

International Journal of  
Engineering Technologies  
**IJET**

# Table of Contents

	Page
<i>From the Editor</i>	<i>vii</i>
<i>Table of Contents</i>	<i>ix</i>
<u>A paradigm change in road safety evaluation: from hypothetico-deductive testing to designing safety systems</u>	
<i>Akin Osman Kazakci, Nicolas Paget, Romain Fricheteau</i>	1-7
<u>Comparison of Microwave and Conventional Driven Adsorption Heat Pump Cycle Duration</u>	
<i>Hasan Demir</i>	8-12
<u>CAE Model Correlation &amp; Design Optimization of a Laminated Steel Oil Pan by means of Acceleration and Strain Measurement on a Fired Engine</u>	
<i>Rıfat Kohen Yanarocak, Abdülkadir Çekiç</i>	13-18
<u>Comparative Study of on and off Grid Tied Integrated Diesel/Solar (PV) Battery Generation System</u>	
<i>Kenneth Okedu, Roland Uhunmwangho, Ngang Bassey</i>	19-25
<u>Multiobjective Pareto Optimal Design of a Clutch System</u>	
<i>Onur Ozansoy, Talat Tevruz, Ata Mugan</i>	26-43
<u>Position Singularities and Ambiguities of the KUKA KR5 Robot</u>	
<i>Géza Husi</i>	44-50

**International Journal of Engineering Technologies, IJET**

**e-Mail:** [ijet@gelisim.edu.tr](mailto:ijet@gelisim.edu.tr)  
**Web site:** <http://ijet.gelisim.edu.tr>  
<http://dergipark.ulakbim.gov.tr/ijet>

# A Paradigm Change in Road Safety Evaluation: From Hypothetico-Deductive Testing To Designing Safety Systems

Akin Osman Kazakci\*<sup>‡</sup>, Nicolas Paget\*\*, Romain Fricheteau\*\*\*

\* Centre for Management Science, Mines ParisTech, 60 Bd. Saint-Michel, 75272 Cedex 06, Paris, France

\*\*LAMSADE, Université Paris Dauphine, Place du Maréchal de Lattre de Tassigny, 75016 Paris

\*\*\*RATP, 54 Port de la rapée 75012 Paris, France

akin.kazakci@mines-paristech.fr, nicolas.paget@lamsade.dauphine.fr, romain.fricheteau@ratp.fr

<sup>‡</sup>Corresponding Author: Akin Osman Kazakçı; Mines ParisTech, 60 Bd. Saint-Michel, 75272 Cedex 06, Paris, France,

Tel: +33627833922,

Fax: +33140519065, akin.kazakci@mines-paristech.fr

*Received: 23.01.2015 Accepted: 22.02.2015*

**Abstract-** Automobile industry is going through important changes with the rise of connected vehicle paradigm. In this context, traditional performance evaluation procedures are becoming obsolete or insufficient. This is particularly the case for road safety evaluation models since new information and communication technologies engender new types of vulnerabilities. This paper claims that traditional hypothetico-deductive evaluation paradigms are no longer adequate to assess road safety. To complement this traditional approach, we present an alternative perspective based on design theory originating from engineering design field. We illustrate the use of design methods in this context. More generally, we argue that a design based approach to road safety evaluation will allow integrating evaluators early in the process, and to give them a set of new tools coming from design theory in order to design better experiments with indicators of safety are better adapted to changing safety situations.

**Keywords** Road safety; safety assessment; evaluation methods; experiment design, design methods.

## 1. Introduction

Road safety is a major concern at the international level. According to the World Health Organization [1, 2] 1.2 million people in the world die each year because of road crashes. Built on a 40 year old practice started in the late 60s, evaluation of road safety seems a well-established, routine practice, with well-known methods and generally accepted norms [3]. This has led to the creation independent and expert structures like the LAB (Laboratory of Accidentology and Biomechanics) – a laboratory co-owned by Renault and Citroën – where evaluation of safety performance of cars can be carried out independently from the internal processes of the car manufacturer [4].

However, automotive industry is seeing major evolutions: energy crisis, sustainable development challenges, global competition, electrical propulsion, assistive technologies, car to car (C2C) and car to infrastructure (C2I) possibilities. These new technologies, inside or outside the car, is equivalent to a change in the evaluation paradigm. Indeed, methods that exclude driver's behavior and environment are no longer sufficient for proper and accurate evaluation even though the usual methods are still valid at some point.

In design terms, the identity of the object “car” is no longer stable as we are on the frontier of breaking a well-established dominant design – that has not seen major changes for decades. This changes inevitably affects the

organization of an entire ecosystem of transportation, including the safety evaluation practices and organizations.

When an object's identity is stable (design completed), its evaluation modalities are also stabilized. The purpose and the intended functionalities of the object are known thus what needs to be evaluated is clear. When the identity becomes subject to change, the evaluation modalities need to be redesigned according to the newly emergent forms. Since automobiles' identity is strongly questioned and subject to evolutions, the classical schemas for the evaluation of its performances (e.g. about safety) need to be reconsidered and redesigned jointly.

The eco-system of road safety evaluation, either not realizing the nature of this shift or lacking adapted theoretical lenses to recognize its properties, tends to adopt a hypothetico-deductive stance for the evaluation of emerging technologies. The efforts are concentrated on what can be measured instead of what does a particular road security issue imply and how evaluators can help with it [5].

The paper proposes that the hypothetico-deductive stance is inadequate and proposes a conceptive perspective where the road safety question is seen as a part of a larger design issue, and evaluation models are adapted to specific variants (i.e. technological or experimental) need to be designed using appropriate design approaches.

We propose that actors, such as the LAB, responsible for the evaluation of safety aspects need to carry out additional responsibilities within the new context and to actively participate to the design of road safety systems - providing input and expertise to the system designers (such as the car manufacturers) early on - they need to become designer of safety evaluation models and they can no longer hold onto an evaluator position solely. These propositions are fundamentally new for the road safety evaluation field and illustrate the contribution design methods and approaches can have in this domain.

Plan of the paper: In Section 2, we review shortly traditional car safety paradigm and current evolutions in the automotive industry. Section 3 presents current philosophies and approaches to safety evaluation. We argue that the most widely used techniques are black-box approaches and give two examples (for a priori and a posteriori evaluations). In Section 4, we present two fundamentally new approaches to extend the role of evaluation expert's role in the car safety eco-system. First method is a functional evaluation approach where evaluators can provide inputs during design of safety system based on the features of different candidate technologies and their match with the safety issue being handled. Second method is the use of a formal design theory in order to map out different road safety scenarios related to a particular safety concern (e.g. road adherence, low friction) and the potential evaluation methods for each. Section 5 concludes with a short discussion.

## **2. Strong Evolution of Automotive Industry: Implied Changes for The Evaluation of Safety**

### *2.1 Traditional Vision of Safety: Within the Confines of a Dominant Design*

The car industry provides the archetypical example of what is often called a dominant design [7]. Its main features, such as the generic architecture, are generally accepted as the best possible combination that maximizes the object's utility and purpose. In such situations, an object's identity is stabilized i.e. its functional design, conceptual models, and associated business models do not see major changes over several development episodes [8].

When languages and parameter spaces for describing an object are stable, design follows a logic of optimization of the current sets of design parameters to achieve maximal performances within the confined description space of the object – including its performance criteria.

One of the key performance criteria for a car is safety of passengers. As Figure 1 shows, this has been a major issue where significant progresses have been achieved over the years. Choice and improvement of materials, numerous additional safety systems (airbag, safety belt, etc.) have been introduced without changing the general architecture and disposition of a car.

Following this logic, where design efforts have been extensively focused on the optimization of the existing systems and definitions, the evaluation of road safety of a car has not seen brutal changes. The major criteria to be considered were the number of dead and injured people in the accidents, depending on the existence (or not) of a given safety system among cars involved in an accident (more details on Section 3). Note that this procedure is often a posteriori evaluation procedure. With the current interest in intelligent vehicles and assistive technologies, globally, car manufacturers became more interested in developing safety systems that would rather prevent an accident from happening. How to evaluate accidents that have never occurred? Such as the question that points to significant changes in the current road safety evaluation paradigm since it is needed to move beyond the passive security paradigm to a more proactive one; Fig. 3.

### *2.2 From Isolated Cars to Communicating Cars*

Automotive industry is going through tremendous change. The return of the electrical vehicles [9] and the efforts to better integrate the car to the city for sustainability is causing rapid and successive changes in major design parameters. Technical changes imposed by economic and sustainability issues create a favorable environment for embedding more intelligent technologies in cars as well. Years of research in automated or assistive technologies on intelligent transportation systems are being industrialized one by one. The trend will be only accelerated with the upcoming 3<sup>rd</sup> generation electrical vehicles.

Followed by these technological changes the evaluation models associated with the car need also changing. The expected performances are not the same, for instance, for a thermic engine or an electric one. To give an example, in case of a crash, an issue to be resolved with thermic engine is fire and explosion risks. For an electrical engine, spill out of dangerous chemical substances is one of the main issues [10]. While both objects can be classified as cars, significant

differences among them imply differences in norms and performance metrics to be used for evaluation purposes.

With C2X (Car to Car or Car to Infrastructure communication; see Fig. 2) new and previously unsuspected safety issues arise. For instance, in a setting where cars can handle most of the driving (at least in particular conditions, such as restricted zones for that purpose), despite all the planning power available to the system, unexpected situations can occur (e.g. unauthorized entry to the zone) where neither the driver nor the car can take appropriate action in time. Current evaluation practices, tailored rather for the optimization of a unique vehicle's performances as explained in Section 2.1 are not adapted for the evaluation of a scenario where the infrastructure and vehicles communicate and coordinate. New evaluation models and practices for a setting whom parameters are yet to be decided need to be constructed. Among other things, these changes implies that in addition to their roles of evaluator (in the traditional sense), structures like the LAB need to become designers of evaluation models [5].



**Fig. 1.** Evolution of car's in-depth accident analysis (65km/h) – Driver dead, injured and finally intact [6].

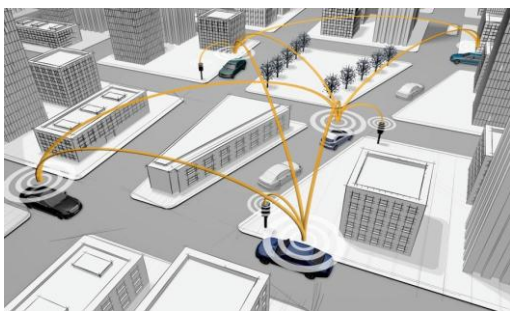


**Fig. 2.** Communicating cars – C2C, car to car and C2I, Car to infrastructure communication.

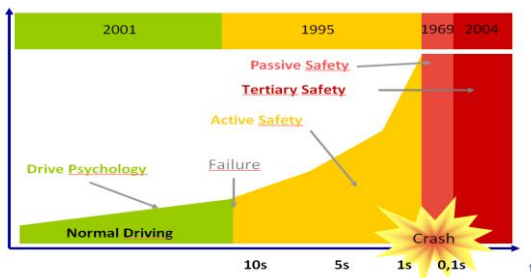


**Fig. 3.** Shift of the foci of road safety systems study over the years.

### 3. Approaches to Safety Evaluation

#### 3.1. Traditional Approaches: Experimental and Epidemiologic Evaluations

With respect to the safety paradigm presented in Section 2.1, a major approach in the evaluation of safety is the classical scientific experimental setting. It consists in conducting a controlled experiment with a well defined experimental plan, defined and isolated variables, devices for measuring and synthesis of results. This process has all the expected advantages of classical scientific methods (controllability, repeatability, etc.). This type of experiences is justified by the need to have accurate information on the driving behaviors and thus for being able to evaluate performances of primary security systems. This practice has limits when it comes to communicating vehicles. In US, recent studies conducted by Michigan University [11] involved 25 vehicles within 50km<sup>2</sup> surface where collecting data in controlled environment proved to be difficult. Facing such challenges, another approach called epidemiologic evaluation is often envisaged. Vehicles, driven by drivers specifically chosen (e.g. for their driving style), are equipped with various sorts of data gathering devices. The aim is to gather data in a realistic and naturalistic setting. This approach has the advantage of gathering enormous quantities of data. The downside is that it is difficult to know how to process all these data and also to what end. For instance, the vehicle can be observed as slowing down, but the reasons for such behavior are multiples and they can be combines: rain, other vehicles stopping, traffic...

This contrast between experimental and naturalistic evaluations points to the real challenges of traditional evaluation methods in road safety. Either, we limit ourselves to a small set of controlled variables and measure mostly their effect a posteriori (the accidents have already happened), or, we have an abundance of data, but what needs to be measured or what the evaluation is for is no longer clear.

#### 3.1.2. Black-box Evaluation: A Priori and A Posteriori Evaluation

There are two very common ways of evaluating a road safety system; a priori and a posteriori evaluation. A priori evaluation is about judging the benefits of a system before it has been developed. Since the system does not exist, it cannot be evaluated with respect to the situations where it saved lives or failed to do so. Rather, considering the existing databases on accidents, it is determined the ratio of accidents that could have been avoided had the system been installed in the vehicle(s) involved in the accident. Such an analysis can be effectively carried out using a black-box scheme [12] Fig. 4.

The result of such an analysis is the partitioning of the set of accidents as in Fig. 5. For the development team who need to decide whether to launch the design project, the important parameter is the size of the effective part i.e. the maximal ration of accidents that could have been avoided.

In Fig. 6. A posteriori evaluation considers the effect of a safety system introduced into the cars and traffic. Again

based on the available databases, the information about the vehicles equipped with a particular safety system and the accidents that are relevant with respect to that system's purpose are retrieved;

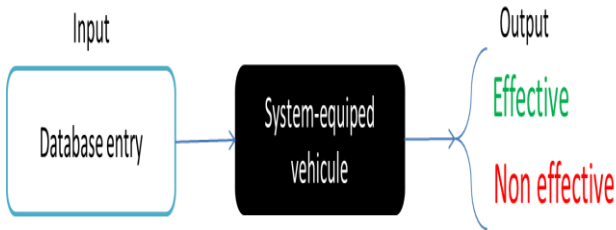


**Fig. 4.** The overall black-box scheme for a priori evaluation [13].

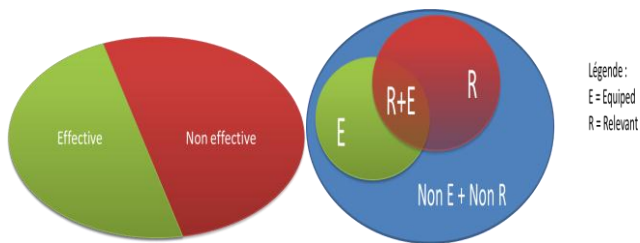


**Fig. 5.** Results of (a) a priori evaluation (b) a posteriori evaluation [13].

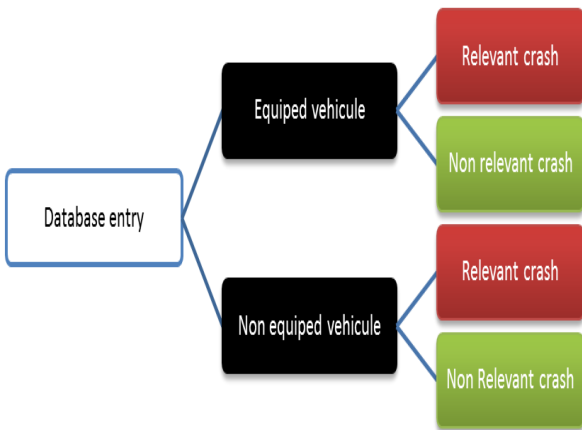


**Fig. 6.** The information compiled for a posteriori evaluation [13].

**3.2 Current Trend: Towards Hypothetico-Deductive FOT**

An approach combining the advantages of the two previous traditions have been used for a European Project, euroFOT [14]. FOT stands for Field Operational Tests. The objective of the project is to provide a testing approach for road safety in quasi-natural environments given the shift towards C2X systems. Test are being made on a variety

subjects such as Adaptive Cruise Control, Blind Spot Monitoring, Curve Speed Warning, to name a few.

For the needs of the platform, a general process has been proposed by FESTA Consortium [15] is a step-by-step approach that preconizes mainly a hypothetico-deductive process where a precise research question and hypotheses must be formulated before proceeding with the collect of data and analysis. A fundamental step in this process is the construction of an evaluation model by the analyst for the research question at hand. This construction involves finding appropriate indicators, performance metrics and thus conditions in a significant way which data should be collected to represent to the best of possible the defined dimensions of evaluation. Kircher [16] has produced a manual for listing some indicators that are advised to the evaluators for use in euroFOT.

We need to stress immediately that this hypothetico-deductive vision for a given safety evaluation issue is reductionist and dissecting the global safety problem into pieces where the analyst may very well loose from sight the interactions – at which point either the study will be biased or the meaning of the result will be lost.

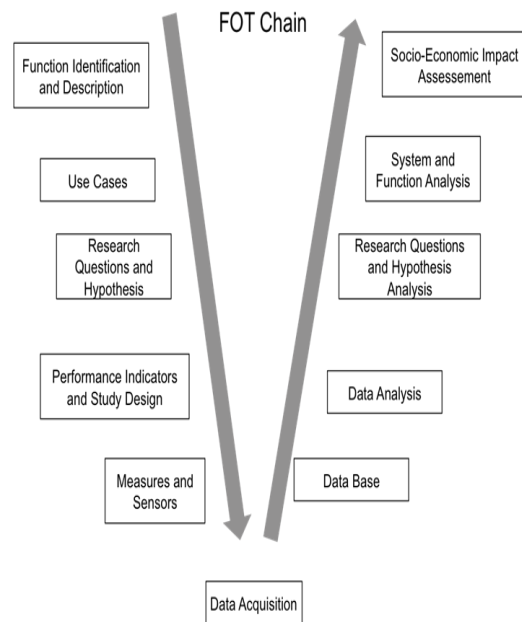


**Fig. 7.** A representation of FOT process.

Let us try to see potential problems of this approach with an example proposed by Kircher [16]:

1. Research Question: What would be the effects and efficiency of a system warning the driver about a zone with low friction of tires?
2. Hypotheses:
  - a) Such a system would increase the average distance between cars when a warning is given
  - b) The average speed will increase when there is no warning
3. Indicators: Average inter-distance / Average speed

There are some fundamental limitations of the implicit reasoning model embedded in this approach. First, as we can see in the example, since the proposed process is disconnected from the global design process of the security system, the research question seems context-free and general- which is an error. What would be the meaning of the collected data if the day of the test it is snowing or there is ice on the test grounds which would cause drivers to slow down? We can see that, despite the attempt to move towards the evaluation within a multiple-cars and natural conditions, the limitations of the isolated car evaluation setting is imported, possibly without recognizing it. More significantly, we can see that the analyst needs precise and accurate knowledge about the behavior of drivers and possible (and various) driving conditions in order to come up with relevant hypotheses which reduce the risk of distorting the phenomena. In order to have such knowledge, the philosophy of an evaluation independent of the design process must be abandoned. It should be acknowledged that the evaluators must now become part of the design process by becoming designers of safety evaluation models in collaboration with car designers.

**4. Re-instating Design Capabilities for the Safety Evaluation Units: From Evaluators to Co-designers of Safety Systems**

Given the previous analysis, we see that it is necessary that road safety evaluators actively participate to the design process in order to give relevant input to system designers but also in order to build appropriate evaluation models for the system being designed is necessary. We shall propose two types of approaches that can be used to this end. These approaches are not meant to replace existing practices, which have their own sphere of validity and relevance. On the contrary, what is targeted is to propose ways to complement existing practices in order to cope with the current transformations in automotive and road safety industries.

*4.1 Functional and Technological Evaluation: The Example of Lane Keeping Assistant Systems*

A first topic about which road safety expert can bring valuable expertise during system design is on the evaluation of functional and technological requirements during the design. Consider the example of Lane Keeping Assistant systems (LKA). Such systems are based on the idea of Lane Departure Warning (LDW) that emits a warning to the driver when the vehicle changes the current lane in a seemingly involuntary way. LKA takes corrective action in an automated way to prevent the drifting [17]. For such a system, the designer might arbitrarily consider very large number of functions. For the sake of example, let us assume that the car designer plans to introduce the following functions:

- F1: Functioning during the night
- F2: Functioning in broad day light

Recent studies in accidentology [18] show that 38,6% of relevant accidents happen during the night whereas only 0,4% happened in broad daylight. Such information allows evaluating functions of the system being designed and it is

important for the system designer to be able to assess alternative design options.

As it is most often the case with rapidly evolving product definitions, there are numerous technologies that can provide the same functionality. Once a safety system design team decides a functional requirement list, they need to evaluate which technological solutions to adopt to continue their design. Once again, the safety evaluation expert may provide inputs to the design process. Consider for instance the following Table1 [18].

With such detailed decomposition of a given safety system, it becomes possible for the safety evaluation expert to pinpoint to relevant portions of database or to proceed to specific tests for each of the considered technologies in a priori manner. The relevance of each property is evaluated according the analysis of real car accidents. Thus one can say that such property is necessary or than another is not. Then, just make the connection between properties/technologies and technology/safety system. Our evaluation through a safety viewpoint is done.

The hypothesis that all the systems with the same purpose (e.g. systems for LKA) are equivalent can be lifted, in favor of a more accurate analysis. The black-box becomes transparent.

At the moment, this type on analysis is not being done in Road Safety evaluation units – more importantly, car or safety system designers do not ask for such inputs. This only shows that, car manufacturers are as much fixated as the road safety evaluation experts on what the role for those latter group is. As depicted in Fig. 8, safety evaluator can become a partner in the design process rather than for the end product – on the specific dimension of safety.

**Table 1.** Properties of different technology for LKA

Technology / Property	Optical	Infra-red	Laser	Radar	GPS
Signal before crossing	Yes	No	Yes	Yes	Yes
Possible extensions	A lot	No	Detect people	Detect people	Already one
Weather restrictions	Bad weather, dust	No	Bad weather	No	No
Range	?	None	Limited : danger	100 m	Infinite
Accuracy	High	High	High	High	Not enough
Speed	High	High	Low	?	High
Need for environment evolution	Low	Low	Low	Huge : reflecting line	Detailed cartography

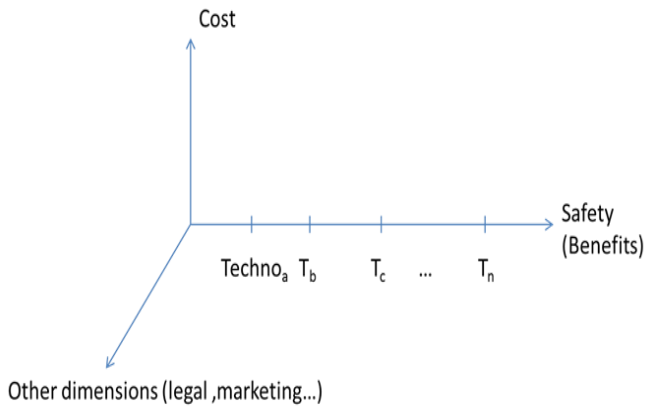


**Fig. 8.** Road safety evaluation expert as a co-designer specialized in safety [13].

4.2 *Becoming Co-Designers for Safety Systems: The Example of Avoidance of Low Friction*

The participation of road safety expert to the design and testing of systems might become more direct and better organized through a better understanding of the overall process and a new type of organization, possibly at the ecosystem level. In paragraph 3.2, we have seen that one of the most significant efforts in today’s ecosystem for improving road safety systems’ evaluation, the euroFOT initiative, suggests essentially a hypothetico-deductive approach. Among many potential difficulties and inaccuracies this approach may cause or simply delay quick convergence towards viable C2X safety systems is the absence of a holistic consideration of the safety issues and the premature reduction to a set of hypotheses and data gathering.

A safety system is seen as an entity whose purpose is uniquely definable and identifiable, whereas in such a rapidly evolving technological contexts, where norms and regulations have not been stabilized yet this is too big an assumption. As we have seen with the example of low friction warning, the system taken in isolation from its use, environment and the driver might lead to invalid or questionable assumptions. In order to provide a rigorous evaluation for a class of objects whose design have not been finalized and whom identity is not stable, a better integration of evaluators with system designers is necessary.

Such integration requires an approach to design that is holistic and provides the possibility to consider multiple potential identities for the system being designed. In the current work, we propose to use C-K theory [19] as a general tool for mapping a messy design process and as a means for coordinating design efforts. Let us consider again the example of low friction to illustrate how the theory can be. In such a case, although the conditions are favorable for a safe driving experience, there are cases where accidents still occur. Normally, such situations are outside the expertise area of the safety system designer – contrary to the safety system evaluation expert. In fact, one such reason for which accidents may occur under those conditions is high speed and the necessity to hit the brakes due to an unforeseen cause. The evaluation experts have a

used to systematically build both the system and the evaluation models associated with each variant. We are going focus on pedagogical aspects, and not the full sized application, since our aim is to illustrate the approach and the project details are confidential [13].

4.2.1 *Avoidance of Low-Friction as a Design Problem*

In order to explore possible meanings of our initial concept C<sub>0</sub>: Avoid low friction, the first step is to better frame what is friction. As we can see from Fig. 9, it is possible to define and explore a variety of combinations regarding the states of the environment, the vehicle and the driver. Once the details about the environment and the vehicle have been defined, it is possible to consider the driver’s reaction (which, currently is not considered in traditional road safety studies). For each unique combination, a different safety system might be required. In case such a system does not exist, its design may be connected to the conceptual description space. Whether it exists or not, the appropriate evaluation model can now be selected or constructed since the precise conditions for which the system is intended is now defined by design.

For instance, in Fig. 9, a situation where the road allows a high friction (>6ms<sup>2</sup>) and the vehicle is equipped with adequate materials (e.g. tires in good conditions) is depicted.

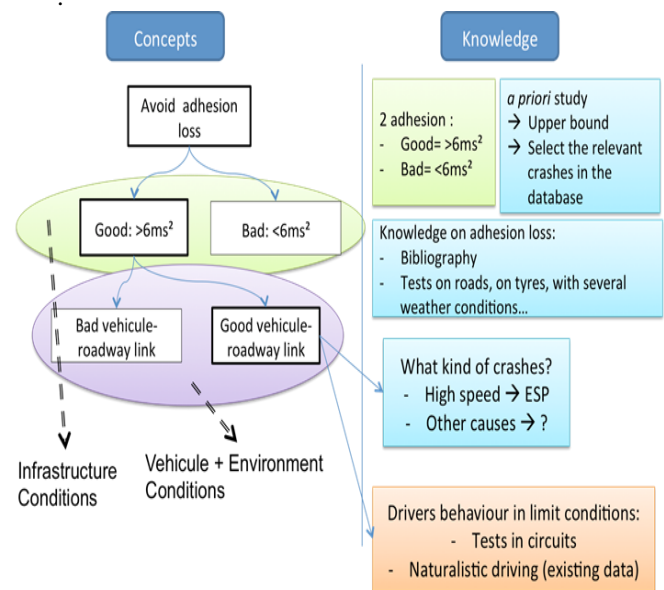


**Fig. 9.** Defining knowledge for friction and low friction for vehicles.

history of test results for similar conditions where ESP (electronic stability program) has been proven to be effective. In addition, relevant cases from the accident databases might be analyzed to determine other possible causes and drivers’ behavior in such conditions. Such analyses are likely to be extremely helpful for the system designer as gradually all the possible situations and potential measures will be mapped out. This, in turn will

give the possibility to better target the necessary functionalities and technologies. Moreover, the road safety system evaluator can devise better-targeted and precise tests in order to reveal both the design need and the performance of the envisaged solutions.

## 5. Conclusion

The automotive industry is going through immense changes. For the rapidly changing technologies for the forthcoming intelligent vehicles, evaluation of road safety is of renewed importance. In this paper, we have presented and analyzed traditional evaluation paradigm that is more centered on passive safety paradigm and stabilized evaluation routines. We argued that, since safety technology is changing and becoming more based on a pro-active approach, given the current communicating vehicles-infrastructure systems being designed, road safety evaluators should be more involved in the design of those systems.

We pointed out that a hypothetico-deductive approach extending the traditional paradigm of safety evaluation will not be sufficient and there is a need for a more holistic approach: Road safety system evaluators need to become co-designers of safety systems, providing inputs to the system designers, while, in turn, they build a new generation of evaluation models and practices. The proposed principles are illustrated with examples on lane keeping assistant system and the analysis of a low-friction system design.

## References

- [1] Peden, M., Hyder, A., Scurfield, R., Mohan, D., Jarawen, E., Sleet, D. and Mathers, C.,(2004). *Rapport mondial sur la prévention des traumatismes dus aux accidents de la circulation*, Organisation mondiale de la santé, Genève.
- [2] World Health Organization, 2004. *World report on trauma prevention*, s.l.: s.n.
- [3] LAB, 2011. *Rapport annuel*, s.l.: s.n.
- [4] Fricheteau, R., 2011. *Cadrage général pour une évaluation des performances des actions de sécurité routière*.
- [5] Labrousse, M., Hermitte, T., Hervé, V., Bertholon, N., Guillaume, A. (2011) Avolution of front car occupants injuries in frontal impacts considering the improvements of passive safety technologies, 13th European Automotive Congress, EAEC 2011, June 2011, Valencia, Spain.
- [6] Abernathy, W. & Utterback, J., 1978. Patterns of Industrial Innovation. *Technology Review*, pp. 40-47.
- [7] Le Masson, P., Weil, B. & Hatchuel, A., 2006. *Les processus d'innovation - Conception innovante et croissance des entreprises*. Paris: Hermès.
- [8] Mock, P., Hülsebusch, D. et al. (2009), *Electric vehicles - A model based assessment of future market prospects and environmental impacts*, International Electric Vehicle Symposium and Exposition (EVS), Stavanger, Norway.
- [9] Hervé, V., Fricheteau, R. (2011). *Etat de l'art sur les véhicules électriques et hybrides*, Confidential Report, LAB – CEESAR.
- [10] Michigan University, 2012. <http://www.umtri.umich.edu/our-results/publications>. [Online].
- [11] Wiener, N., 1948. *Cybernetics, or Control and Communication in the Animal and the Machine*. Cambridge, Mass.: MIT Press.
- [12] Paget, 2012. *Vers de nouvelles méthodes d'évaluation en accidentologie*.
- [13] euroFOT, 2012. [www.eurofot-ip.eu](http://www.eurofot-ip.eu). [Online].
- [14] FESTA Consortium, 2008. *FESTA Handbook*, s.l.: FESTA.
- [15] Kircher, K. (2008) *A comprehensive framework of performance indicators and their interaction*, FESTA Support Action Field operational test support Action, deliverable D2.1.
- [16] Malone, K., 2008. *Introduction: eImpact Final Conference*. Paris, France, .
- [17] Ledon, C., Roynard, M., Simon, MC., Phan, V. (2011) *Les systèmes d'alerte et d'assistance de sorties de voie embarqués sur les véhicules*, Projet ROADSENSE.
- [18] Hatchuel, A. & Weil, B., 2002. La théorie C-K : Fondements et usages d'une théorie unifiée de la conception, Lyon, Colloque sur Herbert Simon.

# Comparison of Microwave and Conventional Driven Adsorption Heat Pump Cycle Duration

Hasan Demir \*<sup>‡</sup>

\* Department of Chemical Engineering, Faculty of Engineering, Osmaniye Korkut Ata University  
hasandemir@osmaniye.edu.tr

<sup>‡</sup>Corresponding Author; Hasan Demir, Department of Chemical Engineering, Faculty of Engineering, Osmaniye Korkut Ata University, hasandemir@osmaniye.edu.tr

*Received: 23.01.2015 Accepted:23.02.2015*

**Abstract-** The present experimental study includes comparison of microwave regenerated and conventional heated adsorbent bed of adsorption heat pump. The novel adsorption heat pump driving with microwave heating system was designed and manufactured. Microwave oven was constructed for providing homogeneous temperature distribution in the adsorbent bed. Temperature and pressure variations in the adsorption heat pump for both microwave and conventional regenerated cycles were measured and investigated. Duration of isobaric desorption process with microwave heating was achieved 98.2% shorter than that of conventional heating system.

**Keywords** Adsorption heat pump; microwave; regeneration; dielectric heating.

## 1. Introduction

Adsorption heat pumps (AHP) that have advantage of being environmentally friendly, provide heating and cooling effects by employing thermal energy sources such as solar and geothermal energies or waste heat of the industrial processes [1]. Although AHPs have high primary energy efficiency, in order to be competitive with conventional heat pumps, researchers should overcome some several important limitations and improve the coefficient of performance. One of the main drawbacks of AHPs is slow heat and mass transport in the adsorbent bed that usually results in low performance criteria. A survey of the literature revealed that the majority of the studies focused on eliminating the above mentioned problem. In these studies, although the thermal conductivity of the adsorbent was able to be improved by different methods, the performance of the adsorption heat pump could not be improved by using these new high thermal conductive adsorbents.

In recent years, dielectric heating systems, or microwave heating systems, have started to be used more frequent than conventional heating systems due to their various advantages, such as: having high heating rate, providing material selective, non-contact, precise and controllable heating, transferring energy rather than heat and providing compact equipment [2]. Kumja et al. [3] and Demir [4] investigated the effect of microwave regenerated adsorbent bed on performance of the adsorption heat pump numerically. A numerical analysis of heat and mass transfer in an adsorbent bed during an adsorption heat pump cycle was performed with both conventional and microwave

heating regeneration methods. The results revealed that the coefficient of performance (COP) of microwave driven cycle was higher than that of conventional one.

The main obstacle for microwave assisted AHP is philosophy of background of adsorption heat pumps in which the adsorption heat pump utilizes thermal energy sources such as solar and geothermal energies or waste heat of the industrial processes. However, it should be kept in mind that the adsorption heat pumps can be used for thermal storage [5]. The microwave assisted adsorption heat pump can use electricity during night time and cool or heat the surrounding throughout day time. Moreover, electricity required for the operation of microwave in the system can be supplied by renewable energy resources such as solar energy with photovoltaic.

The aim of present study was to investigate the effect of microwave and conventional heating systems on the performance criteria of a silica gel-water heat pump experimentally. For this purpose, temperature distributions in the bed for both microwave and conventional heating systems were investigated. Temperature and pressure variations in the intermittent AHP were monitored during the performed cycles.

## 2. Experimental and Method

### 2.1 Experimental Setup

The used adsorbent was Silica gel Rubin with moisture indicator supplied from Sigma Aldrich Chemical Ltd. The equivalent diameter of adsorbent bead varies between 1 and

3 mm. The water adsorption capacity of silica gel is given as 20%.

The designed single bed adsorption heat pump was mainly composed of an adsorbent bed, an evaporator, and a condenser. The main components of adsorption heat pump are shown in Fig.1a. The level of water was viewed and measured from the sight glasses mounted in the casing of evaporator. The evaporator was heated by using water circulated in the heat exchanger inside the evaporator which has  $0.23\text{m}^2$  heat transfer area. The condenser was constructed as shell and tube heat exchanger. The heat transfer area of condenser was  $0.22\text{m}^2$ . The vacuum tight valves were located between the evaporator, condenser and adsorbent to complete intermittent cycle. The valves (V3 and V4) between evaporator and condenser can play the same role of expansion valve if it is carefully opened and closed.

The two adsorbent beds were constructed. One of them was constructed of Pyrex glass and appropriate for the microwave application. The other one also was constructed of Pyrex glass and it has jacket in order to supply heat to the bed with circulating hot water inside the jacket. The heights of the two adsorbent beds were 23 cm. The radii of gap and bed were 10.2 and 2.7 cm, respectively. For microwave application, the adsorbent bed was cooled by four small fans throughout the isosteric cooling and isobaric adsorption processes. Microwave oven was specially designed to have the ability of providing homogeneous temperature distribution in the adsorbent bed. For this purpose, three magnetrons (M1, M2 and M3) were placed with  $120^\circ$  angle to each other as shown in Fig.1b.

Temperature distribution in the adsorbent beds was measured by 5 thermocouples as shown in Fig.1b.

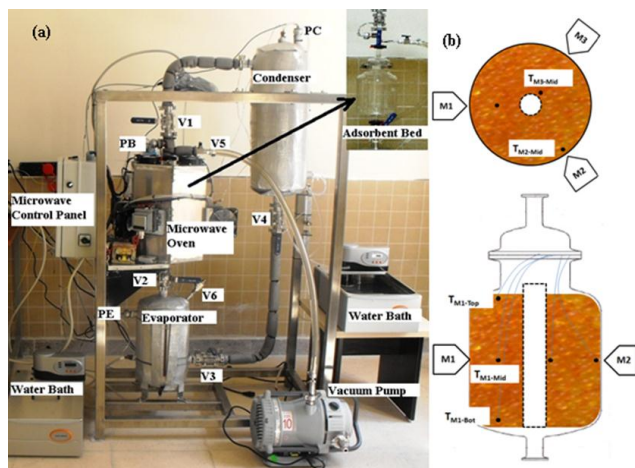


**Fig.1a.** Photograph of the designed intermittent adsorption heat pump, **b.** Location of thermocouples in the adsorbent bed.

Five of the thermocouples were placed across magnetrons for observation temperature distribution in the adsorbent bed. Two of the thermocouples were placed at bottom and top of the adsorbent bed. Three pressure transducers were used for measuring pressure of units. All thermocouples and data logger were calibrated by Fluke 714

temperature calibrator which has  $0.8^\circ\text{C}$  measuring accuracy. The pressure transducers with  $\pm 0.25\%$  accuracy were located at the evaporator, condenser and adsorbent bed. The temperature and pressure were measured by sensors and acquired by using a data logger card and software. The data were transferred to a computer and automatically saved.

Figure 2 presents the microwave oven schematically. Microwave oven consists of three main parts. In the first part, microwave cavity surrounds the adsorbent bed for heating purpose. In the second part, there are three magnetrons (M1, M2 and M3) placed on the hexagonal wall to provide  $120^\circ$  angle to each other as shown in Fig.1b with the aim of providing homogeneous temperature distribution in the adsorbent bed without rotating the bed itself. The power of each magnetron is 1 kW and its working efficiency is around 85%. Frequency is 2450 MHz. Third part is control panel which allows to adjust active/inactive time of magnetrons and total operation time of microwave. The magnetrons do not operate at the same time for safety precaution, hence they work sequentially. At the top of microwave cavity, four small fans are placed for supplying cooling during isobaric adsorption and isosteric cooling processes of cycle.

## 2.2 Experimental Procedure

The adsorbent bed was filled with 4kg of silica gel. The evaporator was filled with 10 L of distilled water. The adsorbent bed was vacuumed while being heated by microwave oven for removing the moisture of silica gel. The silica gel was dried for an hour. After the drying process, system pressure was adjusted and all valves were closed.

The isobaric adsorption process (d-a): For starting the cycle, the valve (V2 as shown in Fig.1a between evaporator and adsorbent bed was slightly opened and evaporation of water was started. The temperature of adsorbent bed increased during the adsorption process; however, the heat of adsorption was removed by four fans which were located at the top of microwave cavity. The isobaric adsorption process was continued until the saturation of silica gel. During the experiment, temperature and pressure of AHP were monitored. The end of isobaric adsorption process was decided according to bed temperature, pressure and the water level of evaporator observing from sight glass.

The isosteric heating process (a-b): After a complete adsorption process, the valve (V2) was closed and adsorbent bed was heated by microwave for 3-4 min for the isosteric heating process. For conventional heating system, hot water was circulated inside jacket of the glass adsorbent bed.

The isobaric desorption process (b-c): When the pressure of the adsorbent bed attained to the desired condenser pressure, the valve (V1) was opened for the isobaric desorption process while the heating of adsorbent bed was continued.

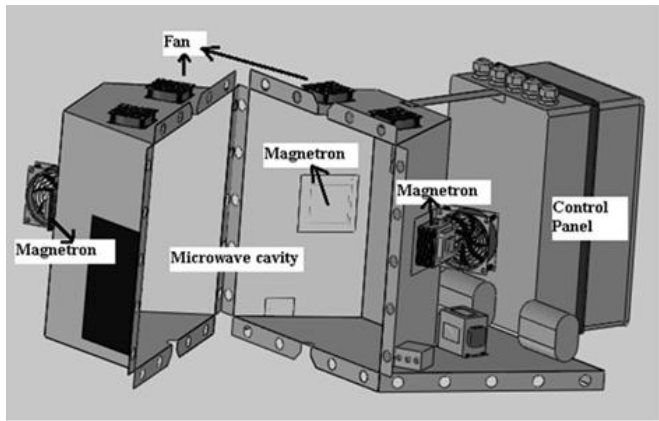


Fig. 2. Schematically illustration of microwave oven

Heating of adsorbent bed during isosteric heating and isobaric desorption processes was supplied by microwave. Each magnetron (M1, M2 and M3) operates for 30s sequentially with 15s break time. Total operation time of microwave can also be adjusted on the control panel. Four different total operation times (20, 25, 30 and 35 min) were investigated for the isobaric desorption process in this study. Electricity consumption was measured by using digital electric meters. For conventional heating system, hot water (85°C) was circulated inside jacket of the glass adsorbent bed.

The isosteric cooling process (c-d): Once isobaric desorption was completed, the isosteric cooling process was started with closing valve (V1) and adsorbent bed was cooled by four small fans. After reducing adsorbent bed pressure to the evaporator pressure, the isobaric adsorption process was performed by opening the valve (V2). The condensed water inside the condenser was transferred to evaporator with opening valves V3 and V4 slightly without change in pressures of units. Hence, the cycle of intermittent adsorption heat pump was completed. The same procedure was repeated for conventionally regenerated cycles and next cycles.

3. Results and Discussions

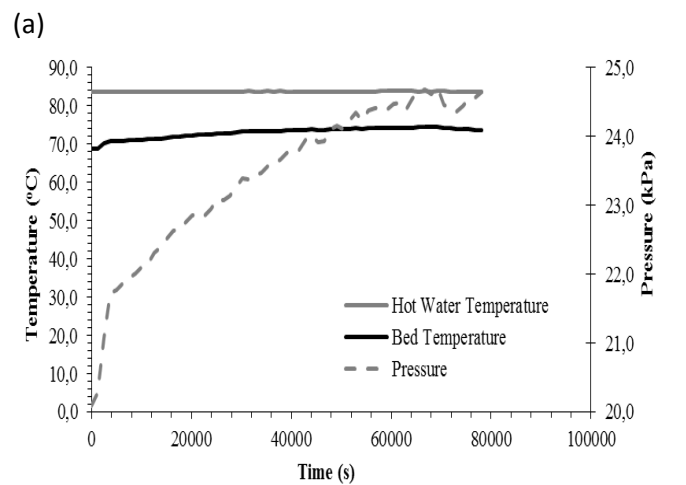
Figure 3 represents the pressure and average temperature of adsorbent bed during desorption processes for conventional and microwave heating systems. In conventional heating system, hot water (85°C) was circulated inside the jacket of adsorbent bed. In Figure 3a, temperature difference between hot water and adsorbent was easily observed. The pressure of adsorbent bed gradually increased and reached 25 kPa at the end of desorption period. Duration of desorption process for conventional heating system was 22.2 h. Poor thermal conductivity of adsorbent bed affected on duration of desorption process. Figure 3b illustrates the adsorbent bed pressure and temperature in the front of magnetrons during desorption process. The adsorbent bed pressure for the case of microwave heating increased gradually and reached 25 kPa as in the case of conventional heating. Three temperature profiles across the magnetrons were very close to each other. This reveals that the magnetrons operate with the similar performances by providing homogenous temperature on adsorbent bed. The zigzag behavior of temperatures indicates active periods of magnetrons. The each magnetron operates for 30 s and break

for 15s sequentially. The duration of desorption process for microwave heating was 0.4 h (26.7 min).

Comparison of desorption periods of conventional and microwave heating systems reveal that desorption of water molecules from adsorbents with microwave heating were faster and easier. The poor thermal conductivity of the adsorbent bed affected on the periods of the desorption process through slow heat and mass transfer. The reason of fast desorption process with microwave is that microwave transferred only energy but not heat. Microwave creates heat in the adsorbent bed by vibrating the water molecules. Thus, this fact clears the questions on that matter and it can be concluded that poor thermal conductivity of adsorbent bed did not influence the periods of desorption process. The long periods of cooling and adsorption processes influenced the performance of AHP which will be discussed in detail below. The bed pressures for both cases reached 25kPa. Insufficient condenser capacity caused to increase the desorption pressure of bed even in conventional heating case which was observed slow heat and mass transfer in the bed.

In Figure 4 the variation of adsorbent bed temperature was illustrated along the bed across the first magnetron. Figure reveals that there is no significant temperature fluctuation through the longitudinal of bed.

The variations of bed pressure and average temperature during the whole cycles for conventionally regenerated bed and microwave regenerated bed were presented in Fig.5. Long desorption period (b-c) for conventionally regenerated adsorption heat pump was easily observed in Fig.5. In microwave heating case, the isosteric heating period (a-b) cannot be observed in Fig.5b because of being too short. The limitation of adsorbent bed was overcome with microwave technique in isosteric heating (a-b) and isobaric desorption processes (b-c). However, effect of the poor thermal conductivity of adsorbent was observed in isosteric cooling (c-d) and isobaric adsorption (d-a) processes for both cases. The microwave technique only reduced the periods of heating processes. The total duration of cycle with microwave heating still needs further improvements.



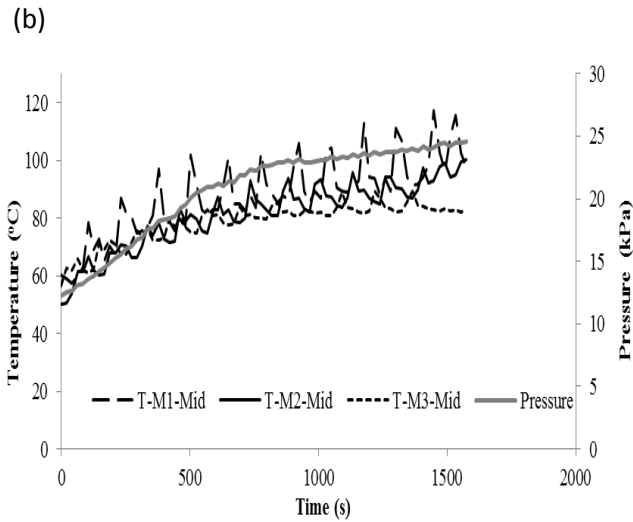


**Fig. 3.** Adsorbent bed temperature and pressure during isobaric desorption process for a) Conventional heating system b) Microwave heating system

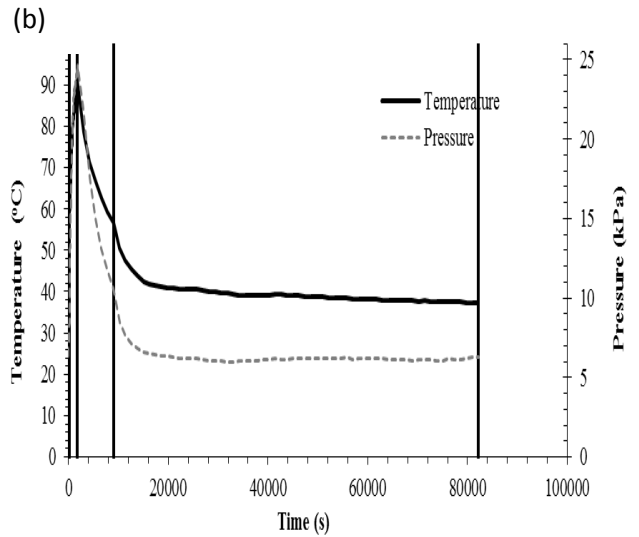


**Fig.5.** Variations of bed temperature and pressure during all cycle process for a) Conventional heating b) Microwave heating

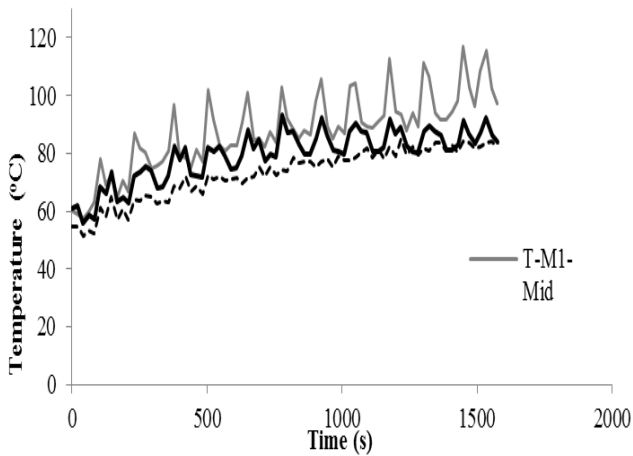
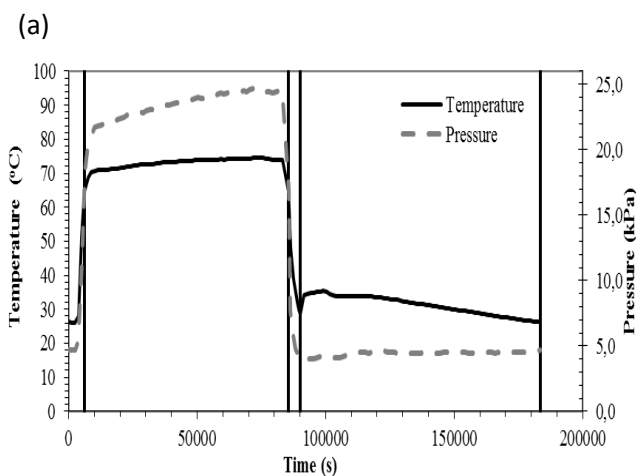


**Fig.4.** Variation of temperature along the adsorbent bed across the magnetron 1.



**4. Conclusions**

The microwave regenerated and conventionally regenerated adsorption heat pumps successfully manufactured and operated to have complete cycles. Following conclusions can be made:

- The cycles were obtained experimentally with microwave regeneration without any problem such as electrical arc, overheating of adsorbent, vacuum leakage etc.
- The designed microwave provided homogenous temperature distribution in the adsorbent bed.
- Heat transfer resistance in adsorbent bed was overcome by microwave heating during heating processes.
- Microwave technique is powerful over conventional heating system since the duration of desorption process with microwave system was 98.2% faster than that of conventional heating system.
- The duration of adsorption processes should be improved in order to reduce the total cycle time.

**Acknowledgements**

The author would like to acknowledge TUBITAK for supporting this study (project no: 110M497) financially.

**References**

[1] H. Demir, M. Mobedi, S. Ulku, “A review on adsorption heat pump: problems and solutions”,

*Renew. Sustain. Energy Rev*, Vol. 12, pp. 2381–2403, 2008.

- [2] K.E. Haque, “Microwave energy for mineral treatment processes: a brief review”, *Int. J. Miner. Process.* Vol. 57, pp. 1-24, 1999.
- [3] M. Kumja, C.K. Ng, C. Yap, H. Yanaghi, S. Koyama, B.B. Saha, A.Chakraborty, “Modeling of a novel desorption cycle by dielectric heating”, *Mod. Physic. Lett. B*, Vol. 23, pp. 425-428, 2009.
- [4] H. Demir, “The effect of microwave regenerated adsorbent bed on the performance of an adsorption heat pump”, *Appl. Therm. Eng.* Vol. 50, pp. 134-142, 2013.
- [5] G. Alefeld, P. Maier-Laxhuber, M. Rothmeyer, “Zeolite heat pump and zeolite heat transformer for load management”, In: *Proc. of solid sorption refrigeration symposium*, Paris, pp. 855-860, November 1992.

# CAE Model Correlation & Design Optimization of a Laminated Steel Oil Pan by means of Acceleration and Strain Measurement on a Fired Engine

Rifat K. Yanarocak\*<sup>‡</sup>, Abdulkadir Çekiç \*\*

\*Ford Otomotiv San. A.S., Department of Design Verification & Test, Design Verification & Test Engineer, Akpınar Mah., Hasan Basri Cad, No: 2, PK: 34885 Sancaktepe/ ISTANBUL/TURKEY

\*\* Ford Otomotiv San. A.S., Department of Powertrain CAE, Structural Analysis Engineer, Akpınar Mah., Hasan Basri Cad, No: 2, PK: 34885 Sancaktepe/ ISTANBUL/TURKEY

ryanaroc@ford.com, acekic1@ford.com

<sup>‡</sup>Corresponding Author: Rifat K. YANAROCAK, Akpınar Mah., Hasan Basri Cad, No: 2, PK: 34885 Sancaktepe/ ISTANBUL/TURKEY, Tel: +90 216 664 9305, Fax: +90 216 664 9305, ryanaroc@ford.com

*Received: 16.01.2015 Accepted: 06.03.2015*

**Abstract-** In this paper, a simultaneous design and development work for a diesel engine oil pan is presented. The interesting point making the design of the oil pan so special is its laminated steel material. Beside its material, due to the deep-drawing production method, to determine the natural frequencies of the structure with Computer Aided Engineering (CAE) methodology is a problem for the design engineer. Especially when the highly nonlinear character of the oil pan and regions at different thicknesses sum up with the hardness of liquid modelling, free vibration modal analysis of the design at virtual environment becomes extremely challenging. Therefore, instead of refining the material characteristics in virtual design, first a primary 3D dummy design is generated. Afterwards, a production method and material intent sample is produced with soft tool. Hammer test is applied on this sample filled with oil, therefore modal shapes and frequencies are gained. As a result, CAE modal analysis is generated and correlated by hammer test results; hence the first challenge of modelling the liquid is overcome. Then, critical stress locations are determined with the CAE durability analysis. After instrumenting the pan with optimum number of accelerometers and strain-gages from these critical locations, a durability test on a fired engine is run. With the measurements here, the CAE durability analysis is refined so the second challenge of material nonlinearity and thinning due to the deep-drawing method is also overcome. Lastly, with the CAE durability simulation, a secondary 3D design proposal is established. Normally the method reach to success here, but to validate it, a secondary sample is produced, instrumented again with accelerometers & gages and tested resulting in significant improvement in terms of durability. With this approach, a method to perform a fail-safe oil pan design in single loop is verified.

**Keywords** Oil pan, laminated steel, deep drawing, CAE durability analysis, advanced instrumentation.

## 1. Introduction

Oil pan is a reservoir usually located at the base of the engine cylinder block enclosing the crankcase. It is manufactured from number of different materials like cast aluminium, stamped mild steel, laminated steels and various plastics & synthetic fibers. [3] Besides transferring lube oil heat to atmosphere, oil pans, can also act as a sort of boom box and amplify engine noise, so they are usually designed to

minimize noise and vibration. [4] The effectiveness of these roles obviously has a lot to do with determination of the right material from which the oil pan is manufactured. As a result in the new generation diesel engines, due to its effective noise reducing and durability improving properties laminated steel is used commonly.

Beside its material, the production method of the oil pan is also an important aspect determining its durability. At this point, the deep drawn part manufacturing technology which

offers a number of benefits over other manufacturing processes is used. It enables the design engineer to produce large, seamless parts with complex axi-symmetric geometries in rapid cycle times and reduce technical labour. [8] But despite of all these advantages, the laminated MPM (metal-plastic-metal) material, combined with the nonhomogeneous thickness problem due to deep drawing, cause the oil pan to show highly nonlinear character during free vibration modal analysis at virtual environment. [6] Especially modelling the unstable liquid inside the pan, determining the damping ratios and gaining modal shapes and frequencies of the structure only with virtual environment is extremely challenging for the design engineer.

Due to all these challenges, instead of trying to refine the material characteristics, optimize the model and create different design recommendations in virtual design, a simultaneous design and development study that would integrate experimental measurements with the CAE durability analysis would be more realistic, accurate and less time consuming. Using this methodology it is also possible to develop a fail-safe oil pan design in single loop.

**2. Experiment**

*2.1. Testing Methodology*

For the simultaneous design & development and optimization study of the oil pan first of all a methodology consists of a fail-safe single loop is generated. The detailed steps of this methodology are listed at Table 1.

Hammer test is applied on this sample filled with oil, therefore modal shapes and frequencies are gained. As a result, CAE modal analysis is generated and correlated by hammer test results. Hence, the first challenge of modelling the liquid is overcome. In Figure 1, the application of the hammer test can be observed. Also, similar CAE model and hammer test frequency results comparison at four different modes are given.

**Table 1.** Single Loop Design Methodology

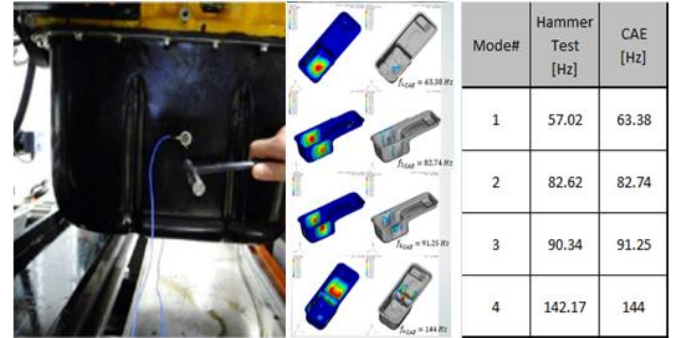
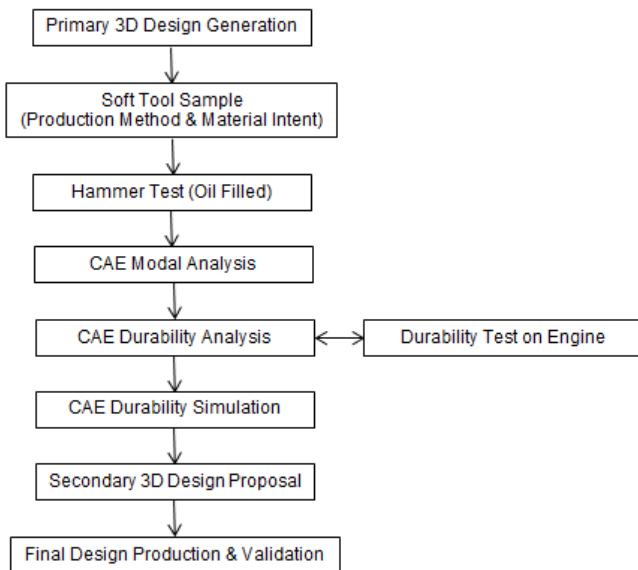


**Fig. 1.** Hammer Test on Oil Pan

Then, critical stress locations, magnitudes, and directions are determined with the CAE durability analysis. This is both important in terms of determining the number and type of the measurement devices. After instrumenting the oil pan with optimum number of accelerometers and strain-gages from these critical locations, a durability test on a fired engine is run. The importance of this test is the engine's being tested until failure, so it is possible to observe and compare the critical stress locations with the model.

Just before the durability test the engine was tested with two different combinations of oil filling amount which has a direct effect to the natural frequency of the oil pan. During this test a power curve is taken at full load to obtain the acceleration values on the oil pan at every 100 rpm increments. Additionally a speed sweep is performed to get strain values at high frequency between the boundary speed limits of the engine. Therefore, this helps the design engineer to determine and compare the critical stress locations on the oil pan with the frequency response analysis by using finite element analysis methods and correlate the dynamic properties of the model accordingly. Another achievement is to eliminate the effect of the level of oil to a possible damage or failure mode on the oil pan. With the measurements here, the CAE durability analysis is refined so the second challenge of material nonlinearity and thinning due to the deep-drawing method is also overcome.

Lastly, with the CAE durability simulation and model refinement, a secondary more robust 3D design proposal is established. A secondary sample is produced, instrumented again with accelerometers & gages. The tests are repeated again from the most critical stress points and significant improvement is gained in terms of vibration characteristics. Also, critical stress locations are moved from side walls of the oil pan to the very bottom of the oil pan side walls with much lower magnitudes and are unlikely to damage the sump. As a result, this methodology is validated.

*2.2. Test Sample Preparation*

Experiments were performed on the oil pan of a diesel engine. In Figure 2 a similar oil pan design is shown.



**Fig. 2.** Similar Oil Pan Design

Four pieces of tri-axial accelerometers and four pieces of rectangular rosette type strain-gages are instrumented very near to the critical stress regions on the left, right, front and bottom of the oil pan. Also four pieces of tri-axial accelerometers are instrumented on the right, front, front-left and rear-left of the block to separate the vibration characteristics of the oil pan from the rest of the engine. In Figure 3 the accelerometer and strain gage instrumentation on the bottom of the oil pan can be observed.

The instrumentations are performed near to the critical stress locations on the oil pan where the vibration characteristics are more stable, therefore, a better CAE model correlation is aimed. Also, special care is applied for the sensors not to be damaged during the instrumentation of the oil pan to the engine. After all the instrumentation and oil filling operations, nulling is applied to the sensors so only the effect of vibration during engine operation is gained. In Figure 4 the exact strain gage and accelerometer locations are shown.



**Fig. 3.** Accelerometer & Strain-gage Instrumentation on the Oil Pan

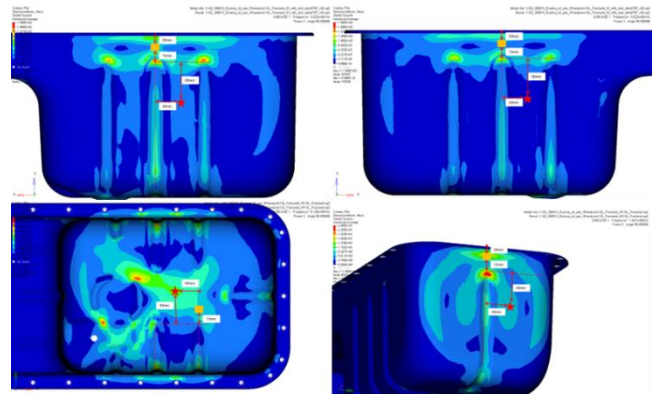


**Fig. 4.** Exact Accelerometer & Strain-gage Locations on the Oil Pan

**3. Experimental Results**

Acceleration data from 4 accelerometers at the block and 4 accelerometers at the oil pan is taken by 1 Hz increments with 100 rpm steps from 2100 rpm to 600 rpm at the power curve. The amplitude – phase and real – imaginary values are obtained for all X, Y and Z directions. In Figure 5 the test cycle is shown.

The data is observed until 600 Hz and 1800 rpm found to be most critical for 30L of oil filling according to the acceleration values at Y direction of oil pan where as for 50L of oil filling 1300 rpm found to be most critical reaching more than 2 times than the values gained in 30L of oil filling, again at Y direction of left side of oil pan.

Strain data from 4 strain gages at the oil pan is taken by 1Hz increments with 1 rpm steps from 600 rpm to 2100 rpm at the speed sweeps. First of all, to eliminate the effects of static and thermal loads a drift offset correction is applied from the data taken. In Figure 6 this successful drifting operation can be observed. The below blue curve shows corrected data.

All max. & min. principle strain & stress values and Von Mises stress values are obtained from the data for all 4 different strain gage locations. By taking the Young Modulus as 210000MPa and the Poisson ratio as 0,28 again the Y direction of left side of the oil pan found to be the most critical stress location. Max. principle stress value is found to be almost 6 times at 50L oil filling compared to 30L.

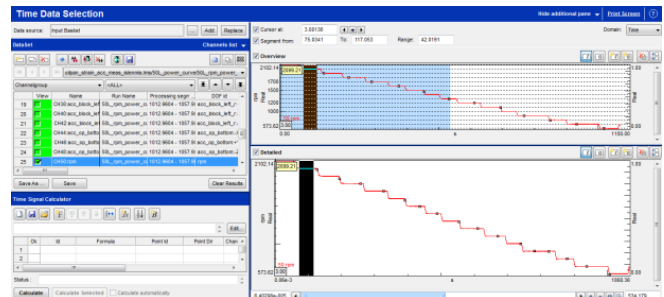


**Fig. 5.** Test Cycle & Determination of the Acceleration Values

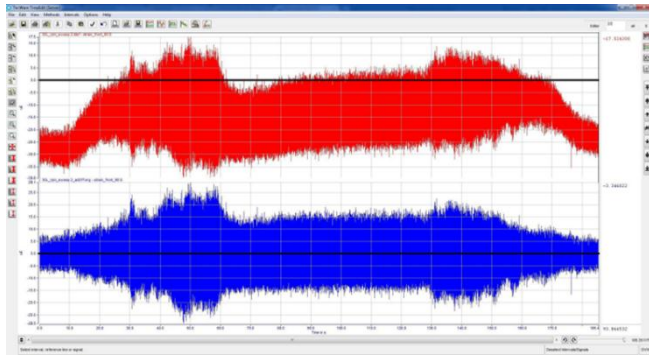


Fig. 6. Drift Offset Correction on the Strain Data

4. CAE Methodology

In this part, brief explanation of CAE model is given. Also, CAE correlation study by using test data is explained and analysis results are shown.

4.1. FEA Model

Oil pan is made of laminated steel and operates with oil inside of it. Difficult part of modelling the oil pan is to model a material which has two layers of steel and between two layers, there is a material that improve damping characteristic of oil pan.(Figure 7)

MSC NASTRAN is used to solve problem. Oil pan is modelled with 2D elements (CQUAD) and oil pan to engine block connection is modelled with bush elements (CBUSH). The effect of oil inside the oil pan is modelled by adding non-structural mass to 2D elements. [9] Figure 8 shows the mesh example of the oil pan.

RKU method, named after its developers Ross, Kerwin and Ungar, is the most commonly used method for characterizing the behaviour of three-layer damping treatments [1]. This method uses a fourth order differential equation for a uniform beam with the sandwich construction of the 3-layer laminate system represented as an equivalent complex stiffness. The advantages of this method are,

- No need to re-mesh if any thickness of layer in laminated steel is changed.
- It has faster run times.
- Only need to change PSHELL & MAT1 cards

By adding bending rigidity into MAT1 card in NASTRAN, material property is modelled.

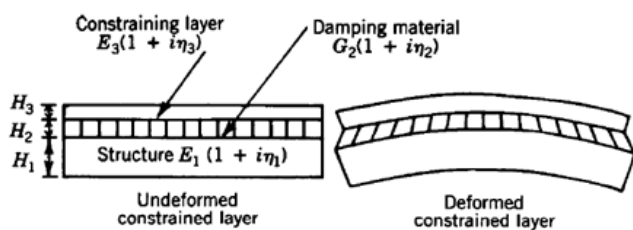


Fig. 7. Example of Laminated Steel

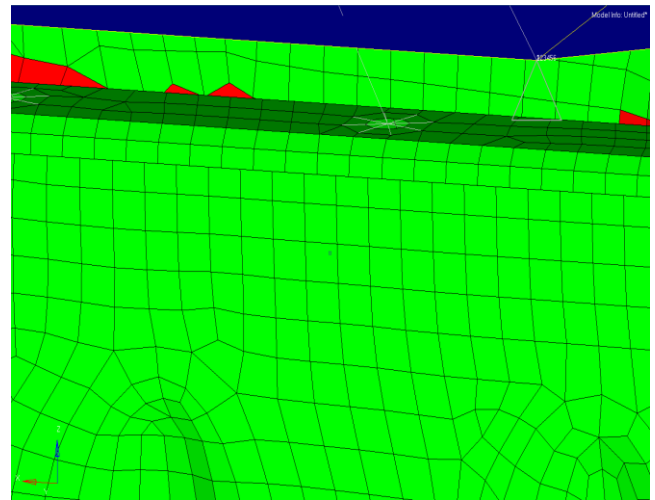


Fig. 8. Mesh Example of Oil Pan

4.2. FEA Correlation

Aim of the correlation is to optimize the design by using the test data. To achieve this, the main steps that are mentioned in Figure 9 are followed. Firstly, critical regions are defined and the test data is acquired with the help of finite element analysis results. To correlate material constants, modal test is required. Bending rigidity of material is optimized with the modal test as seen in Figure 1. With the correlated FEA model (natural frequencies are correlated only), structural damping and stiffness characterization of the connection elements can be modified in order to converge the test data.

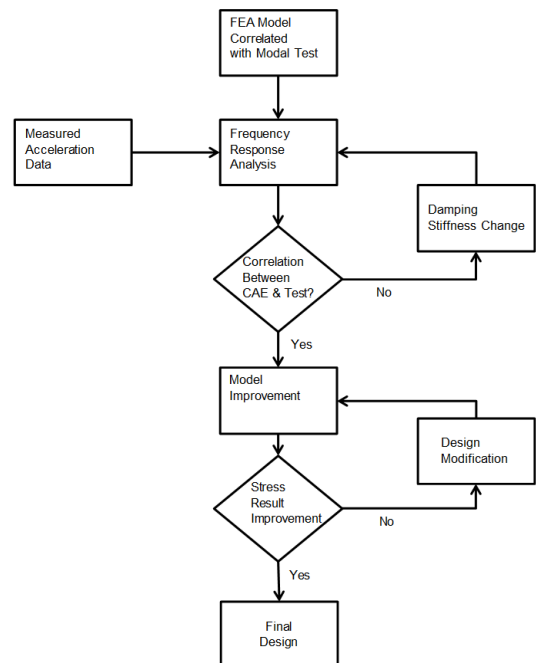


Fig. 9. Flowchart of Correlation Study

By doing fast fourier transformation (FFT) the experimental data is converted to frequency scale and this data is used to perform the frequency response analysis. In the correlation part, RPM range where acceleration response is higher with respect to other RPM values, should be chosen for the study. By changing property of bushing element, non-structural mass of oil and structural damping of laminated steel, best correlation is achieved. As shown in Figure 11 and Figure 12 the correlation between the experimental and CAE result is sustained.

The acceleration data from the block is the input part of the frequency response analysis. By using multiple excitation data, frequency response analysis of the oil pan is performed. In Figure 10, the example of this excitation data is given.

Correlation between accelerations on the oil pan and results of FEA analysis is crucial for the model optimization. The example of the correlated results is shown in Figure 11. Analysis revealed that at lower frequencies there is a good correlation between test data and analysis results. However, correlation is deteriorating because of the sloshing of the oil at higher frequencies. Other important item is stress correlation. RKU model is generally used for the dynamic analysis and stress results are not credible. To assure the stress results, also strain-gages are implemented on oil pan. Von-Misses stress results in Figure 12 which is derived from strain gage test data, show that RKU method gives rational stress results. After correlating FEA model, alternative geometry designs of the oil pan are studied for the optimization. Final design which satisfies the design target is achieved at the end of analysis loops. As a result all the steps mentioned in Figure 9 are completed.

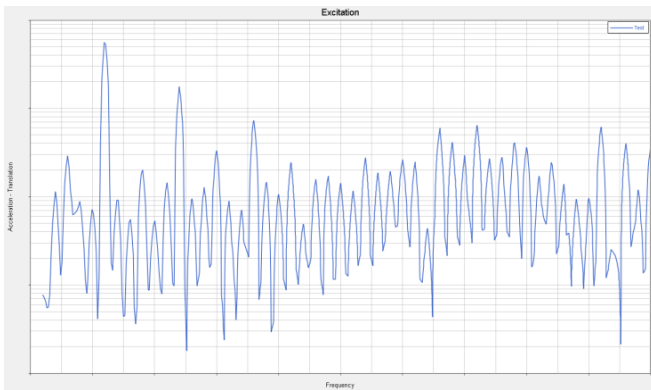


Fig. 10. Example of Excitation

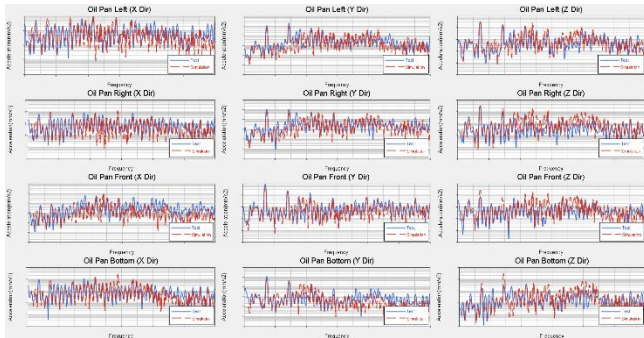


Fig. 11. Correlation Result and Test Result Comparison

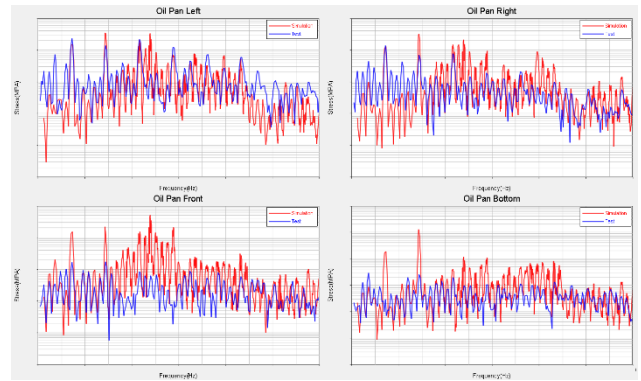


Fig. 12. Von Mises Stress Comparison (CAE Result vs Test Result)

4.3. FEA Results

At the end of study, it is observed that there is a good correlation at the side panels. However, at the bottom of the panel, correlation is not as good as side panels. This is the result of the higher fluid pressure at the bottom panel which is not simulated by adding non-structural mass. This situation is not critical since maximum Von-Misses stress is observed on the side panels. Also at the higher frequencies, correlation is becoming deteriorating because of the sloshing. However, maximum stress is not observed at higher frequencies which are seen both in the analysis result and the test data. As a result, the critical stress location at the first design is moved to the lower part of the side panel and magnitude of Von-Misses stress is decreased to 55% of the first design which is shown in Figure 13.

Acceleration value comparison for the primary and secondary design with 30L and 50L oil filling configurations is given in Figure 14. It can be clearly observed that 50L oil filling is more than 2 times critical than 30L. Also with the secondary oil pan design almost 60% of improvement is gained at both oil filling configurations.

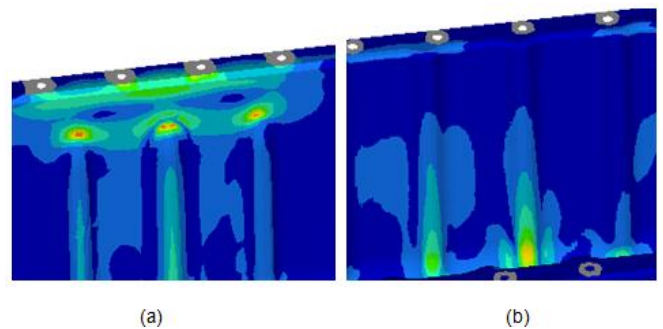
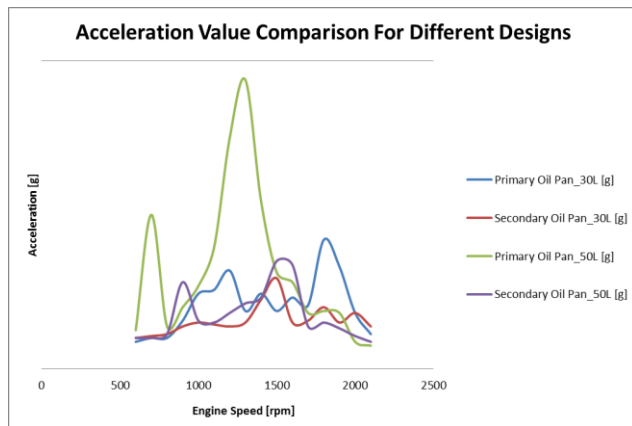


Fig. 13. Von-Mises Stress Location Preliminary Design (a) & Final Design (b)



**Fig. 14.** Acceleration Value Comparison for Different Designs & Oil Filling Configurations

## 5. Conclusion

In today's competitive production market using the right methodology and manufacturing, a fail-safe design at first trial is an important aspect that the research and development companies aim. But due to real life's unpredictable conditions, obtaining this fail-safe design is not always possible in virtual environment, especially on engines and engine components, manufactured with today's complex production methods and working as a thermomechanical end product. Therefore, simultaneous design and development works, integrating CAE analysis with experimental measurement techniques is used more effectively resulting with a single loop design. In this paper, the main steps and advantages of this kind of an approach is explained on a diesel engine oil pan.

First, a primary 3D dummy design is generated and a production method and material intent sample is produced accordingly. Using the modal shape and frequency data gained from the hammer test with the oil filled sump, CAE modal analysis is generated and the first challenge of modelling the liquid is overcome.

Secondly, from the predetermined critical stress locations obtained from CAE durability analysis, the block is instrumented with four accelerometers and the oil pan is instrumented with 4 strain gages and 4 accelerometers. Two configurations of oil filling, 30L and 50L, are tested. With the refined CAE durability analysis, the second challenge of material nonlinearity and thinning is also overcome. According to the acceleration data the 50L oil filling found more than 2 times critical compared to 30L. Also in terms of max. principle stress, 50L oil filling found almost 6 times critical compared to 30L especially at the side panels of the oil pan.

Lastly, with the CAE durability simulation, a secondary 3D design proposal is established, a sample is produced, instrumented again with accelerometers & gages and tested. Almost 55% improvement is gained in terms of Von Misses stresses and the critical stress locations at the first design is moved to the lower part of the side panel with much lower magnitudes. Hence, a method to perform a fail-safe oil pan design in single loop is verified.

## Acknowledgements

The authors are indebted to the Ford Otosan Gölcük Engine Dynamometer Laboratory for the support required to complete project. Special thanks are given to Dr. Serdar AKCA for his support and encouragement throughout this project.

## References

- [1] Anab Akanda, Gregory M. Goetchius, "Representation of Constrained/Unconstrained Layer Damping Treatments in FEA/SEA Vehicle System Models: A Simplified Approach", SAE, 1999.
- [2] Peter Andren, Tommy Falk, Juha Plunt "Analytical and Finite Element Design of Structural Damping using a Parametric Formulation for the Damping Material Properties", Internoise, 1999.
- [3] Sean Bennett, "Modern Diesel Technology: Diesel Engines 2nd Edition", 2014.
- [4] Sean Bennett "Medium/Heavy Duty Truck Engines, Fuel & Computerized Management Systems, 4th Edition", 2013.
- [5] Barry Kluczyk, "High-Performance New Hemi Builder's Guide: 2003-Present", SA Design, 2007.
- [6] Sean Bennett, "Modern Diesel Technology: Light Duty Diesels", 2012.
- [7] "Heat Treating, Including Steel Heat Treating In the New Millennium: An International Symposium in Honor of Professor George Krauss", Sandra J. Midea, George D Pfaffmann, ASM International, 2000.
- [8] "Deep Drawing: Benefits and Industrial Applications", <http://www.thomasnet.com/articles/custom-manufacturing-fabricating/deep-drawing>.
- [9] MSC Nastran User Manual.

# A Comparative Study of on and off Grid Tied Integrated Diesel Solar PV Generation System

Kenneth E. Okedu\*‡, Roland Uhunmwangho\*‡ and Ngang Bassey Ngang\*‡

\* Department of Electrical Engineering, College of Engineering, University of Port Harcourt, Nigeria

kenokedu@yahoo.com, tripodeng@yahoo.com, nbngang@yahoo.com

‡ Corresponding Author; Kenneth E. Okedu, Roland Uhunmwangho, Ngang Bassey Ngang, Department of Electrical Engineering, College of Engineering, University of Port Harcourt, Nigeria

kenokedu@yahoo.com, tripodeng@yahoo.com, nbngang@yahoo.com

*Received: 08.02.2015 Accepted:14.03.2015*

**Abstract-** This paper presents a proposed hybrid system based on diesel generator and solar photovoltaic (PV) as an effective option to power a small remote community. The cost of running diesel generator speedily due to erratic power supply in a small remote community that is not grid connected is highly expensive and not environmentally friendly. A solar PV was used to reduce or augment the continuous diesel generator sets, resulting in reduced cost of operation and maintenance. A proper solar radiation data and sizing based on the specification of the PV system and battery bank was done. In addition, a comparative study was carried out considering two scenarios of the proposed model system. In the first scenario, the diesel generation, solar PV system was treated as autonomous (or standalone). In the second scenario, the proposed model system was connected to the grid system. It is discovered that powering the small remote community with the proposed hybrid system is much more beneficial and encourages competition with other conventional energy sources, because it minimizes both operating costs and pollutants emissions. Furthermore, analysis results obtain from HOMER software shows that is promising to implement the on-grid system.

**Keywords-** Renewable Energy; HOMER; Grid system; Solar PV; Efficiency; Battery

## 1. Introduction

The importance of energy system cannot be overemphasized in modern life style. Most often, there is epileptic power supply to maintain the population and economic growth of developing countries. Also diesel generators are the most used type of power generation in these countries, thus, it is imperative to augment the expensive diesel generation of power with renewable energy. Solar energy is one of the most promising of the renewable energy sources in light of unlimited potential energy. The sun's energy radiation is at a rated value of  $3.8 \times 10^{23}$  kW per second [1-4], and a square meter of the platform of the earth can receive up to 1kW of solar power. However, radiation intensity from solar energy is weak compared with the high energy concentration volume of diesel fossil fuel power supply. One of the most common methods of achieving solar PV radiation to power supply is the use of silicon solar cells made in modules that are connected in a base plate electrically [3, 4, 5, 6].

On the other hand, the cost of fossil fuel based electricity generation in the long term is increasing and the costs of production of renewable energy technologies decreasing due to optimized construction and efficiency improvement.

Reliability and costs are two different important aspects that must be taken into account when working with standalone-hybrid system for electricity generation. Recently studies shows that, the hybrid standalone system are better in terms of reliability and cost than single source of energy supply [7, 8 and 9]. Due to optimized construction and efficiency improvement, renewable electrical systems in off grid application are economically viable, especially in remote areas [10-13].

In light of the above, this work is proposing a solar photo voltaic (PV) renewable energy integration to an existing expensive constant speed diesel generation powering a small remote community. This will not only help reduce the cost of running the present expensive diesel generation system, but also provide reliability of power supply to the remote community with little or no emission of carbon or other contents, hence improving the greenhouse effect. Furthermore, an analysis of connecting the diesel PV-battery integrated system in a grid was compared with an off grid system. The hybrid optimization model for electric renewable (HOMER) software environment was used in carryout this study.

**2. Description of the Model Systems**

Figures 1-3 respectively show the model systems of this work. In Fig. 1, the diesel fueled generator of size 50kW was used to power the small remote community alone and in Fig. 2, the solar PV of size 50kW connected to the dc busbar was introduced and the size of the diesel generator was reduced to 30kW. Fig. 3 shows that the diesel generator, solar PV battery system was connected to the grid. All systems were used to power the small remote community whose load profile is shown in Fig. 4 with 265kWh/day and 41kW peak.

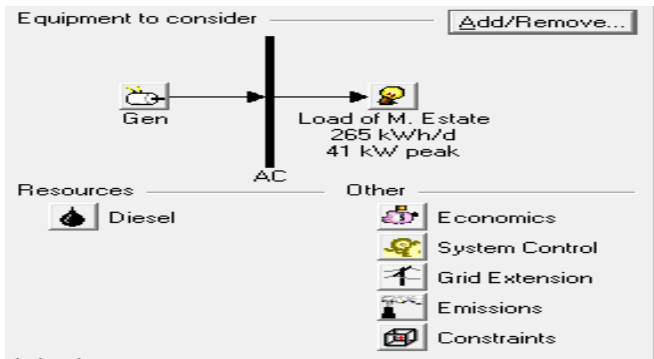


**Fig. 1.** Model System with only Diesel Generator

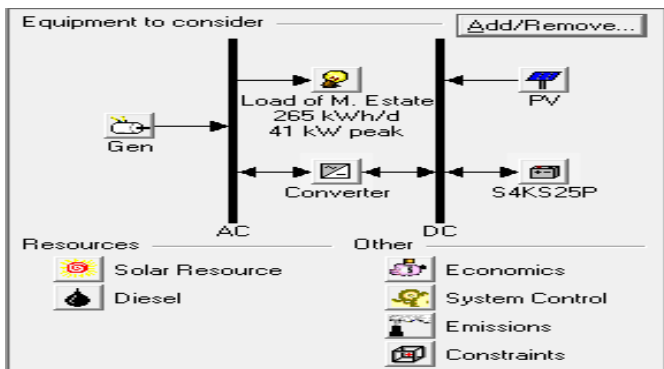


**Fig. 2.** Model System with Diesel Generator and solar PV

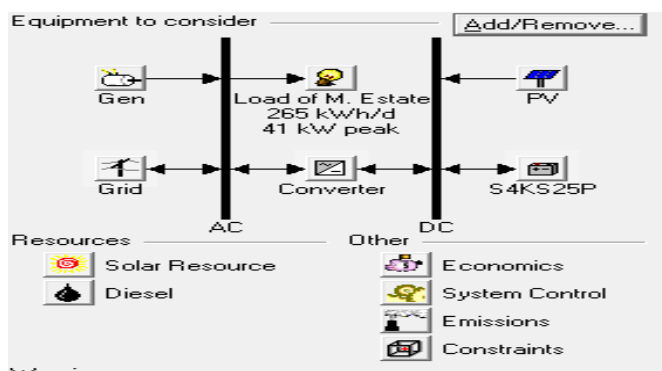


**Fig. 3** Model System with Diesel and solar PV Connected to Grid

The combined output power of diesel generation and PV solar system is slightly higher than the demand in the small remote community load profile to accommodate expansion as more buildings may spring up. Details of the parameters

of the various components used in the model system are shown in Appendix of this work.

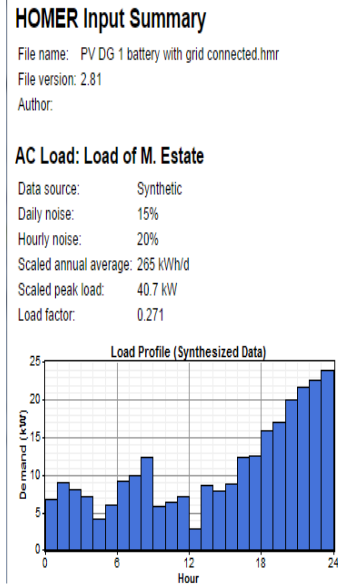


**Fig. 4.** Load Profile of the Small Remote Community

*2.1 The Solar System*

The power produced from the solar PV renewable energy source is dc, from the panels which then goes through a grid interactive inverter, thereby converting the dc into ac used by housing utilities in the small remote community. In scenarios where more power or electricity is produced than the small remote community needs; the excess is fed into the grid system as shown in Fig.3. However, during times of low solar radiation with low generation from the solar PV to augment the supply from the diesel generator to the community demand, the small remote community would take power from the grid. Thus, the grid interactive system eliminates the need for a battery backup during low PV output [14, 15], making the grid serves as a battery.

The power generated by the solar PV panels is given by [16-18]:

$$P_{PV-out} = P_{N-PV} X (G/G_{ref}) X [1 + K_T (T_c - T_{ref})] \quad (1)$$

Where  $P_{pv-out}$  is the output power generated from the PV panel,  $P_{N-pv}$  is the PV rated power at reference conditions,  $G$  is solar radiation ( $W/m^2$ ),  $G_{ref}$  is solar radiation at reference conditions ( $G_{ref} = 1000 W/m^2$ ),  $T_{ref}$  is the cell temperature at reference conditions ( $T_{ref} = 25^{\circ}C$ ),  $K_T$  is temperature coefficient of the PV panel ( $K_T = -3.7 \times 10^{-3} (1/^{\circ}C)$ ) for mono and poly crystalline silicon. The cell temperature  $T_c$  is such that:

$$T_c = T_{amb} + (0.0256 X G) \quad (2)$$

Where  $T_{amb}$  is the ambient temperature in °C. The rated power  $P_{R-PV}$  can be calculated using equation 3 as:

$$P_{R-PV} = (E_L \times SF) / (\eta_R \times \eta_V \times PSH) \quad (3)$$

Where  $E_L$  is daily load energy, SF is stacking factor considered to compensate for resistive and PV temperature losses,  $\eta_R$ ,  $\eta_V$ , are efficiencies of solar charging regulator and bidirectional inverter respectively and PSH is the peak sun shine hours which is numerically equal to the daily average of solar radiation at the specified location.

### 2.2 Battery System

The battery considered in the model systems of this work are rated by the amount of current produced over a period of hours (in Ah). The storage capacity of the battery ( $C_{wh}$ ) is calculated using equation 4 [19];

$$C_{wh} = E_L \times AD / (\eta_V \times \eta_B \times DOD) \quad (4)$$

Where DOD is allowable depth of discharge of the battery, AD is number of autonomy days, and  $\eta_B$  is battery efficiency.

### 2.3 Diesel Generator System

The rated power of the generator and the actual power output affects the fuel consumption of the diesel generator. The fuel consumption of the diesel generator ( $FC_G$ ) in (1/h) is given by equation 5.

$$FC_G = A_G \times P_G + B_G \times P_{R-G} \quad (5)$$

Where  $P_G$ ,  $P_{R-G}$  are the output power and the rated power of the generator in kW respectively.  $A_G$  and  $B_G$  are the coefficients of the consumption curve in (1/kWh), where  $A_G = 0.246$  1/kWh and  $B_G = 0.08145$  for the diesel generation [16, 17].

## 3. Optimal Design of the PV System Components

### PV Solar Array Sizing

The optimal design of the PV solar array sizing, battery sizing, charge controller sizing and inverter sizing can be found in the literature [20].

### 4. Results of Simulations using HOMER Software

The following are the results obtained using the HOMER software in the course of the study. Simulations were run for three different scenarios using the different model system discussed in section 2 of this paper. The results obtained in the three scenarios are discussed in three different sections. The simulation results using model system in Fig .1 for only diesel fuelled generator off grid system serving the small remote community are shown in section A. In section B, model system in Fig .2 was used where solar PV was introduced including the converter and battery units and the system is still off grid. The grid connected system of the diesel, solar PV and battery system as shown in Fig. 3 was analysed in section C.

In section A, Figs 5 and 6 show the optimized and cash flow results for the diesel generation off grid system respectively. It could be seen that the use of the diesel generation incurs very high cost to run with about 2,400 USD net present cost (NPC). The value of the grid extension is also very high of the range of 227km as in Fig. 7, showing that after 227km it would be expensive to use the grid system and the standalone would be cheaper to implement. The emissions of the system in this case is also very high as shown in Table 1, with high carbon, unburned hydrocarbon and nitrogen contents in kg/year.

In section B, in Figs 8 and 9, the optimized results for the diesel, solar PV battery are shown respectively for the off grid system, where it is seen that the NPC of the system dropped drastically compared to the use of only the diesel system, due to the penetration of the solar renewable system. The salvage value of the system for this case is also seen to be appreciative with about 7,000 USD at the end of project life as shown in Fig. 10. The grid extension system dropped drastically from 227km for only diesel system to 139km (Fig. 11) due to the solar PV integration to the system. The emissions of the system are way lower as shown in Table 2 compared to those obtained in section A; this is because a lot of the solar renewable energy technology penetration has made the use of the constant speed diesel power source operation reduced, as compared with when there were no solar PV battery.

The optimized results and the cash flow summary for the on grid tied scenario for the diesel generator and solar PV battery system are shown in Fig. 12, and Fig. 13, respectively in section C. It could be observed that the values of the net present cost (NPC), levelized cost of electricity (COE), and total operating cost were lower than the results obtained in sections A and B. Also, based on Fig. 14, the fuel cost was very low, with reduced and evenly distributed operating and replacement costs, for the on grid system, though the salvage value is lower in this case. Fig. 15 shows the solar radiation used to generate electricity in the solar PV system for all the model systems considered in this study. The global solar and the solar altitude scatter diagram is displayed based on the location where the PV system was sited. Table 3 shows the amount of energy purchased, sold from the grid system and the net purchases in kWh for the year of operation. The peak demand and energy charge for the grid system is also shown in Table 3.

### Section A (Only Diesel Generator off Grid System)

Gen (kW)	Initial Capital	Operating Cost (\$/yr)	Total NPC	COE (\$/kWh)	Fuel Frac.	Diesel (L)	Gen (hrs)
40	\$400	187,004	\$2,401,169	1.942	0.00	69,290	8,759

Fig. 5. Optimized Results using only Diesel Generator

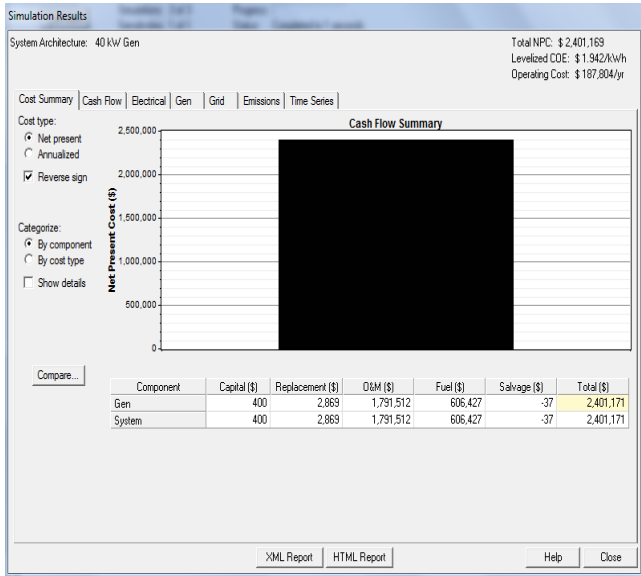


**Fig. 6.** Cash Flow summary using only Diesel Generator

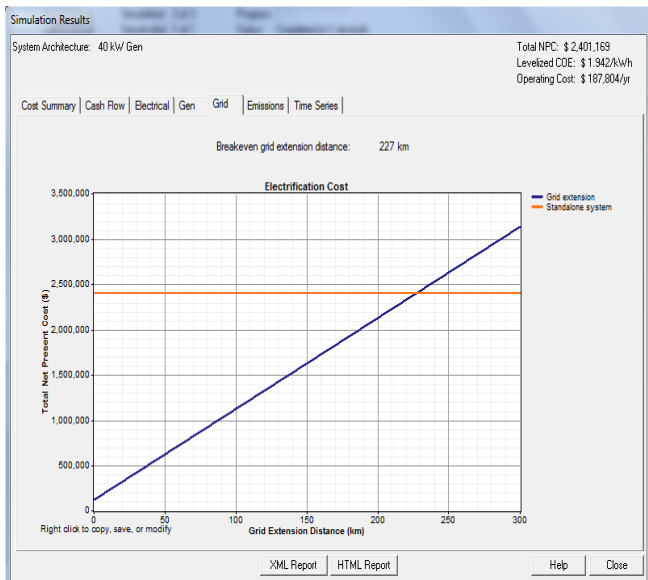


**Fig. 7** Grid Extension using only Diesel Generator

**Table 1.** Emissions of using Diesel Generator

Pollutant	Emission(kg/yr)
Carbon dioxide	156, 152
Carbon monoxide	385
Unburned hydrocarbons	42,7
Particulate matter	29.1
Sulphur dioxide	314
Nitrogen oxides	3,439

**Section B (Diesel Generator and Solar PV Battery off Grid System)**

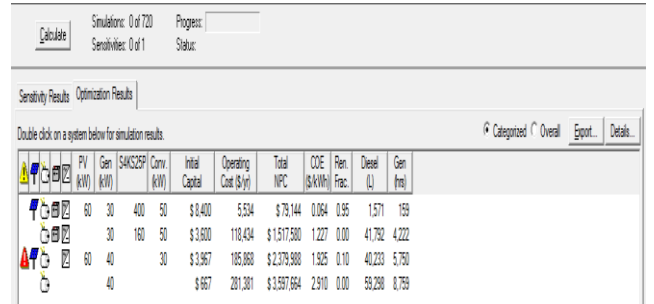


**Fig. 8.** Optimized Results using Diesel Generator, Solar PV

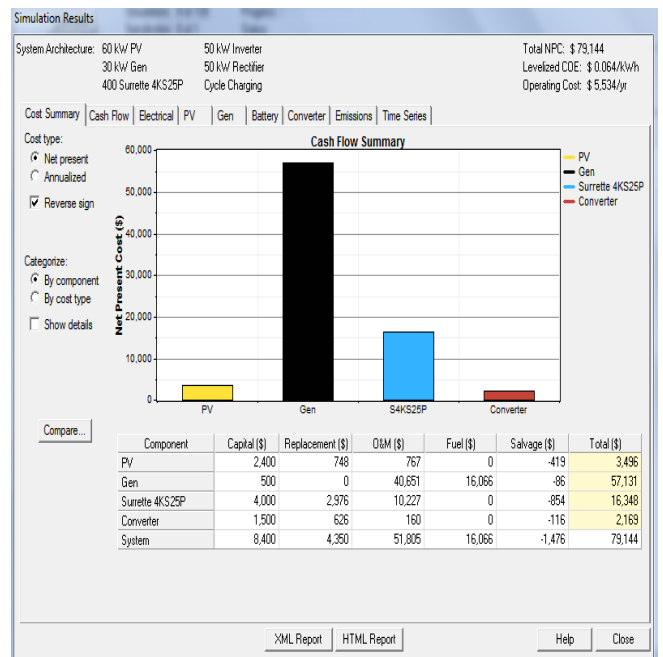


**Fig. 9** Cash Flow Summary using Diesel Generator, Solar PV

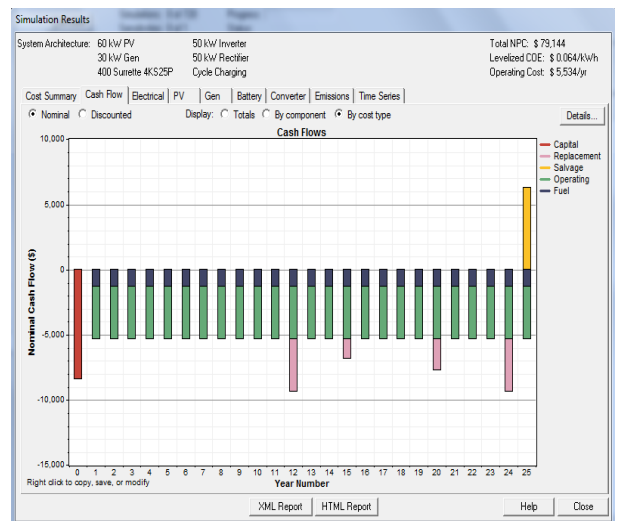


**Fig. 10.** Cost Analyses using Diesel Generator, Solar PV

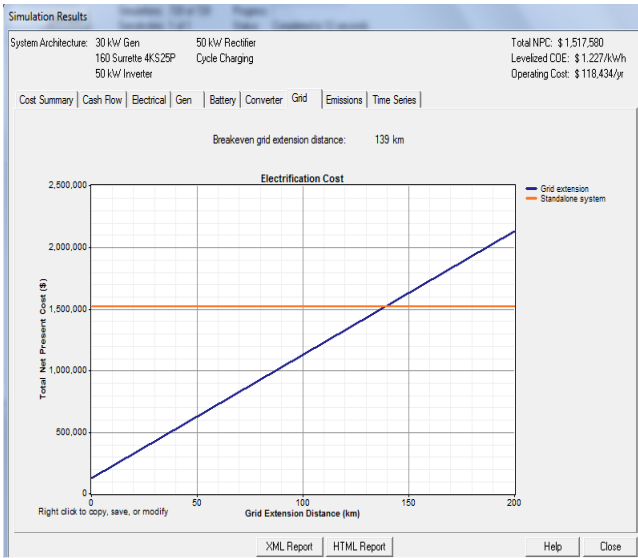


**Fig. 11.** Grid Extension using Diesel Generator, Solar PV

**Table 2.** Emissions for Diesel, Solar PV off Grid

Pollutant	Emission(kg/yr)
Carbon dioxide	4,137
Carbon monoxide	10,2
Unburned hydrocarbons	1,13
Particulate matter	0,77
Sulphur dioxide	8,31
Nitrogen oxides	91,1

**Section C (Diesel Generator, Solar PV Battery System on Grid Connected)**

	PV (kW)	Gen (kW)	SAKCS2SP (kW)	Conv (kW)	Grid (kW)	Initial Capital	Operating Cost (\$/yr)	Total NPC	COE (\$/kWh)	Ren. Frac.	Diesel (L)	Gen (hrs)	
	60	50	1000	\$3,900	2,694	\$38,215	0.017	0.63				0	
	60	30	50	1000	\$4,400	2,675	\$38,601	0.017	0.63			0	
	60	80	50	1000	\$4,700	2,696	\$41,726	0.019	0.63			0	
	60	30	80	50	1000	\$5,200	2,888	\$42,112	0.019	0.63		0	
				1000	\$0	9,673	\$123,647	0.100	0.00			0	
				30	1000	\$500	9,664	\$124,034	0.100	0.00		0	
				40	30	1000	\$1,300	9,807	\$126,670	0.102	0.00	0	
				30	40	30	1000	\$1,800	9,788	\$127,657	0.103	0.00	0

**Fig. 12.** Optimized Results for Diesel Generator, Solar PV on Grid System

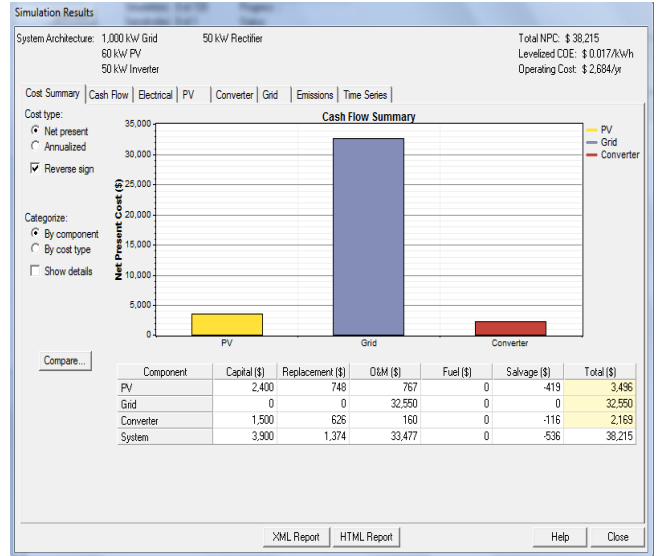


**Fig. 13.** Cash Flow Summary using Diesel Generator, Solar PV on Grid System

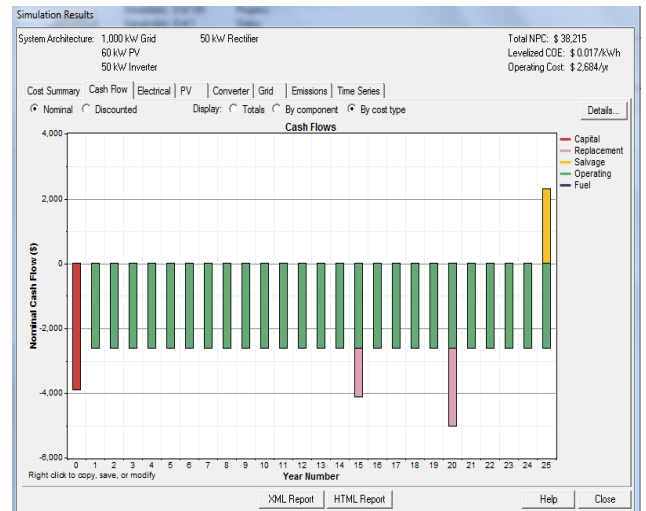


**Fig. 14.** Cost Analyses using Diesel Generator, Solar PV on Grid System

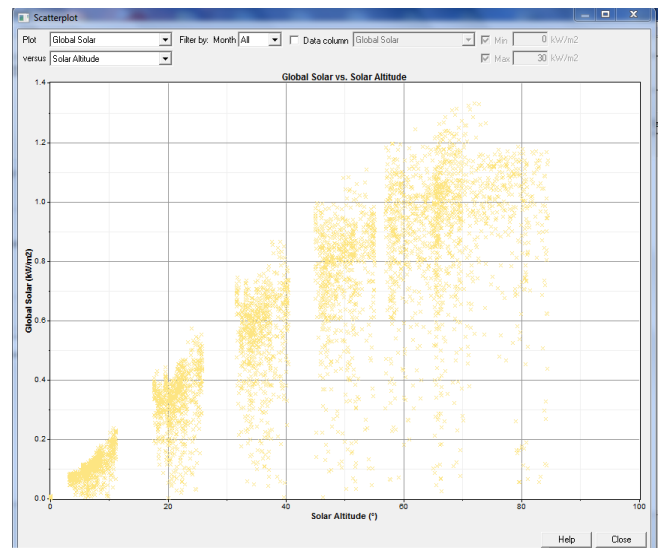


**Fig. 15.** Solar Radiation for all Model Systems

**Table 3.** Diesel Generator and Solar PV on Grid System

Month	Energy Purchased (kWh)	Energy Sold (kWh)	Net Purchases (kWh)	Peak Demand (kW)	Energy Charge (\$)	Demand Charge (\$)
Jan	5,611	5,726	-116	36	275	0
Feb	4,710	6,667	-1,957	37	138	0
Mar	5,650	6,617	-966	34	234	0
Apr	5,272	7,747	-2,475	36	140	0
May	5,394	6,036	-642	34	238	0
Jun	5,437	5,446	-8	37	271	0
Jul	5,277	8,311	-3,034	37	112	0
Aug	5,768	6,050	-282	41	274	0
Sep	5,791	3,766	2,024	37	391	0
Oct	5,305	7,734	-2,429	34	144	0
Nov	5,066	8,642	-3,576	35	75	0
Dec	5,527	5,951	-424	35	255	0
Annual	64,810	78,694	-13,884	41	2,546	0

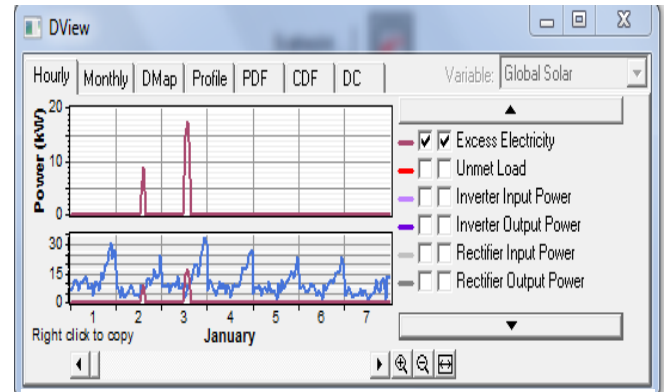


**Fig. 16.** AC load and Excess Electricity (without grid)

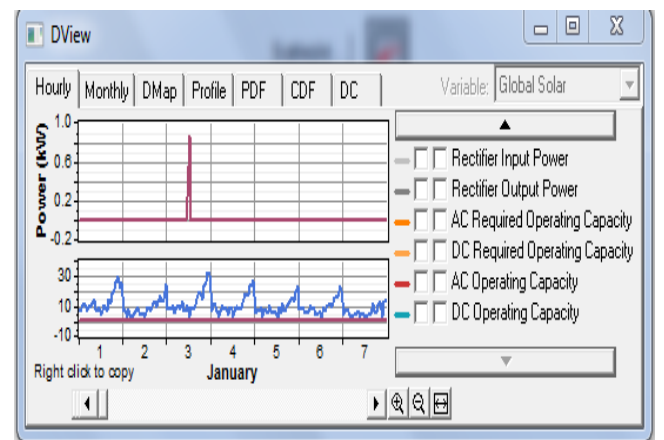


**Fig. 17.** AC load and Excess Electricity (with grid)

**5. Economic Analysis of the System**

The economic analysis of the proposed system was carried out. The responses of the AC primary load and excess electricity produced for without grid and with grid modeled system for this system are shown in Figs. 16 and 17 respectively for the month of January. When the grid was not considered, the excess electricity produced was as high as 18.2kW as against 0.8kW with the grid modeled into the proposed system. A summary of the economic analysis for the scenarios of the proposed diesel solar PV battery system with and without grid is given in Table 4. From the table, it could be seen that when the grid is modeled in the proposed system, the results are more favorable.

**Table 4.** Economic Analysis of Diesel, Solar PV without and with Grid System

Scenarios	NPC (\$)	LCOE (\$/kWh)	Operating Cost (\$/yr)	Excess Electricity (kW)	Renewable Fraction
Without Grid Modeled	79,144	0.064	5,534	18.2	0.95
With Grid Modeled	38,215	0.0017	2,684	0.8	0.63

## 6. Conclusions

Solar photovoltaic (PV) power system has a great potential in future as one of the renewable energy technologies for power generation. This work has presented an off grid connected diesel, solar PV system to power a small remote community. Some of the benefits of the proposed system are reduced cost, reliable and secured power generation for the small remote community, reduced carbon and pollutant emissions because of minimal use of the diesel plant. A comparative analysis was also done for both the off grid and on grid connected system. The simulated results show potential results for favoring on-grid system, thus the long term planning towards on grid diesel hybrid PV systems to power a small remote community would be encouraging. An economic analysis of the proposed system in terms of cost was further carried out for a grid connected and off grid connected scenarios. However, the cost of the proposed system may be high, but commercial use with more customers of the remote community can mitigate the cost of technology and this would be economical for the occupants.

## References

- [1]. Juhari Ab, Kamaruzzaman S, Yusoff Ali, "Optimization of Renewable Energy Hybrid System by Minimizing Excess Capacity", International Journal of Energy, vol. 1, pp. 77-81, 2007.
- [2]. Nathan Johnson, Peter Lilienthal, and Timothy Schoechle "Modeling Distributed Premises-Based Renewables Integration using HOMER", Grid-Interop, Phoenix, Arizona, 2011.
- [3]. Majid Alabdul Salam, Ahmed Aziz, Ali H. A. Alwaeli, and Hussein A. Kazem "Optimal Sizing of Photovoltaic Systems using HOMER for Sohar, Oman", International Journal of Renewable Energy Research, Vol. 3, No. 2, pp. 301-307, 2013.
- [4]. Chiemeka I. U and Chineke T. C. "Evaluating the Global Solar Energy Potential at Uturu, Nigeria", International Journal of Physical Sciences, Vol. 4, No. 3, pp. 115-119, 2009.
- [5]. Gilver T and Lilienthal P. "Using HOMER Software, NREL's Micro Power Optimization Model, to Explore the Role of Gen-sets in Small Solar Power Systems; Case Study: Sri Lanka Technical Report", National Renewable Energy Laboratory, USA, 2005.
- [6]. Al-Badi H. AL-Toobi M., AL-Harthy S., AL-Hosni Z, and AL-Harthy A. "Hybrid Systems for Decentralized Power Generation in Oman", International Journal of Sustainable Energy, Vol. 31, No. 6, pp. 411-421, 2012.
- [7]. Jose L. Bernal-Agustin, and Rodolfo Dufo-Lopez "Simulation and Optimization of Standalone Hybrid Renewable Energy Systems", Renewable and Sustainable Energy Reviews, Vol. 13, pp. 2111-2118, 2009.
- [8]. Muselli M. Notton G., Louche A. "A Design of Hybrid-Photovoltaic Power Generation, with Optimization of Energy Management", Solar Energy, Vol. 65, No. 3, pp. 143-157, 1999.
- [9]. Bagen, Billinton, R. "Evaluation of Different Operating Strategies in Small Standalone Power Systems", IEEE Trans Energy Conversion, Vol. 20, No. 3, pp. 654-660, 2005.
- [10]. Elhadidy M. A. Shaahid S. M. "Parametric Study of Hybrid (Wind + Solar + Diesel) Power Generating Systems", Renewable Energy, Vol. 21, No. 2, pp. 129-139, 2000.
- [11]. Gutierrez Vera J. "Options for Rural Electrification in Mexico", IEEE Trans Energy Conversion, Vol. 7, No. 3, pp. 426-430, 1992.
- [12]. Wichert B. "PV-Diesel Hybrid Energy Systems for Remote Area Power Generation- A Review of Current Practice and Future Developments", Renewable and Sustainable Review, Vol. 1, No. 3, pp. 209-228, 1997.
- [13]. Shaahid SM, Elhadidy MA. "Opportunities for Utilization of Standalone Hybrid Power Systems in Hot Climates", Renewable Energy, vol. 28, no. 11, pp. 1741-53, 2003.
- [14]. Duun P. and Heffers D. *Renewable Energy Sources, Conversion and Application*, Peter Peregrinus Publishing Ltd, Cambridge, 1986.
- [15]. Gwamuri J. and Mhlanga S. "Design of PV Solar Home System for Use in Urban Zimbabwe", Applied Physics and Radiography, pp. 1-6, 2012.
- [16]. Daud A.K and Ismail M. S. "Design of Isolated Hybrid Systems Minimizing Costs and Pollutant Emissions", Renewable Energy, Vol. 44, No.2, pp. 215-224, 2012.
- [17]. Ismail M.S., Moghavvemi M. and Mahlia T.M.I "Design of a PV/ Diesel Standalone Hybrid System for a Remote Community in Palestine", Journal of Asian Scientific Research, Vol. 2, No. 11, pp. 599-606, 2013.
- [18]. California Energy Commission, *A Guide to Photovoltaic (PV) System Design and Installation*, Energy Technology Development Division, 2001.
- [19]. Khatib T, Mohammed A., Sopian K and Mahmoud M. "Optimal Sizing of Building Integrated Hybrid PV/Diesel Generator System for Zero Load Rejection for Malaysia", Energy and Buildings, Vol. 43, No. 12, pp. 3430-3435, 2011.
- [20]. Singh S. N., and Singh A. K. "Optimal Design of a Cost effective Solar Home Power System-An Alternative Solution to DG for Grid Deprived Rural India", International Journal of Research and Reviews in Applied Sciences, pp. 60-66, 2010.

# Multiobjective Pareto Optimal Design of a Clutch System

O. Ozansoy<sup>\*‡</sup>, T. Tevruz<sup>\*\*</sup>, A. Muga<sup>\*\*</sup>

<sup>\*</sup> : Istanbul Technical University, Faculty of Mechanical Engineering, Gumussuyu 34437, Istanbul, Turkey, Ford Otomotiv Sanayi A.Ş. Gebze Engineering, Tubitak Technopark, 41470 Gebze, Kocaeli

<sup>\*\*</sup> : Istanbul Technical University, Faculty of Mechanical Engineering, Gumussuyu 34437

(oozansoy@ford.com, tevruz@itu.edu.tr, muga@itu.edu.tr )

<sup>‡</sup>Corresponding Author; Onur Ozansoy, Ford Otomotiv Sanayi A.Ş. Gebze Engineering, Tubitak Technopark, 41470 Gebze, Kocaeli, oozansoy@ford.com

*Received: 08.02.2015 Accepted:14.03.2015*

**Abstract-** Optimum design of a clutch and dual mass flywheel system is completed. Although the clutch systems are exposed to both rotational and axial vibrations, they are generally designed by considering rotational vibrations of engines and they do not have any component to damp axial vibrations due to the following two reasons: first, the package area of the clutch system is very limited and there is no available space to put additional springs and dampers to reduce these vibrations. Second, axial vibrations are normally insignificant to be considered in the analyses and such vibrations are supposed to be damped by the diaphragm spring and cushion springs. Nonetheless, axial vibrations may lead to some unexpected problems in the power train such as the rattle noise that is examined in this study by using global optimization techniques. The components in the clutch system are modeled analytically. Then, by considering the pedal characteristics and vibrations of pressure plate as objective functions, a multi-objective Pareto optimization problem is solved. It is shown that analytical models agree well with the experimental measurements and vibrations in the clutch system can be reduced significantly by choosing the design parameters with optimization tools.

**Keywords** Optimization; pareto optimality; dynamic systems; vibration; clutch.

## 1. Introduction

Since engineering structures are mostly subjected to dynamic loads, it is important to design these structures in consideration of their dynamic behavior whose optimization is difficult since the associated mathematical models are complicated and computational costs are expensive. In this study, dynamic behavior of a clutch and dual mass flywheel (DMF) system is optimized.

The clutch and dual mass flywheel system existing in manual transmissions of internal combustion engines are important components in a vehicle that affect the ride comfort of the vehicle and may cause noise, fatigue of components and longitudinal vibrations during the cruise of the vehicle. It is noteworthy that the loading on the clutch and dual mass flywheel system is transient and a dynamic model has to be employed in optimization studies. The clutch

systems are essentially designed for damping out rotational vibrations of the engine; thus, it helps increase the ride comfort; nonetheless, they are exposed to axial vibrations as well. They generally do not have any component to annihilate axial vibrations due the following reasons: first of all, packaging area of the clutch system is limited between engine and transmission and there is no available space to add some springs and dampers to annihilate axial vibrations. Second of all, axial vibrations are normally insignificant to be considered in design phase which are supposed to be damped by the diaphragm spring and cushion springs. But, axial vibrations may lead to some unexpected results in the power train such as the rattle noise that is examined in this study by using global optimization techniques.

Many studies on the clutches of different types exist in literature. For instance, wet clutches and dual clutches, which are mostly used on automated manual transmissions,

engagement characteristics and their effects on engine characteristics, shift characteristics and their effects on shaft vibrations, modal frequencies of the clutch system and clutch control mechanisms are some of the investigation topics [1-7]. There are also studies in literature on modeling of one way clutches [8-9]. Manual transmission dry clutch systems and their rotational behavior are examined by some researchers [10-18, 41-42]. For example, Crowther and Zhang studied the torsional behavior of the clutch as an elastic system in the driveline [11]. Duan and Singh formulated the clutch engagement and disengagement as a nonlinear dry friction problem with harmonically varying normal load and investigated the stick-slip motions to understand the clutch response under various torque inputs [12-13]. Awrejcewicz and Grzelczyk studied the wear of clutch friction surfaces [18]. Being one of the most important component of a clutch system, the diaphragm spring (which determines clutch pedal load) is studied by some researchers and optimized for the best release load and durability [19-25]. Some researchers studied the Almen-Laszlo formula (which is used to calculate disc spring characteristics) [26] to improve its accuracy [27-30]. Information about main components of a clutch system can be found in [31-32].

One of the rare investigations on longitudinal vibrations in a clutch system is presented in [33] where Esfahani et al studied in-cycle vibrations on the clutch pedal which is excited by the crank shaft's axial vibration; at this point, the authors remark about the same challenge as we faced in this study which is the lack of an extensive axial clutch vibration studies in literature whilst the problem observed are connected with axial clutch vibrations. They focused on the clutch pedal vibrations around 257Hz, which is originated from the clutch axial vibrations, and their simulation showed the same vibration level around 230-240Hz which is a good correlation with actual condition, e.g., see [33]. But they did not investigate why their system showed the whoop frequency, or in cycle vibration, around 250Hz and did not present a discussion or proposal how this could be reduced. They only suggested using such kind of simulation toolboxes to foresee any possible problems before handling the physical parts.

Reitz et al. worked on a special test bench to investigate NVH problems in a clutch system [46]. They reported that the clutch system is excited by torsional and axial flywheel vibrations. Torsional flywheel vibrations are caused by the 2nd engine order and axial flywheel vibrations are caused by the crankshaft bending vibrations which are excited by the 4th cylinder firing. This means that axial vibrations are caused by the 0.5th engine order which is the same outcome of our investigations as explained in upcoming sections in detail. They also reported the test results of three different clutches but did not share the clutches' specifications due to confidentiality requirements. They presented their test bench that enables to determine the clutch systems' NVH behavior during engagement and disengagement in detail and allow them to predict the behavior of the clutch system in a real vehicle.

Kelly and Rahnejat investigated the pedal vibrations and influence of individual components on the transmission of

the subsequent vibration and noise [47]. They investigated the vibrations in a vehicle and multi-body model of clutch and observed that the pedal vibration and noise occurred due to the 0.5th engine order excitation from the 4th cylinder firing resulting in bending of the crankshaft. This is actually the same root cause of the clutch axial vibrations investigated in this study and although the source is the crankshaft bending vibrations, these vibrations are transmitted by the flywheel and clutch system. They also showed that cable properties and mass fixes can influence the vibrations.

Hasabe and Seiki studied the clutch pedal vibrations which are excited by the clutch axial vibrations [48]. They conducted an experimental study based on an on-vehicle observation of the vibrations and a test bench. They tried to develop a method for a test bench evaluation to predict the levels of vibration and noise in a vehicle having a 4 cylinder engine and observed that the pedal vibrations exist at 4400RPM engine speed when the clutch is half engaged and in the 1st, 3rd and 6th harmonic of the engine vibration. They observed the same behavior on the clutch side which proves that the vibrations are transmitted by the clutch system. They also stated that the clutch system has the major contribution on pedal vibrations. Their measurements showed that their sample clutch has the critical resonance frequency between 200-300Hz. Unlike other studies in literature, since their investigation covered the whole range of release bearing travel, they observed a relatively larger range for critical frequency and they proposed two different clutch behaviors at engaged and disengaged positions which lead to this larger range. They built a correlation between the vibration level and frequency range of two different natural frequencies of engaged and disengaged positions as well.

If the clutch model and its optimization are put aside, there are many studies related to gear rattle phenomenon in literature [14-15, 34-38]. Some of these studies focused on neutral gear rattle [34-35], some of them focused on backlash effects [15, 36-37]. Barthod et al. studied gear rattle phenomenon to understand the rattle threshold and rattle noise evolution in relation with excitations and mechanical gearbox parameters [38]. On the other hand, ergonomic issues of the clutch pedal characteristic for different driver profiles are studied in [39]. There are also some studies to identify the heat energy generation in friction clutch systems. To this end, Shabibi investigated the transient solution of heat conduction problem in solids with insulated boundaries [40].

Padmanabhan and Singh [14] employed a simplified rotational clutch model and showed that if clutch parameters are selected appropriately, it can help reduce the transmission rattle noise; although they employed a simplified clutch model, it is a good example which shows that clutch parameters are very important to reduce transmission rattle noise problem. They proposed a dry friction three-stage clutch with moderate first stage spring stiffness. Although we are using a dry clutch, the clutch examined in this study has one-stage spring set on it and this spring set is selected carefully to accommodate corresponding engine torque. It is noteworthy that three-stage clutches are not normally used with DMF systems; instead, they are used with single mass

flywheel systems due to their relatively higher rotational vibration frequencies. Furthermore, three-stage clutches are more expensive than single stage clutches due to 2 more spring sets and friction surfaces. Nonetheless, since our target should be getting the best results with a competitive price, we avoid bringing add on cost to our system.

On the other hand, analyses of longitudinal dynamic behavior of a clutch system and seeking the solution of corresponding optimization problem have not been pursued in literature. Motivated by these facts, this study is initiated in which dynamic models of components of a clutch system are derived and constructed in Matlab-Simulink, mathematical models are verified by measurements, a multi-objective optimization problem is formulated having two objective functions (i.e., pressure plate vibrations and pedal characteristics) and corresponding Pareto optimal solution is obtained and discussed. A prototype clutch is manufactured by using the design variables obtained by optimization runs and then it is tested. It is shown that analytical models agree well with the experimental measurements and vibrations in the clutch system can be reduced significantly by choosing the design parameters with optimization tools.

**2. Modeling of the Clutch System**

Parameters which affect axial vibrations of the clutch system will also affect clutch release load characteristics which will be discussed in the upcoming sections in detail. Since the clutch pedal load characteristics are dependent on release load characteristics, even if the vibration problem is well resolved, pedal load might be too high which may cause the clutch system becomes unusable. For that reason, clutch release load characteristics will be simulated first, and then optimization problem will be solved.

The clutch and DMF system that are the subject of this study is shown in Fig. 1. Following, dynamic models of components in this clutch system are derived. Please note that primary side of the flywheel and some internal parts could not be shown in the figure not make it more intricate.

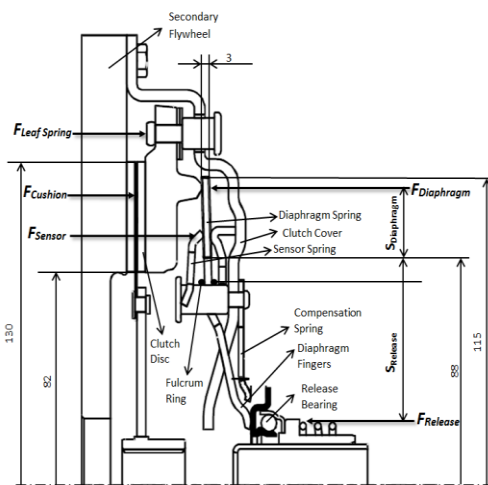


**Fig. 1.** Geometrical data of the simulated clutch and DMF system (at engaged position) [44].

**2.1. Clutch Release Load Characteristic**

Being one of the crucial elements determining the clutch dynamic behavior, clutch release load characteristic is derived from clutch release curve. A typical clutch release curve, pressure plate spring curve and lift off curve are shown in Fig. 2. While clutch diaphragm spring is the most significant component influencing clutch release load characteristic, it is also affected by leaf springs on clutch cover (which helps pressure plate disengagement), cushion springs between friction surfaces of clutch disc and clutch cover stiffness. Following sections explain how these components are modeled.

As mentioned in the abstract, two objective functions such as pressure plate vibrations and clutch pedal curve characteristic are used in this study. Clutch pedal curve characteristic is calculated by dividing the release load curve to release system’s ratio and release load curve gives us the load on the release bearing as the release bearing travel changes. Note that while calculating these curves, they are modeled parametrically by using cubic spline polynomials in the mathematical model of the clutch system and employed in the optimization runs.

**2.2. Diaphragm Spring**

Since the diaphragm spring has two sections having completely different characteristics, it is divided into two parts and their mathematical equations are derived separately, e.g., see Fig. 3. While the disc spring is discussed below in Section 2.2.1, finger springs are studied in Section 2.4 along with the other components that are modeled by using finite element method (FEM).

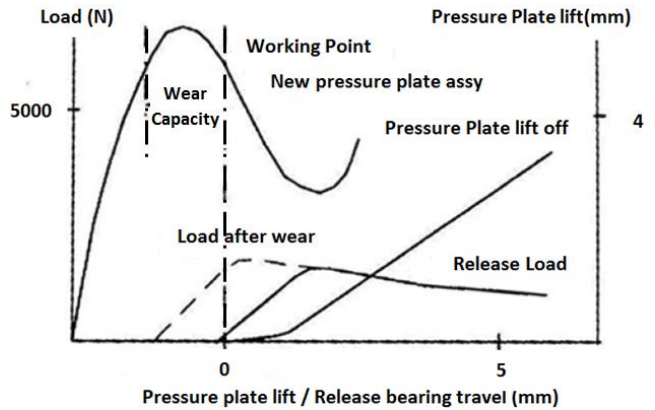


**Fig. 2.** An example of a clutch pedal curve and its important points [45].

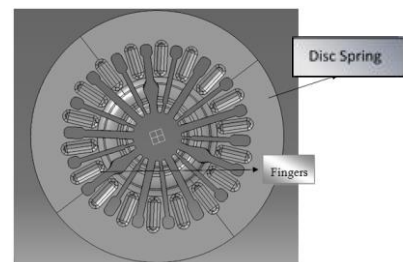


**Fig. 3.** Two sections of the diaphragm spring.

2.2.1. Modeling of Disc Springs.

The Almen-Laszlo formula [26] is commonly used to model the disc springs in practice [19-22].

The load  $P_1$  acting on the outer radius of diaphragm spring can be calculated as follows:

$$P_1 = \frac{\pi Et \lambda_1 \ln\left(\frac{R}{r}\right)}{6(1-\rho^2)(L-l)^2} \left[ \left( h - \lambda_1 \frac{R-r}{L-l} \right) \left( h - \frac{\lambda_1(R-r)}{2(L-l)} \right) + t^2 \right] \quad (2.1)$$

where  $E$  is the elasticity modulus of spring material,  $t$  is the thickness of diaphragm spring,  $\lambda_1$  is the displacement of outer diameter of disc spring,  $R$  is the radius of outer end of disc spring,  $r$  is the inner radius of disc spring,  $\rho$  is the Poisson's ratio of spring material,  $L$  is the position of load  $P_1$ ,  $l$  is the diameter of wire ring and  $h$  is the internal cone height of an unloaded diaphragm spring [20].

The load  $P_2$  acts on the inner radius of diaphragm fingers. This leads to a large deformation  $\lambda_2$  on diaphragm fingers and also  $\lambda_1$  on the outer radius of disc spring as shown in Figure 4a and Figure 4b. The release load  $P_2$  is given by [20]

$$P_2 = \frac{\pi Et \lambda_1 \ln\left(\frac{R}{r}\right)}{6(1-\rho^2)(L-l)(r-r_p)} \left[ \left( h - \lambda_1 \frac{R-r}{L-l} \right) \left( h - \frac{\lambda_1(R-r)}{2(L-l)} \right) + t^2 \right] \quad (2.2)$$

Where  $r_p$  is the inner radius of diaphragm fingers where release bearing connection exists [20].

The cross section of disc spring part of diaphragm spring is presented in Figure 4.b on the right without showing the diaphragm fingers, which is used to derive load equations of disc spring. The Almen-Laszlo formulas assume that the disc spring rotates around a center which can be calculated by using the following formula [31-32]

$$D_0 = \frac{D_e - D_i}{\ln(D_e/D_i)} \quad (2.3)$$

Then, the load on disc spring is given by

$$F = \frac{4E}{1-\rho^2} \cdot \frac{t^4}{K_1 \cdot D_0} \cdot \frac{s}{t} \cdot \left[ \left( \frac{h-s}{t} \right) \cdot \left( \frac{h-s}{2t} \right) + 1 \right] \quad (2.4)$$

$$K_1 = \frac{1}{\pi} \cdot \frac{(\delta-1)^2}{\delta+1} \cdot \frac{2}{\delta-1 - \ln\delta} \quad (2.5)$$

Where  $s$  is the deflection of disc spring,  $D_e$  is the outer diameter of disc spring,  $D_i$  is the inner diameter of disc spring and  $\delta = D_e / D_i$  [31]. The disc spring characteristic which can be found in literature [31-32] is shown in Fig. 5 as  $h/t$  ratio changes.

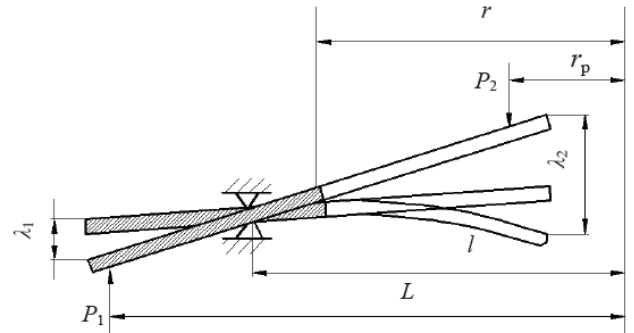


Fig.4a. Deformation of the diaphragm spring when its fingers are loaded. [20]

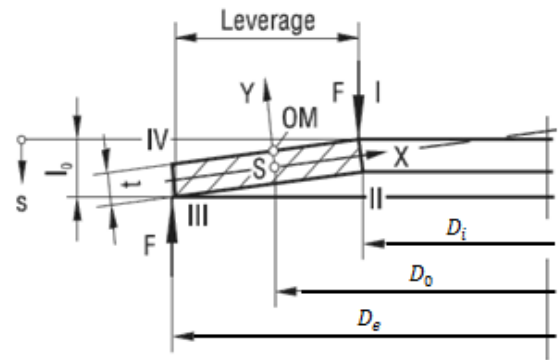


Fig.4b. The cross section at reference position. [31]

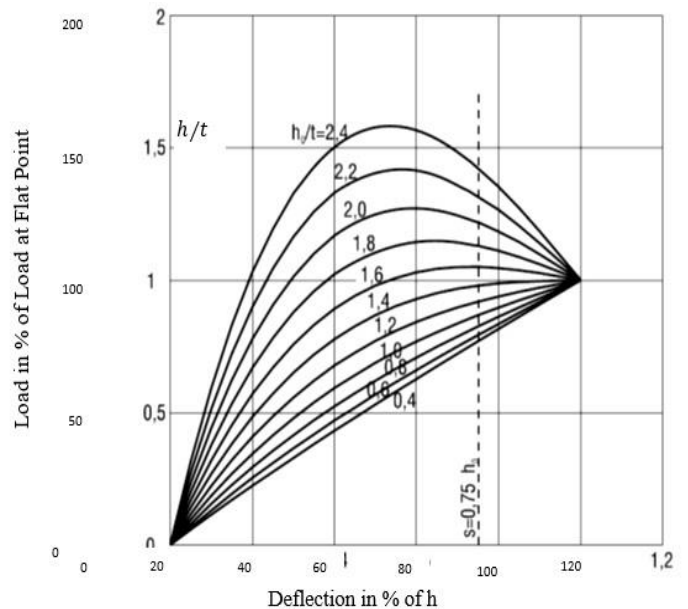
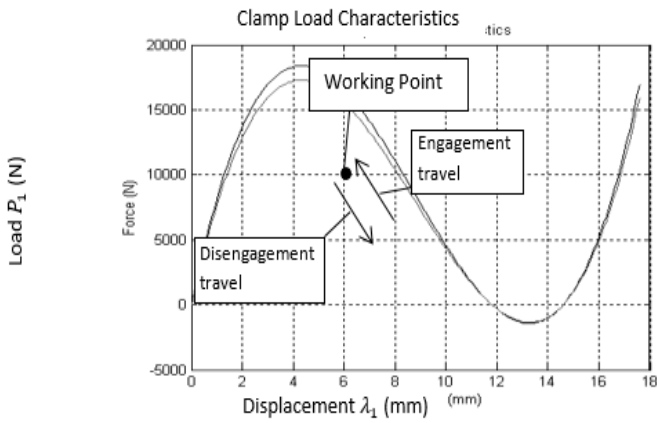


Fig.5. Load-deflection characteristic for Belleville washers [31].

By using the formulations given above and geometrical properties of the clutch employed in this study, the clamp load curve is obtained as shown in Figure 6 where the maximum achievable load is calculated as approximately 18,000N.



**Fig.6.** Clutch clamp load characteristics. The curve at the top shows the spring compression, the curve at the bottom shows the decompression phase.

Once the clamp load curve is built, operation point ( $\lambda_1$ ) on the curve needs to be identified. In order to identify the value of  $\lambda_1$ , clamp load should be known which is the normal force on the clutch pressure plate at the engaged position and must be determined correctly to ensure the transmission of engine torque. A safety factor is also considered to guarantee no slippage on the clutch which is called the Slip Safety Factor (SSF) which is typically chosen as 1.2 [45]. The clamp load is calculated by using Eq. (2.7).

$$D_m = \frac{2}{3} \cdot \frac{D_e^3 - D_i^3}{D_e^2 - D_i^2} = 0.212m \quad (2.6)$$

$$SSF(\text{Slip Safety Factor}) = \frac{F_{\text{clamp}} \cdot D_m \cdot \mu}{T_e} \geq 1.2 \quad (2.7)$$

Where  $D_m$  is the diameter of gyration (centroid of friction facing surface diameter to which torque is applied to calculate the clamp load),  $F_{\text{clamp}}$  is the clamp load at the clutch operation point,  $\mu$  is the friction coefficient of friction and  $T_e$  is the maximum engine torque. By the use of Eq. (2.7), the minimum clamp load is calculated as 9,400N and nominal clamp load can be selected as approximately 10,000N. Considering this clamp load, nominal operation point is calculated as 8.1mm from the Figure 6.

### 2.3. Modeling of Cushion Spring

The cushion spring significantly affects the release load characteristic. Its characteristic load curve used this study is shown in Figure 7 on the left [43] which is obtained from experimental measurements (e.g., see Section 3). It is parametrically modeled by using cubic spline polynomials in the mathematical model of the clutch system and employed in optimization runs. The cushion spring segment of clutch disc provides a smooth release curve and prevents large loads on the pedal load curve. In order to handle release load curve, the difference between diaphragm spring and cushion spring is calculated and divided by clutch ratio. The shaded areas in Figure 7 on the right show this difference and related release load is on the left side.

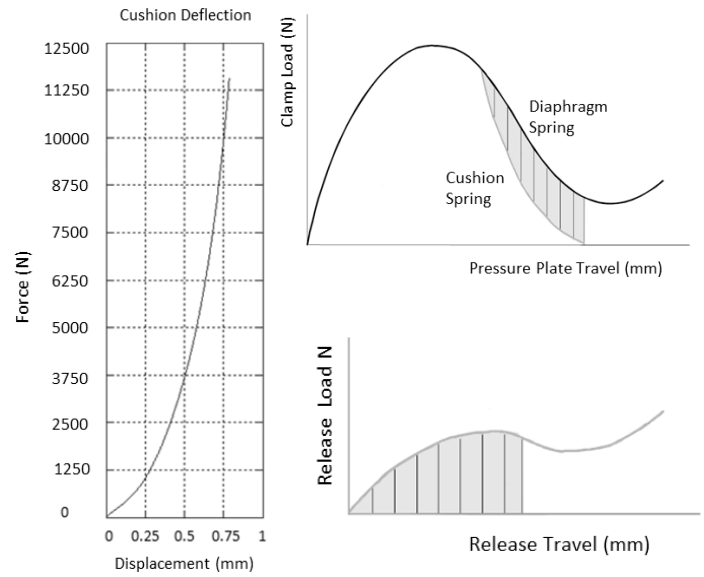


**Fig.7.** The cushion spring and its characteristics for the new and worn springs [43].

### 2.4. Modeling of Diaphragm Spring Fingers, Clutch Cover, Compensation Spring and Leaf Springs

FEM is used to model diaphragm spring fingers, clutch cover, compensation spring and leaf springs. It is noteworthy that diaphragm spring stiffness is strongly related to the clutch release load characteristic.

In order to calculate the diaphragm spring stiffness under loading, it is important to accurately model the stiffness of fingers. To this end, the slave cylinder bearing is modeled as a solid cylinder on the fingers of diaphragm springs and a contact model is defined between the bearing and fingers. There are a number of studies reported in literature used shell elements [24] or tetrahedron solid mesh elements, e.g., [49], [51-52]. Parabolic tetrahedron solid elements (with 10 nodes having three degrees of freedom (DOFs) at each node) are used in our study. In order to analyze only finger area of the diaphragm spring, all DOFs of the fulcrum ring connection are restricted as boundary conditions and distributed pressure is loaded on the release bearing. Based on FEM solutions, characteristics of fingers are found to be similar to a linear spring, which is also verified by experimental measurements, e.g., see Figure 9 (i.e., release load curve). Linear ramp up behavior of first part of the release load curve shows linear spring characteristics of diaphragm fingers. Many measurements and simulations are reported in literature on this issue, e.g., see [22], [24], [49-50].

The clutch cover stiffness is also another important parameter affecting the release load characteristic. By using parabolic tetrahedron solid elements in FEM model, distributed load is applied to fulcrum ring area and all DOFs of the bolt holes around the cover where the cover is connected to flywheel are restricted. Note that the diaphragm spring position, compensation spring position and its end stop position are different between the loaded and unloaded

positions of diaphragm spring. These positions change under the loading during the engagement and disengagement of clutch and significantly affect the release load curve characteristic. In order to identify these positions under different loading conditions, FEM solutions are used and relevant spring coefficients are calculated.

The compensation spring is used to achieve a more flat release load characteristic which also leads to a more flat clutch pedal characteristic. The compensation spring is activated after the maximum loading is reached during its release. After this point, the release load begins to reduce dramatically. In order to prevent this, a linear spring is used to increase the pedal loads starting from the maximum release load to the end of release bearing travel; thus, more flat pedal characteristic can be achieved [44].

Leaf springs are used to pull back the pressure plate from the clutch disc during the disengagement of clutch. These springs are thin planar plates located in front of the diaphragm spring. Due to the clamp load on the pressure plate, these plates are bent and have the function of a spring. They are only used to guarantee that the pressure plate does not touch to clutch disc after the disengagement.

In FEM models of compensation spring and leaf spring, parabolic tetrahedron solid elements with 10 nodes are used and all DOFs of rivet holes of these springs used for the connection to the cover are restricted from movement or rotation. The load between 0 to 400N is applied to leaf spring and distributed pressure is applied to the release bearing which contacts with compensation spring fingers at the release bearing travel where this contact condition is occurred.

FEM solutions of diaphragm spring, clutch cover, compensation spring and leaf spring are shown in Figure 8. Note that these results are used in the mathematical model of clutch system to derive their parametric models which is employed in the optimization runs.

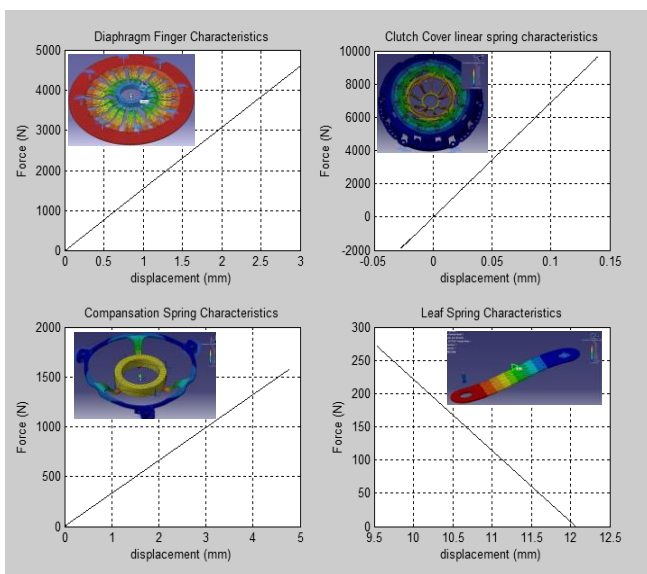


**Fig.8.** FEM solutions of diaphragm spring fingers, clutch cover, compensation spring and leaf springs.

The usage of FEM was necessary since the spring characteristics of subcomponents are needed separately. Experimental results give us only total system behavior as shown in c instead of handling the spring characteristics of all subcomponents separately. Furthermore, once these spring characteristics are identified, it is very easy to change the spring coefficients during optimization runs.

Once these numerical results are obtained and used in the calculations of clutch release load curve, the results are compared with experimental measurements (e.g., see Figure 9).

### 2.5. Derivation of Release Load Curve and Lift Off Curve

By the use of above results, we have all necessary inputs to calculate the release load characteristic and lift off curve. A simplified formulation to calculate the release load for pressure plate movement “s” is given by

$$F_R = \frac{F_D - F_{cushion} - F_{sensor} - F_{leaf}}{i} + F_{comp.} \quad (2.8)$$

where  $F_D$  is the diaphragm spring load,  $F_{cushion}$  is the cushion spring load,  $F_{sensor}$  is the sensor spring load,  $F_{leaf}$  is the leaf spring load,  $F_{comp.}$  is the compensation spring load which is zero at the beginning of disengagement movement of the release bearing and  $i$  is the clutch ratio. These forces are shown in Fig. 1. Then, the clutch ratio is given by

$$i = S_{Release} / S_{Diaphragm} \quad (2.9)$$

Where  $S_{Release}$  and  $S_{Diaphragm}$  are respectively distances between loads and connection rivets shown in Fig. 1.

Sensor spring load in Eq. (2.8) is created by the sensor spring shown in Fig. 1 and it increases as clutch friction faces get worn. After a certain level of load, clutch adjustment system sets in and sensor spring load decreases to the initial value. Detailed information about clutch adjustment system can be found in [44].

It can be seen in Eq. (2.8) that the clutch cover or diaphragm spring finger deflection is not considered in force equilibrium. However, while the load on these components changes during the engagement and disengagement process, their stiffness affects the positions of diaphragm fingers and subsequently the bearing position, which also determines the complete release curve characteristic. These issues are considered in the simulations to determine the mathematical model of the system and calculate the release characteristics of the clutch examined in this study.

The release load on clutch fingers and lift off curve (displacement of pressure plate and clutch finger travel) are simulated and compared with the measurements in Figure 9. These curves are the basic clutch characteristics and can be used to characterize a clutch system [45].



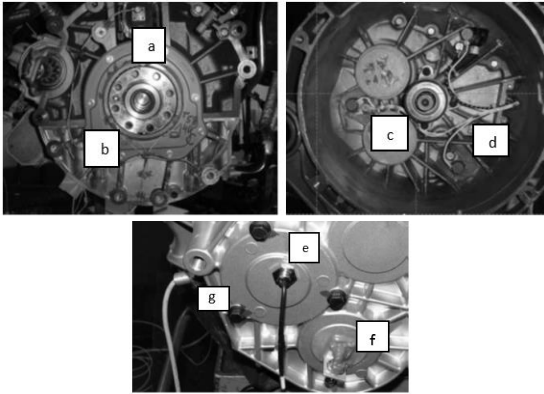


**Fig. 11.** Locations of displacement and speed sensors for vibration analysis: a) 3 displacement sensors for crankshaft vibrations at  $r = 58\text{mm}$ , b) 3 displacement sensors for primary flywheel vibrations at  $r = 140\text{mm}$ , c) 3 displacement sensors for secondary flywheel vibrations at  $r = 97\text{mm}$  d) 3 displacement sensors for pressure plate vibrations at  $r = 118\text{mm}$ , e) 1 displacement sensor at the end of the transmission housing, f) 1 microphone at the end of the transmission housing (bandpass filter 1000-20000 Hz). g) 1 speed sensor for the transmission input shaft speed

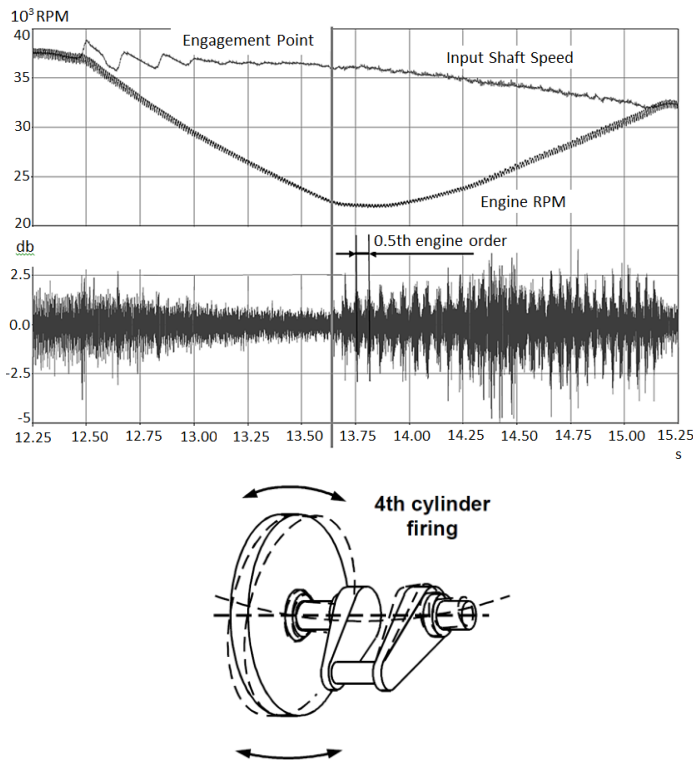


**Fig. 12.** Recorded noise data between 2000-3500 RPM range. Rattle noise exists at the 0.5th engine order (on the left) corresponding to crankshaft bending vibration resulting in axial clutch vibrations (on the right) [33], [46].

As mentioned in Section 1, references [33], [46], [47] reported that axial clutch vibrations are excited by the 4<sup>th</sup> cylinder of engine at the 0.5<sup>th</sup> engine order. Measurements tell us the rattle noise in our experimental setup occurred at the 0.5<sup>th</sup> engine order which is excited by the crankshaft

bending vibrations which is verified by the references as shown in Figure 12 on the right side.

Figure 13 shows the measurements taken from the engine crankshaft, flywheel, clutch cover and pressure plate. It is observed in this figure that the clutch system considered in this study works like an amplifier which results in transmission rattle noise during clutch engagement.

*3.3. Analysis of Vibration Modes on the Clutch and Flywheel*

In order to understand the axial vibration modes of clutch and dual mass flywheel system, a modal analysis test is performed on a shaker test bench and vibrations are measured in response to axial sinusoidal excitations having 5mm release bearing travel between 0-800Hz. The shaker, instrumented clutch and test rig configuration is shown in Fig.14.

Components shown in Figure 14 are listed below:

- a. Shaker
- b. Flywheel primary side
- c. Flywheel secondary side
- d. Pressure plate

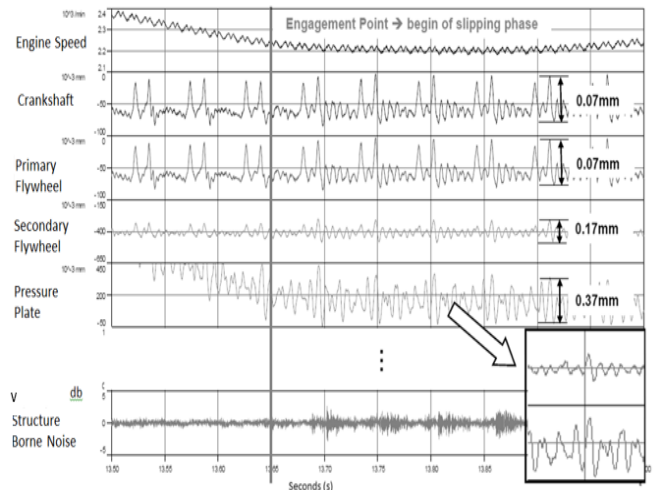


**Fig. 13.** Axial vibration measurements on the crankshaft, primary and secondary flywheels and pressure plate, and its relations with rattle noise measurements.

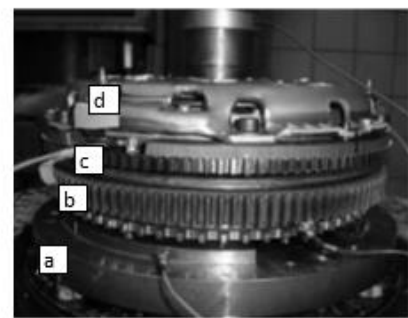


**Fig. 14.** Shaker test rig configuration and instrumented clutch.

Measurements obtained from this setup is presented in Fig. 20 to verify the results of mathematical results where it is observed that the first natural frequency of pressure plate is around 165Hz with a phase difference between the flywheel and pressure plate. Measurements also show that there is a second dominant frequency around 150 Hz with no phase difference between the flywheel and pressure plate whilst pressure plate shows relatively larger amplitudes in compared with the whole frequency range.

**4. Mathematical Model for Pressure Plate Vibrations**

Note that we have flywheel vibration measurements at hand which are excited by the crankshaft bending vibrations (especially 4th cylinder firing is effective on this kind of vibration problem (Fig. 12), e.g., see [33], [46]) and it is not possible to alter these vibrations unless the engine or cranking system is modified. Therefore, flywheel vibrations are used as an input to the vibration model of clutch system in this study.

On the other hand, in order to model the pressure plate axial vibrations, the system is modeled by the components such as the clutch disk, input shaft, pressure plate, diaphragm spring, clutch fingers and clutch cover. Engine vibration transmitted through this flywheel connection is the only source for clutch pressure plate vibration. Such a mathematical model for another clutch system can be found in [33] where a cable clutch system with an external slave cylinder and a lever system is modeled while the model in this study is a hydraulic system with a concentric slave cylinder.

The components of clutch system are shown in Fig. 1. The mathematical model includes the geometrical and physical properties of these sub-components and stiffness properties of the springs. Since excessive vibrations of the pressure plate occur during the engagement (while releasing the clutch pedal), we will simulate the system starting from the disengaged position to the engaged position; that is, this model will be working at the time while the clutch pedal is being released.

It must be underlined that this model is only built to study longitudinal vibrations of the clutch system and no rotational motion is considered. There are two main reasons for this assumption.

- If there are unexpected rotational vibrations in the engine, the noise phenomena would occur at idle or driving conditions as well. Instead, the noise is only heard during engagement phase in which pressure plate does not complete its full travel. Following, the excessive axial vibration causes pressure plate to press the clutch disc intermittently, then torque fluctuation is transmitted to the transmission that causes the rattle noise phenomena.
- Torque fluctuations can also be improved by modifying rotational dampers slightly. But this does not resolve the main source of vibration, only damps out the vibration transmitted to the transmission. This may also cause a negative effect on the dampers life time due to the vibrations on pressure plate.

Simulation results will be compared with the measurements and above mentioned assumption will be proven with the comparisons.

The simplified model of the system is shown in Fig. 15 in which diaphragm fingers are connected to the cover which can rotate around the fulcrum ring connection points. This is completely in line with the detailed representation of the clutch system shown in Fig 1; clutch disc is assumed to be consisting of two separate friction discs. The mass of these friction discs are equally added to the secondary side of flywheel and pressure plate. The cushion spring and its friction surface are shown in the model as a sub-component of the clutch disc.

In Figure 15 on the top side, experimental measurements taken from the engine is shown. As it can be seen from physical measurements, the crankshaft has two main peaks which are due to the 3<sup>rd</sup> and 4<sup>th</sup> cylinder firings which cause the crankshaft bending. These two peaks are repeated in every 720° of crankshaft rotation and used as inputs in the simulation model as shown in the same figure.

By using the simplified model shown in Figure 15, the mathematical model is obtained by using MATLAB software. To this aim, the Simulink® which is a MATLAB tool is employed that helps simulate such vibration models. The high level Simulink model for the pressure plate and clutch cover is shown in Figure 16 on the left.

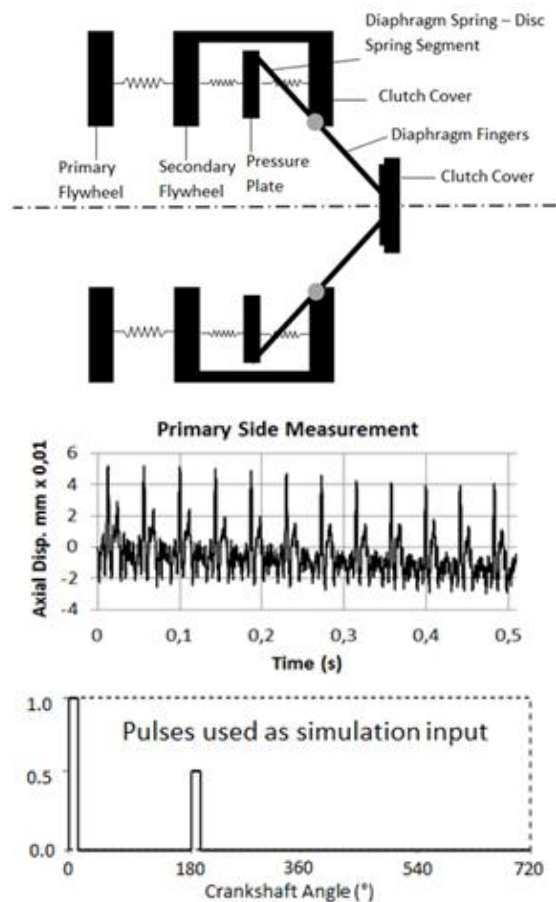


**Fig. 15.** Simplified model of the clutch system by considering axial vibrations and primary side axial vibrations.

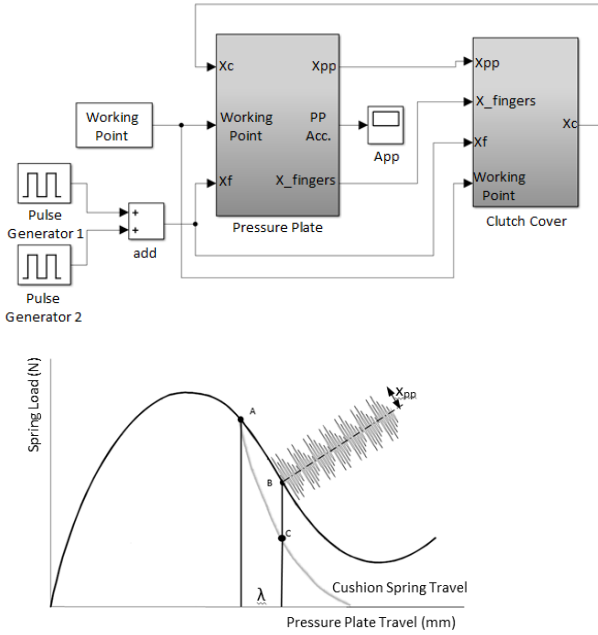


**Fig.16.** High level Simulink model on the left and pressure plate vibration during engagement phase on the right.

The model shown in Figure 16 has two pulse generators as explained in Figure 15, which simulate the engine excitation and is used as an input to the pressure plate and clutch cover. The main purpose is to find the pressure plate excitations. Following, simulation results will be compared with measurements.

In order to build sub-models, the mathematical equations should be obtained for vibrations. The following dynamic equations are of the system shown in Figure 15. Vibrations of the pressure plate are shown in Figure 16 on the right where point A shows the engaged position of the pressure plate (operation point), point B represents the disengagement phase at pressure plate travel  $\lambda$ , and point C shows the cushion spring loading at pressure plate travel  $\lambda$ .

$$m_{pp}\ddot{x}_{pp} + F_{disc\_spring} - F_{cushion} - F_{fingers} = 0 \quad (4.1)$$

$$m_c\ddot{x}_c - F_{cushion} + F_R + k_c \times (x_c - x_f) = 0 \quad (4.2)$$

Where  $m_{pp}$  is the pressure plate mass,  $\ddot{x}_{pp}$  is pressure plate acceleration,  $x_{pp}$  is the pressure plate travel around point B in Figure 15,  $\lambda$  represents pressure plate travel from the point where pressure plate vibrations are calculated,  $F_{disc\_spring}$  is the load on the disc spring,  $F_{cushion}$  is the load on the cushion spring,  $F_{fingers}$  is the load on the pressure plate created by the release load,  $m_c$  is the cover mass,  $\ddot{x}_c$  is the cover acceleration,  $x_c$  is the cover displacement,  $F_R$  is the release load on the diaphragm fingers,  $k_c$  is the cover stiffness given in Figure 8 and  $x_f$  is the secondary flywheel displacement. Now, we will write the terms in Eqs. (4.1) and (4.2) with known parameters as follows

$$F_{disc\_spring} = F_{diaph}(\lambda + x_{pp} - x_c) \quad (4.3)$$

Where  $F_{diaph(.)}$  is the clamp load at any  $x_{pp}$  (characteristic load curve for  $F_{diaph}$  is shown in Figure 6). Moreover,

$$F_{cushion} = F_{cush}(\lambda + x_{pp} - x_f) \quad (4.4)$$

Where  $F_{cush(.)}$  is the cushion spring load at any  $x_{pp}$  which is given in Figure 7. In addition,

$$F_{fingers} = F_R \times i = F_{release}(x_{release} - x_c) \times i \quad (4.5)$$

Where  $F_{release(.)}$  is the release load characteristic dependent on release travel given in Figure 9,  $x_{release}$  is the release bearing travel at  $(\lambda + x_{pp})$  pressure plate travel and  $i$  is the clutch ratio. We can write this equation with  $x_{pp}$  by using lift off curve which is also given in Figure 9 as follows

$$x_{release} = k_{lift}(\lambda + x_{pp}) \quad (4.6)$$

that results in

$$F_{fingers}(\lambda + x_{pp}) = F_{release}(k_{lift}(\lambda + x_{pp}) - x_c) \times i \quad (4.7)$$

Where  $k_{lift(.)}$  is the lift off curve characteristic which gives the pressure plate travel against release travel shown in Figure 9 on the right. We can also write release load  $F_R$  in Eq. (4.2) as follows

$$F_R = F_{release}(x_{release} - x_c) = F_{release}(k_{lift}(\lambda + x_{pp}) - x_c) \quad (4.8)$$

Then, Eq. (4.1) and Eq. (4.2) become as follows

$$m_{pp}\ddot{x}_{pp} + F_{diaph}(\lambda + x_{pp} - x_c) - F_{cush}(\lambda + x_{pp} - x_f) - F_{release}(k_{lift}(\lambda + x_{pp}) - x_c) \times i = 0 \quad (4.9)$$

$$m_c\ddot{x}_c - F_{cush}(\lambda + x_{pp} - x_f) + F_{release}(k_{lift}(\lambda + x_{pp}) - x_c) + k_c \times (x_c - x_f) = 0 \quad (4.10)$$

After deriving the differential equations, we are ready to build the corresponding Simulink models. Since we have a number of non-linear springs and tables, it will be easier to solve the equations in time domain by using the Simulink blocks. Once these equations are solved in time domain, it is easier to examine the solutions in frequency domain.

The mathematical model has the input of 2500 RPM which is in the range such that the rattle noise is in the most noticeable range (i.e., Figure 12). The Simulink sub-models for the pressure plate and clutch cover are shown in Figure 17. These Simulink models help us solve the nonlinear differential equations given by Eq.(4.9) and Eq.(4.10). Simulation results are presented in Figure 18.

Simulink model of the pressure plate is built by using the equation of the pressure plate. The model accepts flywheel vibrations (Figure 15) and pressure plate operation point (Figure 6) as the inputs and then calculates the pressure plate vibrations  $x_{pp}$  and diaphragm finger vibrations.

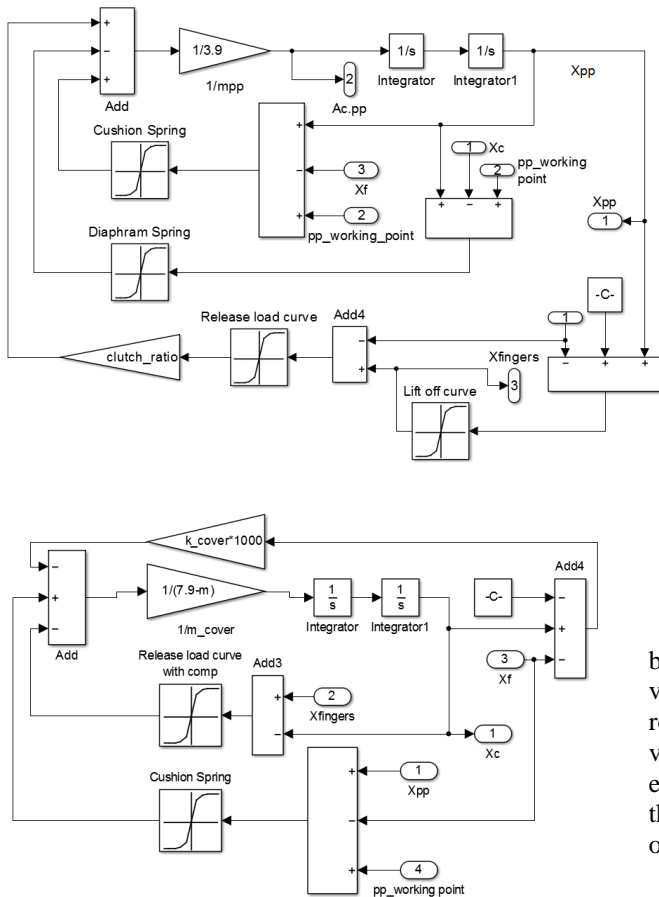


**Fig. 17.** Simulink models for the pressure plate (on the top) and clutch cover (on the bottom).

The model calculates every parameter in Eq. (4.9) by using cushion spring, diaphragm spring and release load characteristics which were explained in Section 2, e.g., see Figure 17 on the top.

Following Simulink model of the clutch cover is constructed by using the equation of the cover. The model accepts pressure plate and diaphragm finger vibrations from the previous Simulink model, pressure plate operation point and flywheel vibrations as the inputs and then calculates the clutch cover vibrations. The model calculates every parameter in Eq. (4.10) by using cushion spring and release load characteristics which were explained in Section 2, e.g., see Figure 17 on the right.

Simulation results and experimental measurements are presented in Figure 18 where it is observed that the simulation results show a good correlation with experimental measurements that are obtained by using the test bench explained in Section 3.2.

For instance, while the vibration amplitude in simulations is approximately 0.35 mm, it is 0.37 mm in experimental measurements at 2500 RPM. As mentioned before, measured flywheel vibrations are used as the excitation data in the simulation. All measurements are sampled during the engagement phase where the rattle noise occurs.

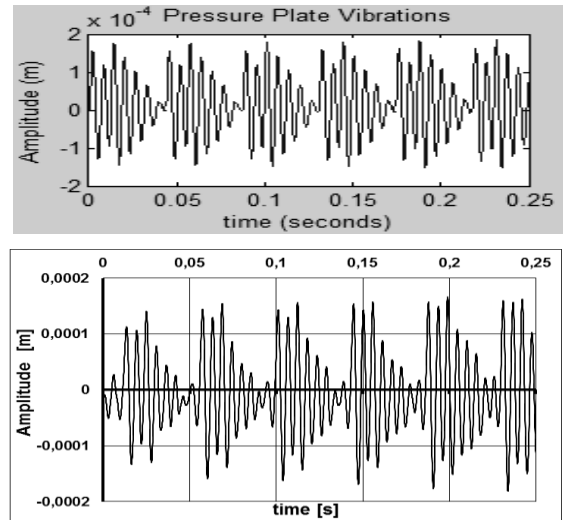


**Fig. 18.** Comparison between simulation results (on the top) and measured vibrations (on the bottom).

By examining Figure 18 in detail, we can observe that basically two different frequency contents exist in the vibrations. It is obvious that the signal content having relatively lower frequency is caused by the crankshaft axial vibrations which are exactly equal to the 0.5<sup>th</sup> order of the engine speed. As a matter of fact, this is expected because this frequency content is one of the most critical frequencies of four cylinder engines.

If we study higher frequency vibrations in Figure 18, we observe that there is a second frequency content in the vibrations having approximately the frequency spectrum of 160Hz as shown in Figure 19 for both measured and simulated data. In sum, both measured and simulated data show a dominant frequency around 160Hz and similar sub-harmonics. The corresponding FFT analyses of measured data and simulation results show that there is another peak around 145Hz as well.

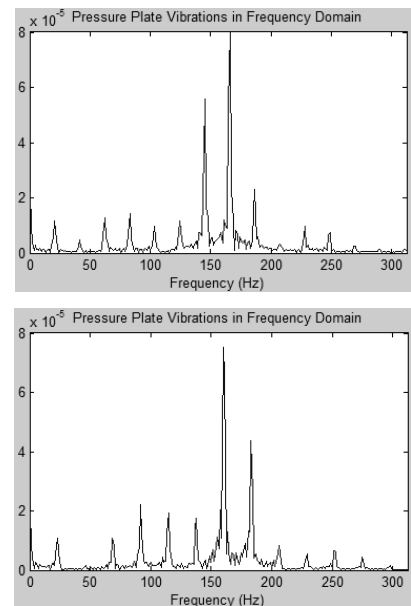


**Fig. 19.** Power spectrum of the pressure plate vibration measurements is on the left and that of simulation results is on the right.

Following, the shaker test is performed to find the natural frequencies of clutch system and reveal the other dominant frequencies as mentioned in Section 3.3. The frequency content of measurements during this test is given in Figure 20 in which it is observed that the first natural frequency of pressure plate is around 165Hz which also confirms our simulation results. These measurements also show that there is a second dominant frequency around 150 Hz which is also close to the observations in simulation results.

As mentioned before and shown in Figure 12, the worst range for the rattle noise problem is around 2500 RPM where the 4<sup>th</sup> engine order around this RPM is 167Hz which is very close to modal analysis and simulation results of axial pressure plate vibrations. Esfahani *et al* also reported the same results that the 0,5<sup>th</sup> engine order excitation caused the clutch pressure plate vibration around 4<sup>th</sup> engine order frequency [33].

To sum up, these measurements are very consistent with the simulation results. R. Esfahani et al. found that the clutch pedal vibration was around 250Hz [33]. They did not investigate the reason of this vibration. The reason was most likely that natural frequency of their clutch was around this frequency value. Since the weight of the clutch they studied was 1.9kg lighter than the one we studied, it is normal that they found the natural frequency higher than what we observed.

Hasebe et al. proposed a modified clutch assembly to change the natural frequency range of the axial clutch vibrations away from the frequency range of flywheel vibrations [48]. But, they did not clearly explain which parameters were modified. In the upcoming sections, we will also identify the most critical parameters of the clutch system and optimize the vibrations of clutch set by using multi-objective genetic optimization method while keeping the clutch release loads as low as possible.

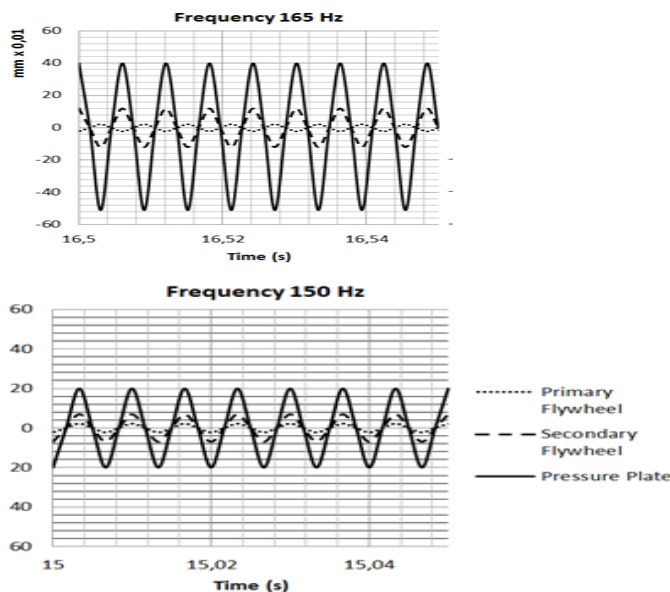


**Fig. 20.** Shaker test results shows that the natural frequency for clutch axial vibration is around 165 Hz and there is also a second axial dominant frequency at 150Hz.

## 5. Multiobjective Pareto Optimal Design of the Clutch System

In this section, a multi-objective Pareto optimal solution of the clutch system is sought by using the pedal characteristic and vibrations of pressure plate as objective functions. The first objective function is the pedal characteristic curve which is affected by a number of variables such as the geometry of diaphragm spring, material properties, release bearing stroke and dimensions of the pedal mechanism. All these variables are chosen as design variables in the related optimization problem.

The other objective function is to reduce the axial vibrations of clutch pressure plate and keep the clutch pedal load as low as possible. If design parameters are selected without considering the axial vibrations of pressure plate, excessive vibrations may emerge and cause interruptions in torque transmission during the engagement and disengagement of clutch disc. Such an interruption in torque transmission is the main cause of the well-known transmission rattle noise problem.

Note that the pressure plate mass may also be considered as an additional design variable which affects both the amplitudes of pressure plate vibrations and heat energy absorbed by clutch friction surfaces. The pressure plate mass should be as big as possible to increase the absorbed heat energy by the clutch for a longer clutch life. Thus, the heat energy absorbed by clutch friction surfaces may be considered in the Pareto optimization problem. However, it was observed in optimization runs that consideration of heat energy absorbed by clutch friction surfaces as the third objective function did not have significant effect on Pareto optimum solutions. Therefore, the heat energy absorption is calculated separately after the optimization runs are completed. Beforehand, we will investigate design variables and objective functions.

### 5.1. Design Variables

There are number of variables affecting the amplitudes of pressure plate vibrations and pedal characteristic. In order to understand the effectiveness of design variables on pressure plate amplitudes, sensitivity analysis is performed and the results are listed in Table 5.1 where all possible design variables and their effects on simulation results are presented.

It is noteworthy that all modifications on the clutch design will bring tooling and test costs to the relevant subcomponents. Therefore, it does not make sense to modify the variables which does not create a significant effect on the vibrations. Considering the effects of design variables on the costs, the best three options are the cushion deflection stiffness, mass of pressure plate and diaphragm spring stiffness. The diaphragm spring stiffness depends on the inner and outer diameters, thickness and its conical height.

**Table 5.1.** Sensitivities of variables on simulation results of pressure plate vibrations.

Variable	Increase Decrease	Effect	Magnitude of Effect
Ratio	↑ ↓	No significant effect	n/a
Pressure Plate Mass	↑	Improvement	Medium
Pressure Plate Mass	↓	Degradation	Medium
Leaf Spring Stiffness	↑	Improvement	Small
Leaf Spring Stiffness	↓	Degradation	Small
Clamp Load	↑	Degradation	Small
Cushion Deflection Stiffness	↓	Improvement	High
Cover Stiffness	↑	Improvement	Small
Cover Stiffness	↓	Degradation	Small
Diaphragm Spring Stiffness ( $h_0$ )	↑	Degradation	Medium
Diaphragm Spring Stiffness ( $h_0$ )	↓	Improvement	Medium

However, in comparison with other design variables, modifying only the conical height is the optimum way to modify the diaphragm spring stiffness due to the ease of tool modification and relatively lower cost. The rest of design variables would result in relatively higher costs, require major modifications on the tools (or may even need a new tool) and very big lead time.

**5.2. Objective Functions and Constraints**

When designing a clutch system, the first issue to be considered is to transfer the maximum engine torque to transmission system. To this end, effective clamp load should be selected carefully. Since the clamp load that is less than the required value may cause excessive slippage on the clutch system and degrades the clutch life significantly; on the other hand, the clamp load which is more than the required value may cause very high clutch pedal efforts and bad clutch feeling during the launch (e.g., very quick engagement and possible undesired stalls).

Subsequently, the first objective function should be the minimization of maximum pressure plate vibration amplitude which is the main source for rattle noise. Since the maximum vibration amplitudes are observed between the frequency range of 100 to 200 Hz (e.g., see Fig. 19 and 20), we will focus on this frequency interval for the first objective function. This frequency range also covers the 4th engine orders of the engine speed between 1500-3000 RPM range which is the critical engine order as discussed in Section 4. Moreover, as another constraint in optimization runs, the clamp load is chosen as 10,000N at the beginning of the design process which is given in the section on modeling of disc spring (i.e., Section 2.2.1).

The other basic function of the clutch system is to cut the torque transfer from the engine to transmission system when requested (to prevent stall or change transmission gear). While fulfilling this function, the maximum clutch pedal effort should be as low as possible. High pedal efforts would cause unsatisfactory drivers. Thus, the second objective function can be defined as the minimization of maximum clutch pedal effort which is directly connected with maximum release load. Considering these objective functions and constraints, the multi-objective optimization problem can be built as shown in Eq. (4.1). That is,

$$\text{minimize } x_{pp}, \text{ minimize } F_R \text{ subject to } \begin{cases} F_{clamp} \geq 10000 \\ 100 < \text{frequency} < 200 \end{cases}$$

$$m_{pp} \ddot{x}_{pp} + F_{diaph}(\lambda + x_{pp} - x_c) - F_{cush}(\lambda + x_{pp} - x_f) - F_{release}(k_{lift}(\lambda + x_{pp}) - x_c) \times i = 0$$

$$m_c \ddot{x}_c - F_{cush}(\lambda + x_{pp} - x_f) + F_{release}(k_{lift}(\lambda + x_{pp}) - x_c) + k_c \times (x_c - x_f) = 0$$

$$F_R = \frac{F_D - F_{cushion} - F_{sensor} - F_{leaf}}{i} + F_{comp}. \tag{5.1}$$

One of the functions of clutch system is to transfer the heat energy generated by the friction on disc surfaces. To this end, the clutch heat energy generation calculations are completed after the optimization runs are completed by using the following [45]

$$Q = \frac{\mu F_{clamp} V_x t_x}{2} \tag{5.2}$$

Where  $Q$  is the dissipated heat energy,  $\mu$  is the friction coefficient of clutch faces,  $F_{clamp}$  is the clamp force on the pressure plate,  $V_x$  is the vehicle speed and  $t_x$  is the time.

The ratio of  $Q/A$  for the cross sectional area  $A$  is widely used to “normalize” heat generation as a sizing parameter. This normalized value is used to evaluate clutch heat effects. In addition,  $Q/m_{pp}$  for the unit pressure plate mass  $m_{pp}$  is also used when considering “heat sink” capability of clutch pressure plate [45].

Since the clutch inner or outer diameters are not chosen as optimization parameters,  $Q/A$  will not be changed. However, we need to check  $Q/m_{pp}$  since pressure plate mass  $m_{pp}$  is an optimization variable and may be changed after the optimization runs. If the pressure plate mass  $m_{pp}$  is reduced, heat sink capability of the pressure plate will be reduced (more heat energy will need to be sank into unit mass).

### 5.3. Optimization of The Clutch System As a Dynamic System

Since we have more than one objective function, multi-objective genetic optimization algorithm in Matlab is used in the optimization runs. The genetic algorithm is a method for solving both constrained and unconstrained optimization problems based on natural selection that drives biological evolution. The genetic algorithm repeatedly modifies a population of individual solutions. At each step, it selects individuals randomly from the current population to be parents and uses them to produce the children for the next generation. At each iteration, the genetic algorithm performs a series of computations on the current population to produce a new population. Each successive population is called a new generation. An individual is any point to which you can apply the fitness functions whose value for an individual is its score. A population is an array of individuals that consist of optimization parameters. The fitness function is the name of the optimization functions for genetic algorithm [53]. Typically, the algorithm is more likely to select parents that have better fitness values.

The genetic algorithm begins by creating a random initial population by using optimization variables. The algorithm then creates a sequence of new populations. To create the new population, the algorithm performs the following steps:

1. Scores each member of the current population by computing its fitness value.
2. Scales the raw fitness scores to convert them into a more usable range of values.
3. Selects members, called parents, based on their fitness.
4. Some of the individuals in the current population that have lower fitness are chosen as elite. These elite individuals are passed to the next population.
5. Produces children from the parents. Children are produced either by making random changes to a single parent (mutation) or by combining the vector entries of a pair of parents (crossover).
6. Replaces the current population with the children to form the next generation.

As an outcome of the above described optimization problem, a Pareto chart is created. The curve in this chart is built with optimum points for both objective functions. It means that we do not have only one optimum solution, instead we have a list of optimum solutions and we need to select one of these solutions which can serve to our aim as the best result.

It must be noted at this point that all relevant optimization parameters are modified at each optimization iterations if the geometry of clutch, mass or stiffness are varied during optimization process. Thus, each iteration is actually an independent simulation which uses new design parameters and re-calculated curves.

Figure 21 shows the Pareto chart of the clutch system and optimum solutions of clutch system. The four solutions having relatively lower values for the objective functions 1

and 2 are encircled in Figure 21, which can be selected as the optimum solution by the designer. Note that the total solution time is 840 seconds on a computer having AMD Athlon 2.8 GHz dual core processor.

As it can be seen in the Pareto chart, global optimum points are calculated as;

- Cushion deflection under max clamp load =  $0.75+0.188=0.938\text{mm}$
- Pressure plate mass = 4.0387 kg
- Diaphragm spring conical height = 8.971mm

However, these values cannot be handled due to the tolerances of clutch manufacturing process. Reasonable values which can be manufactured by manufacturing processes can be found by rounding above design parameters as follows

- Cushion deflection under max clamp load =  $0.75+0.2=0.95\text{mm}$
- Diaphragm spring conical height = 9mm

Table 5.2 shows the comparison between the original parameters of the first physical clutch, optimized parameters and results of the objective functions.

The simulation results which are shown in Figure 22 are calculated by using the variables given in Table 5.2. If the results are compared with the initial system (e.g., Figure 18 and Figure 19), it can be observed that the vibration amplitudes of pressure plate are reduced by 0.06mm that is significant. This makes 0,12mm improvement in total pressure plate displacement which makes approximately 35% improvement on vibration amplitudes. The FFT results also show the same improvement especially around the frequency range of 140-160Hz.

Following, the physical model is produced by using the optimum design variables given in Table 5.2 and then tested. Experimental measurements obtained from the optimized clutch system are shown in Figure 23 in which it is observed that the experimental results give close results to simulation results. Both simulated and measured data have the same dominant frequency around 160Hz and their FFT results are very close to each other. The maximum amplitudes are also very close to each other (around 0,125mm-0,130mm).

Moreover, it is observed in the experiments that the rattle noise is reduced approximately 40% based on microphone measurements that can be observed if Figure 24 is compared with Figure 12. The measurements are performed as explained in Section 3.2. In brief, the simulation results and experimental measurements are encouraging and axial vibrations in the drive line are reduced by optimization process.

Finally, if we check the heat sink capability of optimized mass and compare with that of the initial mass (i.e., 3.9kg), we can see that the heat sink capability is

improved by 3.56% since the mass is increased; that is,  
 $\left\{ \frac{q}{3,9} / \frac{q}{4,0387} \right\} \rightarrow 3,56\%$

**Table 5.2.** Comparison of initial and optimized clutch parameters and their objective functions.

Clutch Type	Cushion Disp. (mm)	Pressure Plate mass (kg)	Diaphragm Spring Height (mm)	Max. Release load (N)	Pressure Plate Amplitudes (mm)
Initial Clutch	0,75	3,9	9,2	2250	0,185
Optimized Clutch	0,95	4,04	9	2170	0,127

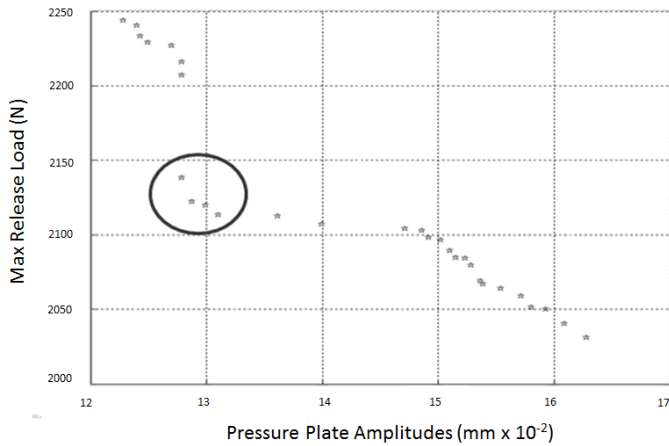


**Fig. 21.** Pareto chart of the optimization problem, where the objective #1 shows the pressure plate amplitude and the objective #2 shows the maximum pedal load.

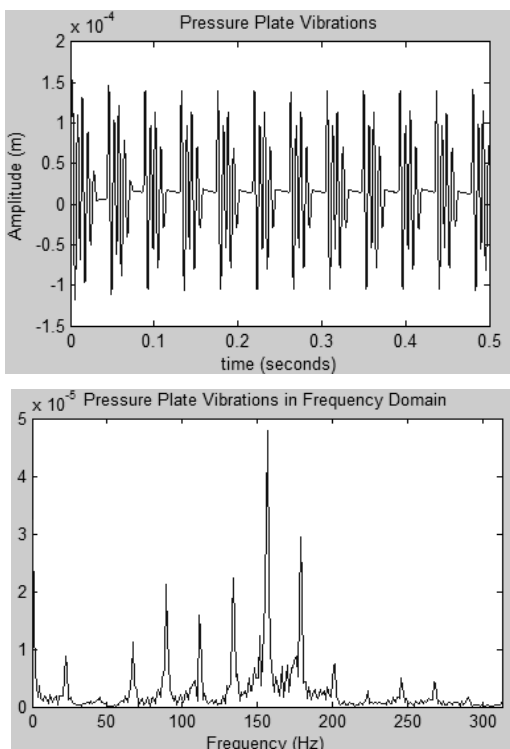


**Fig. 22.** Simulation results of pressure plate vibrations for the optimized clutch (in time domain on the top and in frequency domain on the bottom).

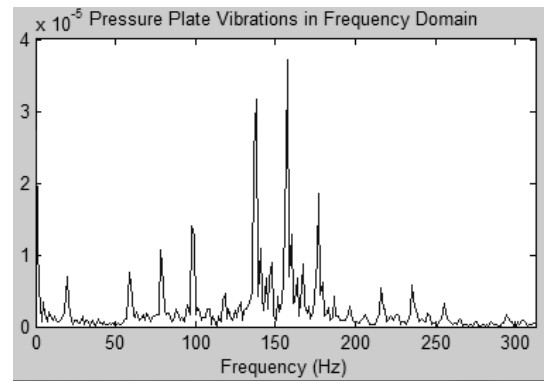
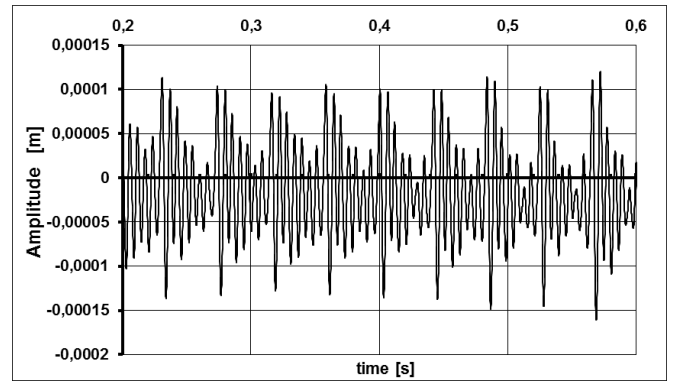


**Fig. 23.** Experimental measurements for pressure plate vibrations measured on the physical model produced by using optimized parameters (in time domain on the top and in frequency domain on the bottom).

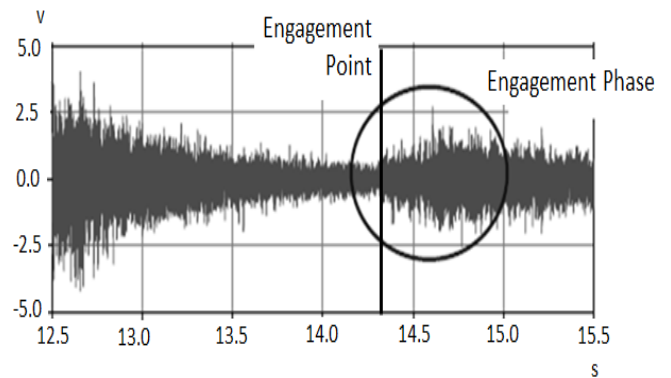


**Fig. 24.** Noise measurements of optimized system.

## 6. Conclusion

Axial vibrations in clutch systems are generally ignored in studies on dynamic behavior of clutch systems in literature, since the clutches are used to damp torsional vibrations instead of the axial ones. However, axial vibrations has to be examined for the driveline noise calculations, in particular in the existence of transmission rattle noise.

On the other hand, axial vibrations and pedal efforts are actually highly related to each other, since they are both derived by the same variables such as stiffness values of springs in the clutch and clutch ratio. To this end, mathematical models for the clutch pedal effort and clutch

pressure plate vibrations are derived and built by using the

Then, these models are verified by making comparisons with experimental measurements. By combining the simulation models together, a multi-objective optimization problem is formulated and solved such that axial vibrations and clutch pedal effort are minimized under some constraints. At the end of the study, a physical model is also produced by using the optimization results and physically tested.

It is observed that experimental measurements and simulation results are quite close to each other and axial vibrations in the drive line is reduced by optimization process. Under the light of findings of this study, it is possible to calculate and design the components of a clutch system in an optimum way, which will help decrease the test and prototype costs significantly.

On the other hand, optimizing a clutch system considering axial vibrations only will not degrade the rotational vibrations and, in order to reduce the different level of rotational vibrations from engine to transmissions (e.g., idle vibrations, creep vibrations or drive vibrations, etc...), different types of rotational dampers are used on clutch discs. However, in our study we tried to reduce the axial vibrations of disengaged clutch, thus effects of these axial vibrations during half engaged clutch position (which can be called slipping phase or engagement phase).

These axial vibrations have no influence on the system when the clutch is fully engaged since very high clamp load is already exerted on the pressure plate that prevents the axial vibrations. However, a further study may also be planned to optimize the rotational dampers so that they can be usable during engagement phase. Thus, the clutch can be optimized to minimize the axial vibrations and rotational dampers can damp the residual vibrations which cannot be fully damped by axial vibration optimization during engagement phase.

### Acknowledgements

This research received no specific grant from any funding agency in the public, commercial or not-for-profit sectors. The authors declare that there is no conflict of interest.

### References

[1] E. Galvagno, M. Velardocchia, A. Vigliani, Dynamic and kinematic model of a dual clutch transmission, *Mech. and Mach. Theory* 46 (6) (2011) 794-805.

[2] Manish Kulkarni, Taehyun Shim, Yi Zhang, Shift dynamics and control of dual-clutch transmissions, *Mech. and Mach. Theory* 42 (2) (2007) 168-182.

[3] Nowshir Fatima, Par Marklund, Roland Larsson, Influence of clutch output shaft inertia and stiffness on the performance of the wet clutch, *Tribol. Trans.* 56 (2) (2013) 310-319.

[4] Y. Zhang, X. Chen, X. Zhang, H. Jiang, W. Tobler, Dynamic modeling and simulation of a dual-clutch automated lay-shaft transmission, *J. of Mech. Des.* 127 (2) (2005) 302-307.

programs MATLAB and MATLAB-Simulink toolbox.

[5] Q. Zheng, K. Srinivasan, G. Rizzoni, Dynamic modeling and characterization of transmission response for controller design, *SAE Int.* 981094 (1998) doi:10.4271/981094.

[6] C. Pan, J. Moskwa, Dynamic modeling and simulation of the Ford AOD automobile transmission, *SAE Int.* 950899 (1995) doi:10.4271/950899.

[7] Z. S. Filipi, D. N. Assanis, A nonlinear, transient, single-cylinder diesel engine simulation for predictions of instantaneous engine speed and torque, *J. of Eng. for Gas Turbines and Power.* 123 (4) (2001) 951-959.

[8] E.M. Mockensturm, E.M. Balaji, Piece-wise linear dynamic systems with one-way clutches, *J. of Vib. and Acoust* 127 (5) (2005) 475-482.

[9] F.R. Zhu, R.G. Parker, Non-linear dynamics of a one-way clutch in belt-pulley systems, *J. of Sound And Vib.* 279 (1-2) (2005) 285-308.

[10] T. Petrun, J. Flaska, M.A. Kegl, *Friction model for dynamic analyses of multi-body systems with a fully functional friction clutch*, *J. of Multibody Dyn.* 227 (2) (2012) 89-105.

[11] A. R. Crowther, N. Zhang, Torsional finite elements and nonlinear numerical modelling in vehicle powertrain dynamics, *J. of Sound and Vib.* 284 (3) (2005) 825-849.

[12] C. Duan, R. Singh, Influence of harmonically varying normal load on steady-state behavior of a 2dof torsional system with dry friction, *J. of Sound and Vib.* 294 (3) (2006) 503-528.

[13] C. Duan, R. Singh, Dynamics of a 3dof torsional system with a dry friction controlled path, *J. of Sound and Vib.* 289 (4) (2006) 657-688.

[14] C. Padmanabhan, R. Singh, Influence of clutch design on the reduction and perception of automotive transmission rattle noise, *Noise-Con 93* (1993) 607-612.

[15] H. Moradi, H. Salarieh, Analysis of nonlinear oscillations in spur gear pairs with approximated modelling of backlash nonlinearity, *Mech. and Mach. Theory* 51 (2012) 14-31.

[16] T. C. Kim, T. E. Rook, R. Singh, Super - and sub-harmonic response calculations for a torsional system with clearance nonlinearity using the harmonic balance method, *J. of Sound and Vib.* 281 (3) (2005) 965-993.

[17] T. C. Kim, T. E. Rook, R. Singh, Effect of nonlinear impact damping on the frequency response of a torsional system with clearance, *J. of Sound and Vib.* 281 (3) (2005) 995-1021.

[18] J. Awrejcewicz, D. Grzelczyk, Modeling and analytical/numerical analysis of wear processes in a mechanical friction clutch, *Inter. J. of Bifurc. and Chaos* 21 (10) (2011) 2861-2869.

- [19] W. Zhang, G. Zhu, Research and application of PSO algorithm for the diaphragm spring optimization, Forth Inter. Conf. on Nat. Comput. (2008) 549-553.
- [20] W. Yong-hai, Multi-objective optimization design of vehicle clutch diaphragm spring, Second Inter. Conf. on Intell. Comput. Technol. and Autom. (2009) 194-197.
- [21] X. Guo, H. Lu, Optimal design on diaphragm spring of automobile clutch, Second Inter. Conf. on Intell. Comput. Technol. and Autom. (2009) 206-208.
- [22] A. Li-jun, L. Tao, S. Bao-yu, Optimum design of automobile diaphragm spring clutch, IEEE Veh. Power and Propuls. Conf. (2008) 1-4.
- [23] G. Ercole, G. Mattiazzo, S. Mauro, M. Velardocchia, F. Amisano, G. Serra, Experimental methodologies to determine diaphragm spring clutch characteristics, SAE Int. (2000) 10.4271/2000-01-1151.
- [24] W. Nam, C. Lee, Y. Chai, J. Kwon, Finite element analysis and optimal design of automobile clutch diaphragm spring, SAE Int. (2000) 2000-05-0125.
- [25] W. Jin, Solid modeling and finite element analysis of diaphragm spring clutch, Manag., Manuf. and Mater. Eng 452-453 (2012) 258-263.
- [26] J. O. Almen, A. Laszlo, The uniform section disk spring, ASME 58 (1936) 305-314.
- [27] G. Wempner, Axisymmetric deflections of shallow conical shells, J. of Eng. Mech. 90 (2) (1964) 181-194.
- [28] G. Curti, M. A. Orlando, New Calculation of Coned Annular Disk Spring, ASME Winter Annual Meet. (1976).
- [29] Y. Zhiming, Y. Kaiyuan. A Study of Belleville Spring and Diaphragm Spring in Engineering. J. of Appl. Mech. 57 (4) (1990) 1026-1031.
- [30] S. Ozaki, K. Tsuda, J. Tominaga, Analyses of static and dynamic behavior of coned disk springs: effects of friction boundaries, Thin-Walled Struct. 59 (2012) 132-143
- [31] E. Fromm, W. Kleiner, Handbook for Disc Springs, Heilbronn, SCHNORR, 2003.
- [32] J. E. Shigley, C. Mischke, Standart Handbook of Machine Design, third ed., McGraw-Hill, San Francisco, 2004.
- [33] R. Esfahani, A. Farshidianfar, A. Shahrjerdi, F. Mustapha, Longitudinal vibrations analysis of vehicular clutch, Aust. J. of Basic and Appl. Sci. 3 (4) (2009) 3633-3641.
- [34] R. Singh, H. Xie, R. J. Comparin, Analysis of automotive neutral gear rattle, J. of Sound and Vib. 131 (2) 1989 177-196.
- [35] S. Theodossiadis, O. Tangasawi, H. Rahnejat, Gear teeth impacts in hydrodynamic conjunctions promoting idle gear rattle, J. of Sound and Vib. 303 (3) (2007) 632-658.
- [36] E. Rocca, R. Russo, Theoretical and experimental investigation into the influence of the periodic backlash fluctuations on the gear rattle, J. of Sound and Vib. 330 (20) (2011) 4738-4752.
- [37] Y. Kadmiri, E. Rigaud, J. P. Laudet, L. Vary, Experimental and numerical analysis of automotive gearbox rattle noise, J. of Sound and Vib. 331 (13) (2012) 3144-3157.
- [38] M. Barthod, B. Hayne, J. L. Tebec, J. C. Pin, Experimental study of gear rattle excited by a multi-harmonic excitation, Appl. Acoust. 68 (9) (2007) 1003-1025.
- [39] X. Wang, B. L. B. Gadegbeku, L. Bouzon, Biomechanical evaluation of the comfort of automobile clutch pedal operation, Int. J. of Ind. Ergon. 34 (3) (2004) 209-221.
- [40] A. Shabibi, Solution of heat conduction problem in automotive clutch and brake systems, Proc. of 2008 ASME Summer Heat Transf. Conf. 321 (2008).
- [41] A. R. Crowther, C. Janello, R. Singh, Quantification of clearance-induced impulsive sources in a torsional system, J. of Sound and Vib. 307 (3-5) (2007) 428-451.
- [42] C. Duan, R. Singh, Super-harmonics in a torsional system with dry friction path subject to harmonic excitation under a mean torque, J. of Sound and Vib. 285 (4-5) (2005) 803-834.
- [43] W. Reik, The self-adjusting clutch – SAC, 05th LuK Symp. (1994) 43-62.
- [44] K. L. Kimming The Self-Adjusting Clutch SAC of the 2<sup>nd</sup> Generation, LuK Symp. (1998) 5-22.
- [45] R. Shaver, Manual Transmission Clutch System, first ed., Warrendale: SAE, (1997), p: 28, 59-63.
- [46] A. Reitz, J. W. Biermann, P. Kelly, Special Test Bench to Investigate NVH Phenomena of the Clutch System, Inst. für Kraftfahrwesen Aachen
- [47] P. Kelly, H. Rahnejat, Clutch Pedal Dynamic Noise and Vibration Investigation, Proc. of the 1<sup>st</sup> Int. Symp. on Multi-Body Dyn.: Monit. and Simul. Tech., Bradford, UK, MEP Press, 1997
- [48] T. Hasabe, U. A. Seiki, Experimental Study of Reduction Methods for Clutch Pedal Vibration and Drive Train Rattling Noise from Clutch System, SAE Int. 932007 (1993). doi:10.4271/932007
- [49] M. Özbakiş, Observation and optimization of the characteristic of the diaphragm springs used in clutch systems, Master Thesis, Dokuz Eylül University, Turkey, 2008.
- [50] A. Hagerodt, F. Küçükay, Optimum Design of Return and Cushion Springs for Automatic Transmission Clutches, SAE Int. 2001-01-870 (2001)
- [51] V. Arora, G. Bhushan, M. L. Aggarwal, Eye Design Analysis of Single Leaf Spring in Automotive Vehicles Using CAE Tools, Int. J. of App. Eng. And Tech. 1 (1) (2011) 88-97.
- [52] V. Arora, M. L. Aggarwal, G. Bhushan, A Comparative Study of CAE and Experimental Results of

Leaf Springs in Automotive Vehicles, Int. J. of Eng. Sci. and Tech. 3 (9) (2011) 6856-6866.

[53] Genetic Algorithm and Direct Search Toolbox™  
User's Guide, Natick, The MathWorks, Inc, (2009), p:48.

# Position Singularities and Ambiguities of the KUKA KR5 Robot

Géza Husi\*‡

\* Head of Department, University of Debrecen, Faculty of Engineering, Department of Electrical Engineering and Mechatronics, Postal address: 4028 Debrecen, Hungary, Ótemető street 2-4

husigeza@eng.unideb.hu

‡ Corresponding Author; Géza Husi, 4028 Debrecen, Hungary, Ótemető street 2-4, Telefon:+36 (52) 415-155 Extension:77743

,husigeza@eng.unideb.hu

*Received: 26.01.2015 Accepted:14.03.2015*

**Abstract-** Recently in the Robot technological laboratory of the Department of Electrical Engineering and Mechatronics (EEM) of the Faculty of Engineering, University of Debrecen there have been several researches concerning the KUKA and SONY Scara robots. The first part of the paper is a theoretical summary deducing the notions concerning robots from the general system technique. I tried to draft all the definitions as precisely as possible to be able rely on them, only to find out the complexity of the required mathematical apparatus necessary for getting to know the nature of this problem, albeit knowing the mathematics of the Denavit–Hartenberg transformation and the use of the Jacobi-matrix. This paper summarizes the singularity of robot positions and their uncertainty by analyzing the KR5 industrial robot in the Robot Technological Laboratory in the EEM. This paper regards the definition of the ISO 8373:2012 standard as a base and deduces all ideas and relations from this standard. ISO 8373 was prepared by the Technical Committee ISO/TC 184, Automation Systems and Integration, Subcommittee SC 2, Robots and Robotic Devices.

**Keywords** KUKA KR5; singularities; style; ambiguities.

## 1. Introduction

At present, more than 1 million programmable industrial robots work in the industries of the world. Programmable industrial robots are suitable for carrying out series of movements and usually move tools and pieces of work seriatim or continuously in accordance with the program in the memory of their controller. Having finished the assigned tasks with their work envelope, they resume their basic position and then repeat the programmed series of movements under the influence of the next starting signal.

Configurations are referred to singular configurations or singularities, where the rank of the Jacobian matrix is not maximal.

Identification of the singularity of the robot arm is an important task on more reason:

- Singularities mark configurations whereby moves of the tool centre point (TCP) in a certain direction cannot be achieved, i.e. the robot arm loses from its degrees of freedom.

- In case of singularities to bounded TCP speeds, unbounded joint speeds belong, because these can extinguish each other.

- In case of singularities to bounded robot arm forces and torques, unbounded joint forces and torques belong.

The singularity of the position of robots and the unambiguous position and orientation of robot arms are some of the most important criteria for carrying out series of movements and for the repeatability and the accuracy of repetition of these movements. This singularity determines the repetition and dynamic accuracy as well as the accuracy of the orientation determined independently from the state of the tools within the work envelope.

6565 of the tool centre point (TCP) in a certain direction cannot be achieved for an undetermined reason, i.e., the robot arm loses its degrees of freedom. In industrial manipulator machines, the position of robot arms defined in relation to each other is determined by their state. The well-selected determination of states and their changes are suitable to avoid this problem.

Singularity issues need to account for its specific deployment and usage in industry and business and how this

impacts on the various stakeholders and constituents along the robotic continuum, given the impacts and influences of research and the overriding and even overarching impacts of robotic theorists, practitioners and others involved in this processes, from conceptualization, drawing board stage, design and assembling, mounting and operationalizing and finally its deployment in industry and business for gains.

Mathematically, a Jacobian mathematical matrix formulation can be used to relate the movement in joint space to the movement in Cartesian space. A singularity occurs when the inverse Jacobian becomes singular (determinant = 0).

## 2. Theoretical Summary

A body will stand underneath a force and its movement will be a constrained movement if its six possible coordinates cannot have optional values and if the connection between them is a constrained condition. The constrained condition includes the accessory geometric conditions delimiting the effect of the free forces affecting a system, which consists of mass points, systems of points and rigid bodies and therefore the movement of the system. Due to constrained conditions, these systems perform a constrained movement. In practice, the movements are usually constrained movements because all elements of a mechanism shall perform a movement designated by another structural element as a force. Forces prescribing constrained movements may be at a standstill, but they can also move (standing and moving forces). Forces are usually functions of the location, time and relative speed.

The mechanism is a moving structure consisting of rigid bodies in connection with each other causing constrained movement. Connected rigid bodies are called the members of the mechanism. A selected member is “the base frame” (the movements of all other members of the mechanism are analysed in comparison to the base frame) The relationship between coordinates can be described by means of the constrained movement equations below if out of six possible coordinates, three indicate a relative displacement ( $x_{12}$ ,  $y_{12}$ , and  $z_{12}$ ) and the other three indicate angular rotation ( $\varphi_{x12}$ ,  $\varphi_{y12}$ ,  $\varphi_{z12}$ ):

$$s_{12} = f(x_{12}, y_{12}, z_{12}, \varphi_{x12}, \varphi_{y12}, \varphi_{z12}). \quad (2.1)$$

(Interpretation: member 2 is displaced in comparison to the first member by the  $x_{12}$  value, etc.). If the relationship between coordinates depends on time, the previous equation can be described in the form:

$$s_{12} = f(x_{12}, y_{12}, z_{12}, \varphi_{x12}, \varphi_{y12}, \varphi_{z12}, t). \quad (2.2)$$

and these two equations have a serious importance. If the relationship between coordinates does not depend on time, the force is a passive force; if the relationship also depends on time, the force is called an active force.

In the case of a body or mechanism, the degree of freedom is the number of free coordinates independent of each other that evidently determine the position of the body (mechanism). In the case of a force, this means the number

of free coordinates independent of each other that evidently determine the position of members in comparison to each other. There are three different degrees of freedom connected with each other.

- Geometric degree of freedom – the degree of freedom of forces as passive forces is indicated by  $\gamma$  (this parameter also means the registration number of the system, force).
- Kinematic degree of freedom - the degree of freedom of forces as active forces is indicated by  $\sigma$ .
- Degree of restriction – the number of restricted coordinates, coordinates in the function are indicated by  $\kappa$ .

The degree of restriction and the degree of freedom are complementary properties, and their sum is always equal to the degree of freedom, with restriction as high as possible.

In the case of force, the number of degrees of freedom is equal to 6, so the

- Geometric degree of restriction:

$$\kappa_g = 6 - \gamma. \quad (2.3)$$

- Kinematic degree of restriction:

$$\kappa_s = 6 - \sigma. \quad (2.4)$$

The degree of restriction is equal to the number of constrained movement equations to be written.

A kinematic linkage may be opened (opened kinematic linkage) if its last member is not connected to any previously denoted member. The last member of the robot may work free and not be connected to any other member except the member position in front of it through the joint. This last member (terminal member) is called a peripheral member.

Definition: The main property of six-axis industrial robots functioning as mechanisms with an opened kinematic linkage is that the member has separate drivers on all of its joints. The structure can be described on the basis of the structural formula.

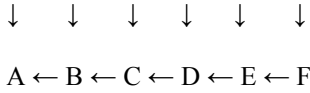
A robot arm having six degrees of freedom (6 DOF) is necessary to grasp a subject in a certain position from an optional direction (3 spatial coordinates + 3 orientation angles). All of these require at least six joints independent of each other. As far as the types of joints are concerned, they may be rotating (R) or dislocating (T). These joints are called elementary joints, i.e., joints having a degree of freedom of one. For one joint it is valid that

$$x_{12} = y_{12} = z_{12} = 0 \text{ and } \varphi_{x12} = \varphi_{y12} = 0 \quad (2.5)$$

and  $\varphi_{z12}$  can be optimally determined (certainly within geometric limits).

A 6-DOF industrial robot manipulator consists of six joints assuring rotating movements, and the first member is regarded as the base frame because it is fixed and thus does not move during the operation of the robot. This property makes it suitable for bearing the inertia system of the robot called world system of coordinates.

Its structural formula is below.



The open-linkage robot arms are determined by enumerating the types of joints advancing from the base towards the arm, e.g., RRP. Roll joints perform a rotation around an axis, while slider-crank joints perform a sliding action along an axis. This axis is called the effect axis of the given joint. The position of all joints can be determined by means of only one parameter: roll value or slide value. This is the  $q = (q_1, \dots, q_n)$  vector called the configuration of the manipulator machine. The number parameters (i.e., joints) are called the degrees of freedom of the robot arm.

The industrial robot is a mechanism consisting of rigid bodies in a constrained connection with each other. Its specialty lies in that all of its members can be driven at the same time, and the movement of a given member can be described in a relatively simple way.

The kinematic linkage is called an opened linkage if both of its ends are connected by only one sequence of segments. The contrary case is referred to as a closed linkage.

Robot kinematics applies geometry to the study of the movement of multi-degree of freedom kinematic chains that form the structure of robotic systems. [1] [2]. A robot usually measures its inner kinematic parameters and joint coordinates directly. Those coordinates measure the position of the joints. We usually denote them as  $q$ . The joint coordinate of the revolute joint is denoted as  $\theta$ , and the joint coordinate of the prismatic joint is denoted as  $d$ . The user is interested in the position of the end effector or the position of the manipulated rigid body. The robot has six DOFs and could be described in a number of ways, e.g., by the transformation matrix describing the position of the end effector coordinate system in the world coordinate system. During the operation of the robot, two tasks are possible:

- When the robot parameter vectors are known (direct geometric modelling), the column vector determining the position of moved points shall be determined, and the tool centre point values can be calculated by means of robot joint values (forward kinematic).
- When the column vector determining the position is known, the vector of robot parameters shall be determined (inverse geometric task), and joint values are calculated by means of the tool centre point values.

In the general case, when the trajectory covered by the programmed point is known and on the basis of this knowledge, the vector of robot parameters describing the position and movement of robot arms in comparison to each other shall be determined. This vector is the solution of an inverse geometric task (inverse kinematic).

As far as general embodiment of the connection of robot arms by means of joints is concerned, the connection produces the connection chain shown in Fig.1.

The position of the coordinate systems fixed to arms with respect to their transformation into each other can generally be presented as shown in Fig. 2. Let us regard the two coordinate systems, one succeeding the other, determined with the features indicated in Fig. 2.

$$R_{i-1,i} = \begin{bmatrix} \cos q_i & -\sin q_i \cos \alpha_i & \sin q_i \sin \alpha_i \\ \sin q_i & \cos q_i \cos \alpha_i & -\cos q_i \sin \alpha_i \\ 0 & \sin \alpha_i & \cos \alpha_i \end{bmatrix} \tag{2.6}$$

The beginning point of the  $(x_{i-1}, y_{i-1}, z_{i-1})$  coordinate system shall be moved a distance  $P$  so that the two coordinate system cover one another.

$$P = \begin{bmatrix} a_i \cos q_i \\ a_i \sin q_i \\ d_i \end{bmatrix} \tag{2.7}$$

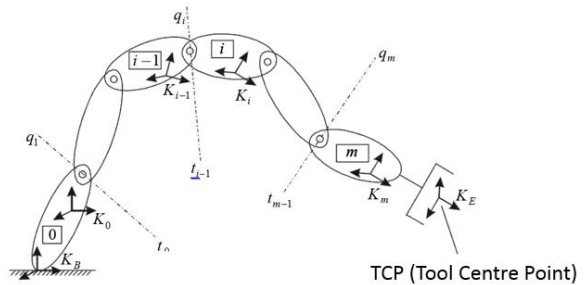


Fig.1. Principal scheme of a robot having an opened chain without embranchment [3]

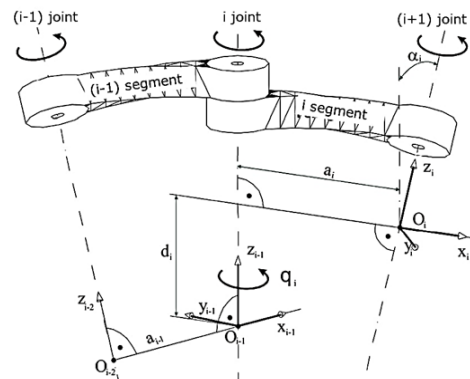


Fig.2. Denavit-Hartenberg method [4].

The  $R_{i-1,i}$  matrix can be extended with the P vector. When using homogeneous coordinates after rotation around the  $x_i$  and  $z_i$  axes and movement along the  $x_i$ ,  $y_i$  and  $z_i$  axes, we obtain the so-called Denavit–Hartenberg matrix by simultaneously interpreting the rotation and movement [5].

$$DH_{i-1,i} = \begin{bmatrix} \cos q_i & -\sin q_i \cos \alpha_i & \sin q_i \sin \alpha_i & a_i \cos q_i \\ \sin q_i & \cos q_i \cos \alpha_i & -\cos q_i \sin \alpha_i & a_i \sin q_i \\ 0 & \sin \alpha_i & \cos \alpha_i & d_i \\ 0 & 0 & 0 & 1 \end{bmatrix} \quad (2.8)$$

The transformation of joint coordinates into world coordinates occurs by means of the Denavit–Hartenberg transformation matrix. Denavit and Hartenberg published this method in 1955, so it is named Denavit–Hartenberg method [4]. The substance of the method lies in transforming a system of coordinates into another system of coordinates by means of two translation and two rotating movements. The Denavit–Hartenberg parameters used in robot manipulator machines are the distances  $d$  and  $a$  and the angles  $\alpha$  and  $q$ .

The transformation between coordinate systems (j and k) can be written by means of the

$$\bar{j} = DH_{jk} \bar{k} \quad (2.9)$$

matrix equation.

### 3. The K5 Robot

The KR5 robot consists of six joints that assure rotating movements, so its basic configuration is RRR. The recurring elements of the robots are robot arms and joints connecting arms. The connection object is oriented. One joint connects two arms, and one arm connects two joints. The KR5 robot consists of six joints that assure rotating movements, and the first member is regarded as the base frame because this member is fixed and does not move during the operation of the robot. This property makes it suitable for bearing the inertial system of the robot called the world coordinate system. Fig.3 shows the coordinate systems of robot. For controlling KUKA robots, four types of Descartes systems of coordinates are determined:

- WORLD
- ROBROOT
- BASE
- TOOL.

All robots have a controlling unit, the most important task of which is regulation of driving, as mentioned before in accordance with incoming signals and previously programmed commands. The Controller Cabinet has been given the name KUKA KR C2.

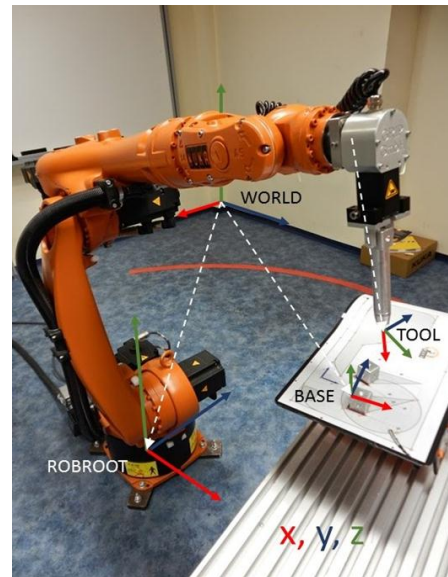


Fig.3. Robot systems of coordinates.

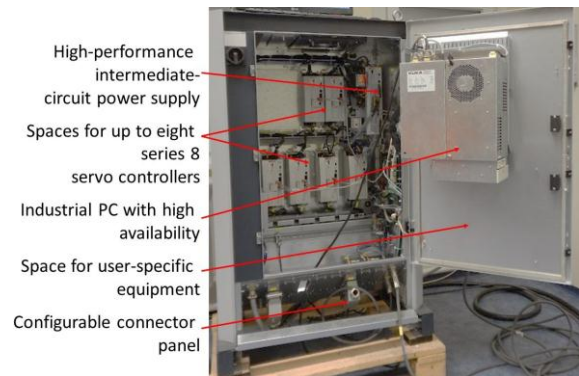


Fig.4. KUKA KR C2 controller cabinet

Two processors are in the Controller Cabinet because two servo units, two processors interpreting and running the program as well as another moving processor coordinating the axis movements of the robot are necessary for driving servo-motors because the synchronisation of the movement of six axes is an important task. The controlling unit is connected with the robot by a CAN bus cable of DeviceNet type. This unit is a serial bus system enabling the contact between the robot and tool connected to it (reception and sending).

Industrial robots can be classed into two groups on the basis of their programming. Different robots carry out different working processes, so different working processes require different programming techniques. The two large groups are ON-LINE and OFF-LINE programming. KUKA can be programmed by using both of these programming methods using KRL 5.5 (KUKA Robot Language 5.5).

### 4. Synchronising Problems in Different Coordinate Systems

A serious problem may arise in planning the movement of the KRS robot when right-angled coordinate systems (WORLD, ROBROOT, BASE, TOOL) are used for the plan as the actual movement is realized in a polar coordinate

system due to the structure of the robot (robot with opened chain and without embranchment) and the rotating movement of its arms in a polar coordinate system. This property means that the position and orientation determined in the right-angled coordinate system are determined by the angular position of the 6 joints of the 6-axis robot.

In any case, when the programmer employs a right-angled coordinate system to program the movement of the robot, the controller transforms the values determined in the right-angled coordinates into the joint angular turn of the arm and then processes the feedback signal from the motor conducting the movement. A permanent coordinate transformation (Fig. 5.) occurs in the controller during the movement.

The situation gets more complicated, as 4 right-angled coordinate systems (WORLD, ROBROOT, BASE, TOOL) can be used, and positions in each can be transformed into the others. The position and orientation of the robot can in principle be defined in the following coordinate systems. In the AXIS-specific coordinate system (A), each axis can be moved individually in a positive or negative direction. The ROBROOT coordinate system (R) is a Cartesian coordinate system that is always located at the robot base. It defines the position of the robot relative to the WORLD coordinate system. By default, the ROBROOT coordinate system is identical to the WORLD coordinate system. ROBROOT allows the definition of an offset for the robot relative to the WORLD coordinate system. The WORLD coordinate system (W) is a permanently defined Cartesian coordinate system. It is the root coordinate system for the ROBROOT and BASE coordinate systems. By default, the WORLD coordinate system is located at the robot base. For achieving the 3 degrees of freedom in positioning, the base configuration of the robot is necessary. The axis-specific coordinate of the robot is a scalar value defining the relative position of a segment of the kinematic match in comparison to the other segment. In the rotation joint, the joint coordinate corresponds to the rotation angle of the joint. The axis-specific coordinate of the robot is indicated as follows:

$$q_i \quad i=1,2,\dots,n \quad (4.1)$$

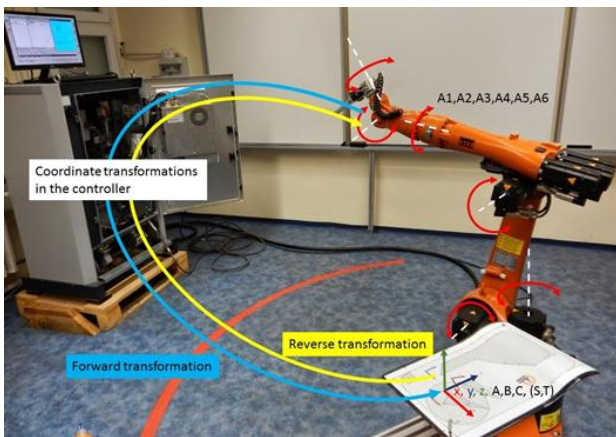


Fig.5. Coordinate transformations in the controller.

While the vector of coordinates is:

$$q = [q_1 \ q_2 \ \dots \ q_n]^T \quad (4.2)$$

The axis-specific axis of the KR5 robot, which has 6 degrees of freedom. All axis-specific coordinates can change within certain limits:

$$q_{imin} \leq q_i \leq q_{imax} \quad (4.3)$$

During the positioning of the joints, an important condition is that the orientation of the effector also changes so that the orientation of the effector will be corrected after all movements occurring in axis-specific coordinates. Robot coordinates define the position and orientation of the manipulator machine of the robot in a Cartesian (Descartes) right-angled coordinate system. This coordinate system is fixed to the base of the robot. The position of the effector can be represented as the three Descartes right-angled coordinates (x, y, z). In practice, the world coordinates and robot coordinates correspond to each other. In the coordinate system of the robot, the lower plane of the robot base and the cutting point of the rotation axis (first axis) of the first motor define the origin, while the x axis is the bisector of the angle defined by the end points ( q\_1min and q\_1max ) of the first axis and the origin. The orientation of the effector can be represented as modified Euler angles: φ, θ, ψ. These angles define the angular rotation of the moving coordinate system fixed to the effector with respect to the robot coordinate system. The effector has its own coordinate system, termed the TOOL coordinate system.

The TOOL coordinate system (T) is a Cartesian coordinate system that is located at the tool centre point. By default, the origin of the TOOL coordinate system is located at the flange centre point (in this case it is termed the FLANGE coordinate system.) The TOOL coordinate system is offset from the tool centre point by the user. The optional position and orientation of a robot can be represented in the world coordinate system as follows:

$$S_W = [x, y, z, \varphi, \theta, \psi]^T \quad (4.4)$$

Where,

- The x, y, z coordinates represent the vector (position) from the origin of the world coordinate system to the TCP (tool coordinate system);
- The φ, θ, ψ rotations indicate the rotation of the axes of the world coordinate system in parallel with those of the tool coordinate system (positioning).

If the world coordinates and robot coordinates correspond to each other as,

$$O_W = O_R \text{ and } x_W = x_R; y_W = y_R; z_W = z_R, \quad (4.5)$$

The  $S_W$  vector will correspond to the optional position and orientation of the robot in the ROBROOT coordinate system:

$$S_W = S_R. \tag{4.6}$$

**5. Ambiguities**

During the solution of the inverse kinematic task, the number of solutions is  $> 1$ . This means that the TCP is in the appropriate position, but the position of the arm is not unambiguous. As an example, let us consider Fig. 6. The example in the upper part of the figure shows that, with respect to joint 2, joint 5 can achieve the same position in two different ways, depending on the relative positions of joint 2 and 3. In the example in the lower part of Fig. 5, it is clear that the grasping position will not change as long as a turn by axis 4 in any direction is countered by the same degree of turn by axis 6 in the opposite direction. In this latter case, the ambiguity of position value of the arm is not two but infinite, and this state can be maintained not only in the case of discrete values but also permanently over time. The problems concerning robot arm ambiguities of position can only partially be managed by the KRC 2 robot controller of the KUKA KR5 robot and the KRL 5.5 robot programming language. During programming, the positions of an arm in comparison to each other (S Status) and the direction of a turn (T Turn) can be separately given. The entries “S” and “T” (Fig.7) in a position (POS) specification serve to select a specific, unambiguously defined robot position when several different axis positions are possible for the same point in space (because of kinematic singularities).

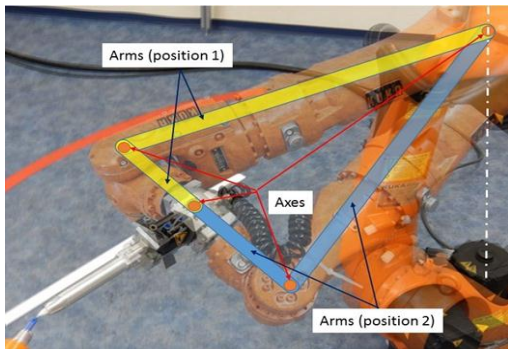


**Fig.6.** Examples of ambiguous robot kinematics.

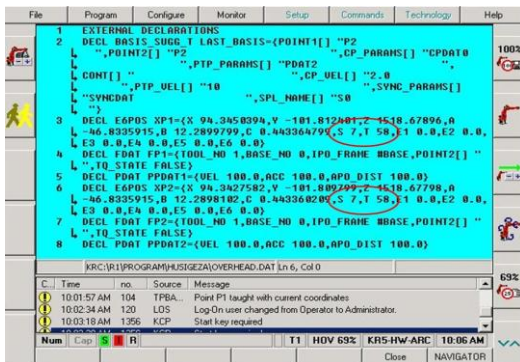


**Fig.7.** Status and Turn.

**6. The Singularity**

The singularity is defined as the configuration of a robot position that is accompanied by the loss of a degree of freedom. Configurations for which the rank of the Jacobi matrix does not have the maximum value are called singular configurations, or singularities. The examination of Jacobi matrix ranks is important in the inverse velocity aspect, as it becomes obvious that, in the whole rank case, the solution can be calculated very easily. A further denomination is that the singularities of the  $B(\alpha)$  matrix are termed representative singularities [6].

It can be easily shown on the basis of the formula [6]:

$$B(\alpha) = \begin{bmatrix} \cos \psi \sin \theta & -\sin \psi & 0 \\ \sin \psi \sin \theta & \cos \psi & 0 \\ \cos \theta & 0 & 1 \end{bmatrix} \tag{6.1}$$

That, in the case of  $\sin \theta \neq 0$ ,  $B(\alpha)$  can be inverted, which is important for the complete rank state on the basis of the equation

$$J_a(q) = \begin{bmatrix} I & 0 \\ 0 & B(\alpha)^{-1} \end{bmatrix} J(q) \tag{6.2}$$

These equations show that the singularities of the analytic Jacobi matrix include representation of the singularities of the geometric Jacobi matrix. According to its definition, the  $6 \times n$   $J(q)$  Jacobi matrix determines a value

$$\xi = J(q)\dot{q} \tag{6.3}$$

mapping between the  $dq/dt$  vector of the velocity of the joint and the

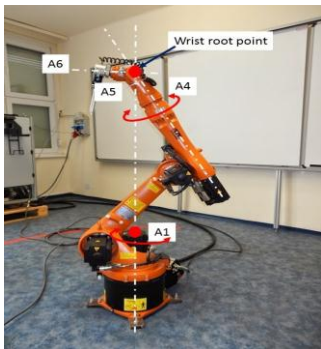
$$\xi = (v, \omega)^T \tag{6.4}$$

vector of the velocity of the arm.

In the standard KUKA kinematic system, a distinction is made among 3 different singularity positions. These are the overhead singularity, the extended position and the wrist axis singularity. One characteristic of a singularity is that an unambiguous reverse transformation (conversion of Cartesian coordinates to axis-specific values) is not possible, even though Status and Turn are specified. Small Cartesian changes in the immediate vicinity of a singularity give rise to major changes in the axis angles [7]. The wrist root point, located at the intersection of axes A4, A5 and A6, is positioned directly on axis 1 (Fig. 8).

The position of axis 1 cannot be determined unambiguously by means of the reverse transformation and can thus have any value. If the end point of a PTP motion results in the overhead singularity, the controller offers the following options:

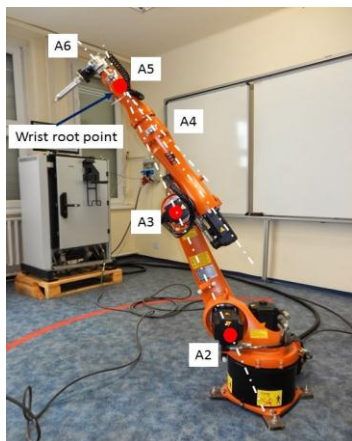
- Axis 1 is moved to “0” degrees (default position) during the PTP motion.
- The axis angle for axis 1 remains the same for both the start point and the end point.



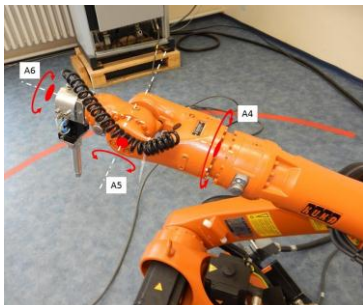
**Fig.8.** The wrist root point, located at the intersection of axes A4, A5 and A6.

Figure 9 shows when the extension of A2-A3 intersects the wrist root point. In this case, the robot is at the limit of its work envelope. Although reverse transformation does provide unambiguous axis angles, low Cartesian velocities result in high axis velocities for axes 2 and 3.

In the wrist axis singularity (A5 position, Fig. 10) the axes 4 and 6 are parallel. It is not possible to unambiguously determine the positions of these two axes by means of reverse transformation, as there is an infinite number of axis positions for A4 and A6 for which the sum of the axis angles is identical.



**Fig.9.** The extension of A2-A3 intersects the wrist root point.



**Fig.10.** Axes 4 and 6 are parallel.

## 7. Conclusion

This paper has at length delved into the basic aspects of Different singularity positions Standard 6R 6DOF kinematic system. The subject is not only complex and far entailing but also evolving and dynamic one, wherein the technology is subject to major changes over time and new technooog9 that supplants earlier ones are occurring on recurrent and periodic basis so it is rather difficult to place best industry practices in the realms of position Singularities of 6R 6DOF of Robots in its proper and definitive perspectives. Moreover, it is also necessary to admit that globally, different manufacturers, assemblers and sellers have different norms and practices with regard to the overwhelming and preponderance of Standard 6R 6DOF kinematic system and most robust systems that are diligent, committed and laborious have withstood the test of time and changing technology in these domains The realms of Standard 6R 6DOF kinematic system are indeed major issues that need to be considered in the realms of manipulators and it is also important to consider the preponderance of major issues like that of representations of designs for Jacobean theories and its enforcement in the realms of Standard 6R 6DOF kinematic system.

## References

- [1] R. Paul, Robot manipulators: mathematics, programming, and control : the computer control of robot manipulators, Cambridge, MA. ISBN 978-0-262-16082-7.: MIT Press, 1981.
- [2] J. M. McCarthy, Introduction to Theoretical Kinematics, Cambridge, MA: MIT Press, 1990.
- [3] L. Béla, Robotok programozása (egyetemi jegyzet), Budapest: BME, 2002.
- [4] R. H. J. Denavit, "A kinematic notation for lower-pair mechanisms based on matrices," J.Appl. Mech, vol. 22, pp. 215-221, 1955.
- [5] B. Kulcsár, *Robottechnika II.*, Budapest: Typotex, 2012.
- [6] M. W. Spong, S. Hutchinson and M. Vidyasagar, *Robot Modeling and Control*, New York: John Wiley and Sons ISBN: 9780471649908, 2005.
- [7] A. KUKA Roboter GmbH, *KR 5 arc Specification*, Augsburg: KUKA Roboter GmbH, Augsburg Spez KR 5 arc V1.1, 21.03.2011.

**Guide for Authors**

---

The *International Journal of Engineering Technologies (IJET)* seeks to promote and disseminate knowledge of the various topics of engineering technologies. The journal aims to present to the international community important results of work in the fields of engineering such as imagining, researching, planning, creating, testing, improving, implementing, using and asking. The journal also aims to help researchers, scientists, manufacturers, institutions, world agencies, societies, etc. to keep up with new developments in theory and applications and to provide alternative engineering solutions to current.

The *International Journal of Renewable Energy Research* is a quarterly published journal and operates an online submission and peer review system allowing authors to submit articles online and track their progress via its web interface. The journal aims for a publication speed of **60 days** from submission until final publication.

The coverage of IJET includes the following engineering areas, but not limited to:

All filed of engineering such as;

**Chemical engineering**

- Biomolecular engineering
- Materials engineering
- Molecular engineering
- Process engineering

**Civil engineering**

- Environmental engineering
- Geotechnical engineering
- Structural engineering
- Transport engineering
- Water resources engineering

**Electrical engineering**

- Computer engineering
- Electronic engineering
- Optical engineering
- Power engineering

**Mechanical engineering**

- Acoustical engineering

- Manufacturing engineering
- Thermal engineering
- Vehicle engineering

#### **Systems (interdisciplinary) engineering**

- Aerospace engineering
- Agricultural engineering
- Applied engineering
- Biological engineering
- Building services engineering
- Energy engineering
- Railway engineering
- Industrial engineering
- Mechatronics
- Military engineering
- Nano engineering
- Nuclear engineering
- Petroleum engineering

Types of Articles submitted should be original research papers, not previously published, in one of the following categories,

- Applicational and design studies.
- Technology development,
- Comparative case studies.
- Reviews of special topics.
- Reviews of work in progress and facilities development.
- Survey articles.
- Guest editorials for special issues.

## Editorial Board

---

### *Editor-in-Chief:*

*Professor ILHAMI COLAK*

### *Associate Editors:*

*Dr. Selin ÖZCIRA*

*Dr. Mehmet YESILYAPRAK*

## Ethic Responsibilities

---

The publication of an article in peer-reviewed “*International Journal of Engineering Technologies*” is an essential building block in the development of a coherent and respected network of knowledge. It is a direct reflection of the quality of the work. Peer-reviewed articles support and embody the scientific method. It is therefore important to agree upon standards of expected ethical behavior for all parties involved in the act of publishing: the author, the journal editor, the peer reviewer, the publisher and the society of society-owned or sponsored journals.

All authors are requested to disclose any actual or potential conflict of interest including any financial, personal or other relationships with other people or organizations within three years of beginning the submitted work that could inappropriately influence, or be perceived to influence, their work.

Submission of an article implies that the work described has not been published previously that it is not under consideration for publication elsewhere. The submission should be approved by all authors and tacitly or explicitly by the responsible authorities where the work was carried out, and that, if accepted, it will not be published elsewhere in the same form, in English or in any other language, including electronically without the written consent of the copyright-holder.

Upon acceptance of an article, authors will be asked to complete a “Copyright Form”. Acceptance of the agreement will ensure the widest possible dissemination of information. An e-mail will be sent to the corresponding author confirming receipt of the manuscript together with a “Copyright Form” form or a link to the online version of this agreement.

### *Author Rights*

As a journal author, you retain rights for a large number of author uses, including use by your employing institute or company. These rights are retained and permitted without the need to obtain specific permission from *IJREER*. These include:

- ❖ The right to make copies (print or electronic) of the journal article for your own personal use, including for your own classroom teaching use;
- ❖ The right to make copies and distribute copies (including via e-mail) of the journal article to research colleagues, for personal use by such colleagues for scholarly purposes;
- ❖ The right to post a pre-print version of the journal article on internet web sites including electronic pre-print servers, and to retain indefinitely such version on such servers or sites for scholarly purposes

- ❖ the right to post a revised personal version of the text of the final journal article on your personal or institutional web site or server for scholarly purposes
- ❖ The right to use the journal article or any part thereof in a printed compilation of your works, such as collected writings or lecture notes.

## Article Style

---

Authors must strictly follow the guide for authors, or their articles may be rejected without review. Editors reserve the right to adjust the style to certain standards of uniformity. Follow Title, Authors, Affiliations, Abstract, Keywords, Introduction, Materials and Methods, Theory/Calculation, Conclusions, Acknowledgements, References order when typing articles. The corresponding author should be identified with an asterisk and footnote. Collate acknowledgements in a separate section at the end of the article and do not include them on the title page, as a footnote to the title or otherwise.

### *Abstract and Keywords:*

Enter an abstract of up to 250 words for all articles. This is a concise summary of the whole paper, not just the conclusions, and is understandable without reference to the rest of the paper. It should contain no citation to other published work. Include up to six keywords that describe your paper for indexing purposes.

### *Abbreviations and Acronyms:*

Define abbreviations and acronyms the first time they are used in the text, even if they have been defined in the abstract. Abbreviations such as IEEE, SI, MKS, CGS, sc, dc, and rms do not have to be defined. Do not use abbreviations in the title unless they are unavoidable.

### *Text Layout for Peer Review:*

Use single column layout, double spacing and wide (3 cm) margins on white paper at the peer review stage. Ensure that each new paragraph is clearly indicated. Present tables and figure legends in the text where they are related and cited. Number all pages consecutively; use 12 pt font size and standard fonts; Times New Roman, Helvetica, or Courier is preferred.

Research Papers should not exceed 12 printed pages in two-column publishing format, including figures and tables.

Technical Notes and Letters should not exceed 2,000 words.

Reviews should not exceed 20 printed pages in two-column publishing format, including figures and tables.

### *Equations:*

Number equations consecutively with equation numbers in parentheses flush with the right margin, as in (1). To make equations more compact, you may use the solidus (/), the exp function, or appropriate exponents. Italicize Roman symbols for quantities and variables, but not Greek symbols. Use an dash (–) rather than a hyphen for a minus sign. Use parentheses to avoid ambiguities in denominators. Punctuate equations with commas or periods when they are part of a sentence, as in

$$C = a + b \tag{1}$$

Symbols in your equation should be defined before the equation appears or immediately following. Use “Eq. (1)” or “equation (1),” while citing.

### **Figures and Tables:**

All illustrations must be supplied at the correct resolution:

- \* Black and white and colour photos - 300 dpi
- \* Graphs, drawings, etc - 800 dpi preferred; 600 dpi minimum
- \* Combinations of photos and drawings (black and white and color) - 500 dpi

In addition to using figures in the text, upload each figure as a separate file in either .tiff or .eps format during submission, with the figure number.

Table captions should be written in the same format as figure captions; for example, “Table 1. Appearance styles.”. Tables should be referenced in the text unabbreviated as “Table 1.”

### **References:**

Please ensure that every reference cited in the text is also present in the reference list (and viceversa). Any references cited in the abstract must be given in full. Unpublished results and personal communications are not recommended in the reference list, but may be mentioned in the text. Citation of a reference as “in press” implies that the item has been accepted for publication. Number citations consecutively in square brackets [1]. Punctuation follows the bracket [2]. Refer simply to the reference number, as in [3]. Use “Ref. [3]” or Reference [3]” at the beginning of a sentence: “Reference [3] was ...”. Give all authors’ names; use “et al.” if there are six authors or more. For papers published in translated journals, first give the English citation, then the original foreign-language citation.

#### *Books*

- [1] J. Clerk Maxwell, *A Treatise on Electricity and Magnetism*, 3rd ed., vol. 2. Oxford:Clarendon Press, 1892, pp.68-73.

#### *Journals*

- [2] Y. Yorozu, M. Hirano, K. Oka, and Y. Tagawa, “Electron spectroscopy studies on magneto-optical media and plastic substrate interface”, *IEEE Transl. J. Magn. Japan*, vol. 2, pp. 740-741, August 1987.

#### *Conferences*

- [3] Çolak I., Kabalci E., Bayindir R., and Sagiroglu S, “The design and analysis of a 5-level cascaded voltage source inverter with low THD”, *2nd PowerEng Conference*, Lisbon, pp. 575-580, 18-20 March 2009.

#### *Reports*

- [4] IEEE Standard 519-1992, Recommended practices and requirements for harmonic control in electrical power systems, *The Institute of Electrical and Electronics Engineers*, 1993.

### ***Text Layout for Accepted Papers:***

A4 page margins should be margins: top = 24 mm, bottom = 24 mm, side = 15 mm. Main text should be given in two column. The column width is 87mm (3.425 in). The space between the two columns is 6 mm (0.236 in). Paragraph indentation is 3.5 mm (0.137 in). Follow the type sizes specified in Table. Position figures and tables at the tops and bottoms of columns. Avoid placing them in the middle of columns. Large figures and tables may span across both columns. Figure captions should be centred below the figures; table captions should be centred above. Avoid placing figures and tables before their first mention in the text. Use the abbreviation “Fig. 1,” even at the beginning of a sentence.

Type size (pts.)	Appearance		
	Regular	<b>Bold</b>	<i>Italic</i>
10	Authors’ affiliations, Section titles, references, tables, table names, first letters in table captions, figure captions, footnotes, text subscripts, and superscripts	<b>Abstract</b>	
12	Main text, equations, Authors’ names, <sup>a</sup>		<i>Subheading (1.1.)</i>
24	Paper title		

### **Submission checklist:**

---

It is hoped that this list will be useful during the final checking of an article prior to sending it to the journal's Editor for review. Please consult this Guide for Authors for further details of any item. Ensure that the following items are present:

- ❖ One Author designated as corresponding Author:
  - E-mail address
  - Full postal address
  - Telephone and fax numbers
- ❖ All necessary files have been uploaded
- Keywords: a minimum of 4
- All figure captions (supplied in a separate document)
- All tables (including title, description, footnotes, supplied in a separate document)
- ❖ Further considerations
  - Manuscript has been "spellchecked" and "grammar-checked"
  - References are in the correct format for this journal
  - All references mentioned in the Reference list are cited in the text, and vice versa

- Permission has been obtained for use of copyrighted material from other sources (including the Web)
- Color figures are clearly marked as being intended for color reproduction on the Web (free of charge) and in print or to be reproduced in color on the Web (free of charge) and in black-and-white in print.

# Article Template Containing Author Guidelines for Peer-Review

First Author\*, Second Author\*\*‡, Third Author\*\*\*

\*Department of First Author, Faculty of First Author, Affiliation of First Author, Postal address

\*\*Department of Second Author, Faculty of First Author, Affiliation of First Author, Postal address

\*\*\*Department of Third Author, Faculty of First Author, Affiliation of First Author, Postal address

(First Author Mail Address, Second Author Mail Address, Third Author Mail Address)

‡Corresponding Author; Second Author, Postal address, Tel: +90 312 123 4567, Fax: +90 312 123 4567, corresponding@affl.edu

*Received: xx.xx.xxxx Accepted:xx.xx.xxxx*

**Abstract-** Enter an abstract of up to 250 words for all articles. This is a concise summary of the whole paper, not just the conclusions, and is understandable without reference to the rest of the paper. It should contain no citation to other published work. Include up to six keywords that describe your paper for indexing purposes. Define abbreviations and acronyms the first time they are used in the text, even if they have been defined in the abstract. Abbreviations such as IEEE, SI, MKS, CGS, sc, dc, and rms do not have to be defined. Do not use abbreviations in the title unless they are unavoidable.

**Keywords-** Keyword1; keyword2; keyword3; keyword4; keyword5.

## 2. Introduction

Authors should any word processing software that is capable to make corrections on misspelled words and grammar structure according to American or Native English. Authors may get help by from word

processor by making appeared the paragraph marks and other hidden formatting symbols. This sample article is prepared to assist authors preparing their articles to IJET.

Indent level of paragraphs should be 0.63 cm (0.24 in) in the text of article. Use single column layout, double-spacing and wide (3 cm) margins on white paper at the peer review stage. Ensure that each new paragraph is clearly indicated. Present tables and figure legends in the text where they are related and cited. Number all pages consecutively; use 12 pt font size and standard fonts; Times New Roman, Helvetica, or Courier is preferred. Indicate references by number(s) in square brackets in line with the text. The actual authors can be referred to, but the reference number(s) must always be given. Example: "..... as demonstrated [3, 6]. Barnaby and Jones [8] obtained a different result ...."

IJRER accepts submissions in three styles that are defined as Research Papers, Technical Notes and Letter, and Review paper. The requirements of paper are as listed below:

- Research Papers should not exceed 12 printed pages in two-column publishing format, including figures and tables.
- Technical Notes and Letters should not exceed 2,000 words.
- Reviews should not exceed 20 printed pages in two-column publishing format, including figures and tables.

Authors are requested write equations using either any mathematical equation object inserted to word processor or using independent equation software. Symbols in your equation should be defined before the equation appears or immediately following. Use "Eq. (1)" or "equation (1)," while citing. Number equations consecutively with equation numbers in parentheses flush with the right margin, as in Eq. (1). To make equations more compact, you may use the solidus ( / ), the exp function, or appropriate exponents. Italicize Roman symbols for quantities and variables, but not Greek symbols. Use an dash (–) rather than a hyphen for a minus sign. Use parentheses to avoid ambiguities in denominators. Punctuate equations with commas or periods when they are part of a sentence, as in

$$C = a + b \tag{1}$$

Section titles should be written in bold style while sub section titles are italic.

### 3. Figures and Tables

#### 3.1. *Figure Properties*

All illustrations must be supplied at the correct resolution:

- Black and white and colour photos - 300 dpi
- Graphs, drawings, etc - 800 dpi preferred; 600 dpi minimum
- Combinations of photos and drawings (black and white and colour) - 500 dpi

In addition to using figures in the text, Authors are requested to upload each figure as a separate file in either .tiff or .eps format during submission, with the figure number as Fig.1., Fig.2a and so on. Figures are cited as “Fig.1” in sentences or as “Figure 1” at the beginning of sentence and paragraphs. Explanations related to figures should be given before figure. Figures and tables should be located at the top or bottom side of paper as done in accepted article format.



Figure 1. Engineering technologies.

Table captions should be written in the same format as figure captions; for example, “Table 1. Appearance styles.”. Tables should be referenced in the text unabbreviated as “Table 1.”

Table 1. Appearance properties of accepted manuscripts

Type size (pts.)	Appearance		
	Regular	<b>Bold</b>	<i>Italic</i>
10	Authors’ affiliations, Abstract, keywords, references, tables, table names, figure captions, footnotes, text subscripts, and superscripts	<b>Abstract</b>	
12	Main text, equations, Authors’ names, Section titles		<i>Subheading (1.1.)</i>
24	<b>Paper title</b>		

#### 4. Submission Process

The *International Journal of Engineering Technologies* operates an online submission and peer review system that allows authors to submit articles online and track their progress via a web interface. Articles that are prepared referring to this template should be controlled according to submission checklist given in “Guide f Authors”. Editor handles submitted articles to IJET primarily in order to control in terms of compatibility to aims and scope of Journal.

Articles passed this control are checked for grammatical and template structures. If article passes this control too, then reviewers are assigned to article and Editor gives a reference number to paper. Authors registered to online submission system can track all these phases.

Editor also informs authors about processes of submitted article by e-mail. Each author may also apply to Editor via online submission system to review papers related to their study areas. Peer review is a critical element of publication, and one of the major cornerstones of the scientific process. Peer Review serves two key functions:

- Acts as a filter: Ensures research is properly verified before being published
- Improves the quality of the research

## 5. Conclusion

The conclusion section should emphasize the main contribution of the article to literature. Authors may also explain why the work is important, what are the novelties or possible applications and extensions. Do not replicate the abstract or sentences given in main text as the conclusion.

## Acknowledgements

Authors may acknowledge to any person, institution or department that supported to any part of study.

## References

- [1] J. Clerk Maxwell, *A Treatise on Electricity and Magnetism*, 3rd ed., vol. 2. Oxford:Clarendon Press, 1892, pp.68-73. (Book)
- [2] H. Poor, *An Introduction to Signal Detection and Estimation*, New York: Springer-Verlag, 1985, ch. 4. (Book Chapter)
- [3] Y. Yorozu, M. Hirano, K. Oka, and Y. Tagawa, "Electron spectroscopy studies on magneto-optical media and plastic substrate interface", *IEEE Transl. J. Magn. Japan*, vol. 2, pp. 740-741, August 1987. (Article)
- [4] E. Kabalci, E. Irmak, I. Çolak, "Design of an AC-DC-AC converter for wind turbines", *International Journal of Energy Research*, Wiley Interscience, DOI: 10.1002/er.1770, Vol. 36, No. 2, pp. 169-175. (Article)
- [5] I. Çolak, E. Kabalci, R. Bayindir R., and S. Sagiroglu, "The design and analysis of a 5-level cascaded voltage source inverter with low THD", *2nd PowerEng Conference*, Lisbon, pp. 575-580, 18-20 March 2009. (Conference Paper)
- [6] IEEE Standard 519-1992, Recommended practices and requirements for harmonic control in electrical power systems, *The Institute of Electrical and Electronics Engineers*, 1993. (Standards and Reports)

# Article Template Containing Author Guidelines for Accepted Papers

First Author\*, Second Author\*\*<sup>‡</sup>, Third Author\*\*\*

\*Department of First Author, Faculty of First Author, Affiliation of First Author, Postal address

\*\*Department of Second Author, Faculty of First Author, Affiliation of First Author, Postal address

\*\*\*Department of Third Author, Faculty of First Author, Affiliation of First Author, Postal address

(First Author Mail Address, Second Author Mail Address, Third Author Mail Address)

<sup>‡</sup>Corresponding Author; Second Author, Postal address, Tel: +90 312 123 4567,

Fax: +90 312 123 4567, [corresponding@affl.edu](mailto:corresponding@affl.edu)

*Received: xx.xx.xxxx Accepted:xx.xx.xxxx*

**Abstract-** Enter an abstract of up to 250 words for all articles. This is a concise summary of the whole paper, not just the conclusions, and is understandable without reference to the rest of the paper. It should contain no citation to other published work. Include up to six keywords that describe your paper for indexing purposes. Define abbreviations and acronyms the first time they are used in the text, even if they have been defined in the abstract. Abbreviations such as IEEE, SI, MKS, CGS, sc, dc, and rms do not have to be defined. Do not use abbreviations in the title unless they are unavoidable.

**Keywords** Keyword1, keyword2, keyword3, keyword4, keyword5.

## 1. Introduction

Authors should use any word processing software that is capable to make corrections on misspelled words and grammar structure according to American or Native English. Authors may get help by using word processor by making sure the paragraph marks and other hidden formatting symbols are visible. This sample article is prepared to assist authors preparing their articles to IJRER.

Indent level of paragraphs should be 0.63 cm (0.24 in) in the text of article. Use single column layout, double-spacing and wide (3 cm) margins on white paper at the peer review stage. Ensure that each new paragraph is clearly indicated. Present tables and figure legends in the text where they are related and cited. Number all pages consecutively; use 12 pt font size and standard fonts; Times New Roman, Helvetica, or Courier is preferred. Indicate references by number(s) in square brackets in line with the text. The actual authors can be referred to, but the reference number(s) must always be given. Example: "..... as demonstrated [3,6]. Barnaby and Jones [8] obtained a different result ...."

IJRER accepts submissions in three styles that are defined as Research Papers, Technical Notes and Letter, and Review paper. The requirements of paper are as listed below:

➤ Research Papers should not exceed 12 printed pages in two-column publishing format, including figures and tables.

➤ Technical Notes and Letters should not exceed 2,000 words.

➤ Reviews should not exceed 20 printed pages in two-column publishing format, including figures and tables.

Authors are requested to write equations using either any mathematical equation object inserted to word processor or using independent equation software. Symbols in your equation should be defined before the equation appears or immediately following. Use "Eq. (1)" or "equation (1)," while citing. Number equations consecutively with equation numbers in parentheses flush with the right margin, as in Eq. (1). To make equations more compact, you may use the solidus ( / ), the exp function, or appropriate exponents. Italicize Roman symbols for quantities and variables, but not Greek symbols. Use an dash (-) rather than a hyphen for a minus sign. Use parentheses to avoid ambiguities in denominators. Punctuate equations with commas or periods when they are part of a sentence, as in

$$C = a + b \quad (1)$$

Section titles should be written in bold style while sub section titles are italic.

## 6. Figures and Tables

### 6.1. Figure Properties

All illustrations must be supplied at the correct resolution:

- Black and white and colour photos - 300 dpi
- Graphs, drawings, etc - 800 dpi preferred; 600 dpi minimum
- Combinations of photos and drawings (black and white and colour) - 500 dpi

In addition to using figures in the text, Authors are requested to upload each figure as a separate file in either .tiff or .eps format during submission, with the figure number as Fig.1., Fig.2a and so on. Figures are cited as “Fig.1” in sentences or as “Figure 1” at the beginning of sentence and paragraphs. Explanations related to figures should be given before figure.



**Fig. 1.** Engineering technologies.

Figures and tables should be located at the top or bottom side of paper as done in accepted article format. Table captions should be written in the same format as figure captions; for example, “Table 1. Appearance styles.”. Tables should be referenced in the text unabbreviated as “Table 1.”

**Table 1.** Appearance properties of accepted manuscripts

Type size (pts.)	Appearance		
	Regular	<b>Bold</b>	<i>Italic</i>
10	Main text, section titles, authors’ affiliations, abstract, keywords, references, tables, table names, figure captions, equations, footnotes, text subscripts, and superscripts	<b>Abstract-</b>	<i>Subheading (1.1.)</i>
12	Authors’ names,		
24	<b>Paper title</b>		

### 6.2. Text Layout for Accepted Papers

A4 page margins should be margins: top = 24 mm, bottom = 24 mm, side = 15 mm. The column width is 87mm (3.425 in). The space between the two columns is 6 mm (0.236 in). Paragraph indentation is 3.5 mm (0.137 in). Follow the type sizes specified in Table. Position figures and tables at the tops and bottoms of columns. Avoid placing them in the middle of columns. Large figures and tables may span across both columns. Figure captions should be centred below the figures; table captions should be centred above. Avoid placing figures and tables before their first mention in the text. Use the abbreviation “Fig. 1,” even at the beginning of a sentence.

## 7. Submission Process

The International Journal of Renewable Energy Research operates an online submission and peer review system that allows authors to submit articles online and track their

progress via a web interface. Articles that are prepared referring to this template should be controlled according to submission checklist given in “Guide f Authors”. Editor handles submitted articles to IJRER primarily in order to control in terms of compatibility to aims and scope of Journal. Articles passed this control are checked for grammatical and template structures. If article passes this control too, then reviewers are assigned to article and Editor gives a reference number to paper. Authors registered to online submission system can track all these phases. Editor also informs authors about processes of submitted article by e-mail. Each author may also apply to Editor via online submission system to review papers related to their study areas. Peer review is a critical element of publication, and one of the major cornerstones of the scientific process. Peer Review serves two key functions:

- Acts as a filter: Ensures research is properly verified before being published
- Improves the quality of the research

## 8. Conclusion

The conclusion section should emphasize the main contribution of the article to literature. Authors may also explain why the work is important, what are the novelties or possible applications and extensions. Do not replicate the abstract or sentences given in main text as the conclusion.

## Acknowledgements

Authors may acknowledge to any person, institution or department that supported to any part of study.

## References

- [7] J. Clerk Maxwell, A Treatise on Electricity and Magnetism, 3rd ed., vol. 2. Oxford:Clarendon Press, 1892, pp.68-73. (Book)
- [8] H. Poor, An Introduction to Signal Detection and Estimation, New York: Springer-Verlag, 1985, ch. 4. (Book Chapter)
- [9] Y. Yorozu, M. Hirano, K. Oka, and Y. Tagawa, "Electron spectroscopy studies on magneto-optical media and plastic substrate interface", IEEE Transl. J. Magn. Japan, vol. 2, pp. 740-741, August 1987. (Article)
- [10] E. Kabalcı, E. Irmak, I. Çolak, "Design of an AC-DC-AC converter for wind turbines", International Journal of Energy Research, Wiley Interscience, DOI: 10.1002/er.1770, Vol. 36, No. 2, pp. 169-175. (Article)
- [11] I. Çolak, E. Kabalcı, R. Bayindir R., and S. Sagirolu, "The design and analysis of a 5-level cascaded voltage source inverter with low THD", 2nd PowerEng Conference, Lisbon, pp. 575-580, 18-20 March 2009. (Conference Paper)
- [12] IEEE Standard 519-1992, Recommended practices and requirements for harmonic control in electrical power systems, The Institute of Electrical and Electronics Engineers, 1993. (Standards and Reports)

**INTERNATIONAL JOURNAL OF ENGINEERING TECHNOLOGIES (IJET)  
COPYRIGHT AND CONSENT FORM**

This form is used for article accepted to be published by the IJET. Please read the form carefully and keep a copy for your files.

**TITLE OF ARTICLE (hereinafter, "The Article"):**

.....  
.....  
.....

**LIST OF AUTHORS:**

.....  
.....  
.....

**CORRESPONDING AUTHOR'S ("The Author") NAME, ADDRESS, INSTITUTE AND EMAIL:**

.....  
.....  
.....

**COPYRIGHT TRANSFER**

The undersigned hereby transfers the copyright of the submitted article to International Journal of Engineering Technologies (the "IJET"). The Author declares that the contribution and work is original, and he/she is authorized by all authors and/or grant-funding agency to sign the copyright form. Author hereby assigns all including but not limited to the rights to publish, distribute, reprints, translates, electronic and published derivatives in various arrangements or any other versions in full or abridged forms to IJET. IJET holds the copyright of Article in its own name.

Author(s) retain all rights to use author copy in his/her educational activities, own websites, institutional and/or funder's web sites by providing full citation to final version published in IJET. The full citation is provided including Authors list, title of the article, volume and issue number, and page number or using a link to the article in IJET web site. Author(s) have the right to transmit, print and share the first submitted copies with colleagues. Author(s) can use the final published article for his/her own professional positions, career or qualifications by citing to the IJET publication.

Once the copyright form is signed, any changes about the author names or order of the authors listed above are not accepted by IJET.

**Authorized/Corresponding Author**

**Date/ Signature**